MELTING OF A PHASE CHANGE MATERIAL IN HORIZONTAL ANNULI

Dipendra B. Khillarkar

Department of Chemical Engineering
McGill University
Montreal, Quebec, Canada

A thesis submitted to the Faculty of Graduate Studies and Research in partial fulfillment of the requirements for the degree of Master of Engineering

0-612-50629-0

ABSTRACT

Numerical experiments were carried out to determine tube geometries for more efficient thermal storage. A finite element simulation code developed earlier, which solves the two dimensional governing conservation equations was employed to examine the thermal performance of horizontal annuli of the following configurations:

(a) Square external tube with a circular tube inside - Annulus Type A

(b) Circular external tube with a square tube inside - Annulus Type B

Effects of the Rayleigh number as well as heating of the inside, outside or both walls at a temperature above the melting point of the material were studied. Flow and temperature patterns within the melt, local heat flux distributions at the heating surface and the cumulative energy charged as a function of time are presented and discussed.

To enhance the heat transfer rate during melting in horizontal annular containers various innovative passive methods were examined. Eccentric annular configurations are identified as superior to concentric tubular geometries due to the vertically upward orientation of the buoyancy force in the melt phase at higher Rayleigh numbers. In addition to this the effect of flipping the container at pre-selected times after initiation of melting as a measure to increase the heat transfer rate during the last stage of the melting process is also examined and discussed.

RÉSUMÉ

Des expériences numériques ont été réalisées dans l'optique de déterminer des formes optimales de tubes pour le stockage thermique. Un programme de simulation basé sur les éléments finis développé antérieurement résout les équations de conservation à deux dimensions. Cette technique est utilisée pour examiner les performances thermiques des anneaux horizontaux des configurations suivantes :

(a) Tube de section extérieure carrée avec une section interne circulaire- Anneau de type A

(b) Tube de section extérieure circulaire avec une section intérieure carrée- Anneau de type B

Les effets de la constante de Rayleigh comme l'échauffement de l'intérieur, de l'extérieur ou des deux surfaces à une température supérieure au point de fusion du matériau ont été étudiés. L'évolution du flux et de la température dans la phase de fusion, les distributions du flux de chaleur sur la surface chauffée et l'énergie thermique cumulée emmagasinée sont présentés et commentés en fonction du temps.

Pour améliorer le rendement du transfert de chaleur, pendant la fusion dans des récipients horizontaux et annulaires, différentes méthodes innovatrices et passives ont été examinées. Des modèles d'anneaux excentrés ont obtenu de meilleures performances que des formes tubulaires concentriques. Ceci est principalement du à l'orientation ascendante verticale des forces de poussée dans la phase de fusion pour des nombres de Rayleigh élevés. De plus le récipient est retourné à des temps prédéfinis après le début de la fusion, pour augmenter le taux de transfert thermique pendant la dernière étape du procédé de fusion. L'effet sur le système est examiné et commenté.

ACKNOWLEDGEMENTS

I wish to express my sincere appreciation and gratitude to my research advisor, Professor A. S. Mujumdar, for his advice, fruitful suggestions, guidance and encouragement throughout the course of this work. I am also grateful to Dr. Z. X. Gong of Hyprotech, Co., for his original work on computer code development along with his judicious suggestions and constant collaboration which made the successful completion of this thesis possible.

I would also like to thank my friends Sakamon Devahastin and Ka Wing Ng for their expert comments and valuable suggestions during the crucial moments of this work. I am also thankful to all the staff of the Chemical Engineering Department without whom this work would not have been accomplished.

Thanks are also due to my friends Anand, Mihir, Sanjay, Arvinder and Dinesh for their help, support and consistent encouragement while being away from home. Acknowledgment is due to my friend R. Dumortier for his help in the preparation of the French abstract.

Last, but not least, I am greatly indebted to my parents and sister for their patience, understanding and continuous moral support without which this work would not have been attempted. The least I can do is to dedicate this thesis to them.

TABLE OF CONTENTS

LIST OF FIGURES

LIST OF TABLES

Chapter 1

Introduction

1.1 GENERAL INTRODUCTION

Heat transfer during melting and/or freezing of a phase change material has attracted considerable attention over the past several decades due to its relevance to many technological applications such as latent-heat energy storage systems, casting and crystal-growth processes, latent-heat thermal storage devices, to name a few. Literally several thousand papers have examined various aspects of melting and freezing phenomena both from the fundamental as well as applications point of view. The non-linearity of the governing energy equation and a wide variety of geometric and thermal boundary conditions provide a fertile ground for challenging basic research problems. Also, numerous industrial applications in diverse industries provide the necessary incentive for engineering research and development. Time-dependant boundary conditions, under some conditions can lead to interesting and unique multiple moving boundaries as well.

Although a number of experimental and numerical studies have been devoted to convection dominated melting of a phase change material (PCM) for various geometric configurations, particular attention is given to melting in a horizontal annulus as a model for thermal energy storage system A number of numerical/analytical studies [1-3] have been performed in an attempt to model the melting phenomenon based on the Boussinesq approximation. Rieger *et al.* [4] and Ho and Viskanta [5] investigated experimentally the evolution of the solid-liquid interface during melting of a PCM contained in a horizontal cylinder. They also presented results of a numerical simulation of the melting process using a finite difference numerical method. In addition to this, recently Ng *et al.* [6]

studied the free convective melting of a phase change material in a horizontal cylindrical annulus heated isothermally from the inside wall and their results indicate that an increase in Rayleigh number promotes the heat transfer rate. However no prior work exists on the problem of melting in a horizontal annulus of arbitrary cross-section.

The present investigation is motivated by both a fundamental heat transfer problem and the need to identify container geometries and thermal boundary conditions that may lead to enhanced thermal energy storage as heat of fusion in a phase change material. PCM thermal storage devices compete with sensible heat and chemical heat storage devices as possible alternatives to store heat during the melt cycle and discharge it during the freezing cycle. PCM stores provide the key advantages of high energy density, small floor space, stable temperature of discharged heat etc. Gong [7] has discussed this aspect of PCM stores in considerable detail.

1.2 OBJECTIVES

The main objectives of this study are as follows:

1. To simulate using a mathematical model the free convection-dominated melting heat transfer characteristics of a PCM contained in arbitrary-shaped annular geometry, and
2. To identify and numerically examine simple ways of enhancing such heat transfer rates

The model used in this work is an extension of the one developed by Gong[7]. The computational code is based on a finite element discretization of the governing conservation equations [7] This work is confined to melting heat transfer when effects of temperature dependant melt density leads to buoyancy forces driving the free convective motion in the melt zone

1.3 OUTLINE OF THE THESIS

This thesis is divided into five chapters with introduction as the first chapter. Chapter 2 presents a brief review of the literature associated with melting heat transfer of a PCM with heating along horizontal wall, vertical wall in annulus of different cross-section. In Chapter 3, the finite element model used to simulate melting of a PCM including free convection in the liquid phase is described. Results of the simulations for melting in horizontal annulus of arbitrary cross-section and passive innovative ways to enhance the heat transfer rate are presented in Chapter 4. The conclusions based on the results are enumerated in Chapter 5.

REFERENCES

1. Prusa, J. and Yao, L.S., 1984, "Melting around a Horizontal Heated Cylinder: Part I- Perturbation and Numerical Solution for Constant Heat Flux Boundary condition, " *J. Heat. Transfer*, Vol. 106, pp. 376-384.
2. Rieger, H., Projahn, U. and Beer, H., 1982, "Analysis of the Heat Transport Mechanisms during Melting around a Horizontal Circular Cylinder," *Int. J. Heat Mass Transfer*, Vol 25, pp. 137-147.
3. Ho, C.J. and Chen, S., 1986, "Numerical solution of melting of Ice around a Horizontal Cylinder," *Int. J. Heat Mass Transfer*, Vol.29, pp. 1359-1369.
4. Rieger, H., Projahn, U., Bareiss, M. and Beer, H., 1983, "Heat Transfer during Melting inside a Horizontal Tube," *J. Heat Transfer*, Vol. 105, pp.226-234.
5. Ho, C.J. and Viskanta, R, 1984, " Heat Transfer during inward Melting in a Horizontal tube," *Int. J. Heat Mass Transfer*, Vol. 27, pp. 705-716.
6. Ng, K.W., Devahastin, S. and Mujumdar, A.S., 1998, "Free Convective Melting of a Phase Change Material in a Horizontal Cylindrical Annulus," *Transactions TSTU*, Tom 4., No. 1., pp 40-52.
7. Gong, Z. X., 1997, "Time-dependant Melting and Freezing Heat Transfer in Multiple Phase Change Materials," Ph.D Thesis, Department of Chemical Eng., McGill University, Canada

Chapter 2

Literature Review

Free convective heat transfer studies, both experimental and analytical, have been reported in the literature very extensively in view of their industrial significance in many processes. This review is confined to sub-areas of free convection which are directly relevant to the theme of this thesis viz. melting heat transfer for a pure phase change material in horizontal containers of various geometries under conditions such that a two dimensional free convective flow develops in the melt zone due to the temperature-induced density variations leading to buoyancy forces. The aspect ratio of the container is such that three dimensional effects are not considered. Gong [E21] provides an extensive listing of relevant literature published prior to 1997.

2.1 CONVECTION-CONTROLLED MELTING

2.1.1 Melting along a Horizontal and Vertical Wall

The heat transfer from a vertical heated wall to a PCM contained in a rectangular enclosure has received considerable research attention due to its simple geometry as well as fundamental importance in several technological applications. A number of experimental studies in this area [A1-A6] have demonstrated the enhancement effects of natural convection on the melting heat transfer along a vertical wall in rectangular cavities. Also several numerical/analytical studies [A7-A17] have also been published over the last decade based on the Boussinesq assumption. Only a selected few are cited here due to space limitations.

Hale and Viskanta [A1] studied experimentally the melting of n-octadecane from a heated vertical wall of a rectangular test cell. The melt shapes, the temperature histories and the local heat transfer coefficients at the solid-liquid interface demonstrated the dominant role played by natural convection during melting from a vertical heat source. The experiments of Bareiss and Beer [A2] clearly showed that the local enhancement in melting at the top of the wall overrides the decrease occurring near the bottom, and that the melt volume increases linearly with time.

Benard, Gobin and Martinez [A3] observed the development of a thermal boundary layer along the heated wall and solid liquid interface with a central stratified zone in between, once the melt zone is sufficiently large. According to Ho and Viskanta [A4] sub-cooling of the solid is found to significantly impede the melting process because of the required sensible heating of the solid and the delay in the occurrence of the convection stage which the reduced melt zone causes. The role of natural convection on the shape and motion of the phase change interface of gallium and tin from a vertical wall were investigated by Gau and Viskanta [A5] and Wolff and Viskanta [A6], respectively. Their results indicate that the melting of the solid from the top of the PCM could be greatly accelerated and near the bottom region could be significantly retarded or even terminated by buoyancy driven convection in the liquid phase.

Gadgil and Gobin [A7] numerically simulated the two dimensional melting of a solid phase change material in a rectangular enclosure heated from one side. They divided the process into a large number of quasi-static steps and for each quasi-static step natural convection in the liquid phase was calculated by directly solving the governing equations with a finite difference technique. Webb and Viskanta [A8] developed a numerical model to predict the melting of a pure metal from an isothermal vertical wall. They used a control volume based discretization scheme adapted for irregular geometries. The moving boundary was immobilized by employing the quasi-steady assumption with an algebraically generated grid.

Lacroix [A9] employed a vorticity-velocity formulation with body-fitted co-ordinates to model a similar problem to that modeled by Webb and Viskanta [A8] and obtained similar results Costa *et al.* [A10] carried out a fixed grid finite difference analysis of melting in rectangular cavities using the SIMPLEC algorithm. Usmani *et al* [A11] performed a fixed grid finite element analysis of melting in rectangular enclosures.

Rady and Mohanty [A12] employed an enthalpy-porosity fixed grid method for simulating the natural convection during melting of pure metal in a rectangular cavity.

Keller and Bergman [A13] modeled numerically the steady state melting and freezing in an open rectangular cavity including both buoyancy and surface tension forces in the liquid phase. They found that surface tension induced flow could affect the solid geometry and, ultimately the melting and freezing rates. Liu *et al.* [A14] modeled both numerically and experimentally the melting and solidification of a pure metal in an open cavity with liquid phase buoyancy and surface tension forces and their numerical results were verified by comparing them with experimental data. Ho and Chu [A15, A16] simulated conduction-convection controlled melting of n-octadecane in a vertical square enclosure imposed with a time-dependant sinusoidal oscillatory wall temperature. Ho and Chu [A17] also simulated coupled melting and free convection heat transfer in two vertical rectangular composite cells one of which is filled with a PCM and the other is an air layer.

Sasaguchi *et al.* [A18] numerically studied the utilization of melting of a phase change material for cooling of a surface heated at a constant rate. Two orientations of the heated surface, i.e., at the bottom and at the side of the cavity, were examined. In addition, they studied the effects of uniform and discrete heating conditions on the cooling of the heated surface. They observed that the discrete arrangement of the heated portions strongly affected the cooling rate of the surface. They found that if the uniformly heated surface is located at the side of the cavity, the maximum temperature becomes much larger than that for the heated surface located at the bottom. They concluded that, if possible the heat-generating surfaces should be located at the bottom of the cavity for effective cooling.

Little prior work exists on the problem of melting of a PCM heated by a horizontal wall. Benard [A19] was the first to observe the convective instabilities, which develop during the melting of a horizontal layer of a PCM heated from below. An experimental investigation was carried out by Yen *et al.* [A20, A21] and Seki *et al.* [A22] on the melting of a horizontal ice slab heated from below. Seki [A22] *et al.*

experimentally determined the Rayleigh number marking the onset of free convection, when the heat transfer mode changed from conduction to convection from the fact that the temperature distribution in the melted water layer started to deviate from its linear profile. Hale and Viskanta [A23] carried out experiments for melting from below and solidification from the top of a n-octadecane slab in a rectangular cavity. However, in their paper they did not present flow patterns and phase change interface shapes. Gau *et al.* [A24] presented flow visualization results for melting from below of an n-octadecane slab in a rectangular cavity. Diaz and Viskanta [A25] extended the experiments of Gau *et al.* [A24] to the observation of the morphology of the liquid/solid interface. Lacroix and Benmadda [A26] did a numerical study of melting from a horizontal heated wall with vertically oriented fins embedded in the phase change material. Their results show that melting is enhanced with a bottom finned heated wall and increasing Rayleigh number. Later Lacroix and Binet [A27] carried out a numerical study for natural convection dominated melting inside uniformly and discretely heated rectangular cavities using the computational methodology based on the enthalpy method for the phase change. Gong and Mujumdar [A28] have simulated the melting of a pure PCM in a rectangular container heated from below using the streamline Upwind/ Petrov Galerkin finite element method. They obtained several complex and time-dependant flow patterns at different Rayleigh numbers, which are quantitatively consistent with published results.

For more information on melting problems the reader is referred to the reviews by Yao and Prusa [A29], Viskanta [A30-A32] , Samarskii *et al.* [A33], Fukusako and Yamada [A34].

2.1.2 Melting inside a Horizontal Cylinder

One important geometric arrangement in view of technical applications particularly in phase change thermal storage is the phase change process occurring inside horizontal enclosures of various geometries. There are two possible cases: solid-constrained melting and close contact melting. Both of these cases have received considerable research attention in the past several years and are summarized in Table 2.1 in the interest of brevity

Table 2.1 Summary of Literature for Melting inside a Horizontal Cylinder

<table>
<tr><th>Author(s)</th><th colspan="2">Configuration</th><th>Conclusions</th></tr>
<tr><td>Rieger, H. et al. (1983) [B1]
Bareiss, M. & Beer, H. (1984) [B2]
Ho, C. J. & Viskanta, R. (1984a) [B3]
Sparrow, E. M. & Geiger, G. T. (1986) [B4]
Hirata, T. and Nishida, K. (1989) [B5]</td><td>• Experimental Studies</td><td rowspan="2">• Melting inside a Horizontal cylinder
• Solid PCM was maintained at a fixed position inside the heated horizontal cylinder</td><td rowspan="2">• Period of heat conduction is quite short, but dependant on Rayleigh number
• For smaller Rayleigh numbers, a streamlined shape for the solid occurs.
• For larger Rayleigh numbers ($\geq 10^6$) three dimensional, unsteady roll cell appears at the bottom of the solid, resulting in an inverted, pear-shaped, solid region.</td></tr>
<tr><td>Pannu, J. et al. (1980) [B6]
Saitoh, T & Hirose, K (1982) [B7]
Ho, C. J. & Viskanta, R. (1984) [B3]
Sparrow, E. M. & Geiger, G. T. (1986) [B4]
Prasad, A. & Sengupta, S. (1987) [B8]
Prasad, A. & Sengupta, S. (1988) [B9]
Park, C. E. & Chang, E. P. (1992) [B10]
Ro, S. T. & Kim, C-J. (1994) [B11]</td><td>• Theoretical / Numerical Studies</td></tr>
<tr><td>Nicholas, D. and Bayazitoglu, Y.(1980)[B12]
Bareiss, M. & Beer, H. (1984) [B13]
Sparrow, E. M. & Geiger, G. T. (1986) [B4]
Saitoh, T et al. (1992) [B15]
Saitoh, T & Kato, K. (1993) [B14]
Chen, W. Z. et al. (1998) [B16]</td><td colspan="2">• Investigated Heat transfer during melting of an unfixed solid phase change in a horizontal cylindrical enclosure</td><td>• If solid phase has higher density, the solid sinks to the bottom of the cylinder, giving rise to a region of close-contact melting
• Close-contact melting is the dominant mode of heat transfer when stefan number is small and contribution to free convection becomes significant as Stefan number increases</td></tr>
</table>

Pannu *et al* [B6] modeled the melting of a PCM inside a horizontal cylinder over the Rayleigh number range of 1.0×10^5 and 2.0×10^5 and for a Prandtl number of 145. For the case of Rayleigh number of 1.0×10^5 they observed secondary flow at the top of the melted annular zone. Saitoh and Hirose [B7] simulated the problem of Pannu *et al.* using the Landau transformation and an explicit finite difference method. Over a wide range of Rayleigh numbers, they predicted two vortex circulation cells at the bottom part of the melt annular which was different from that obtained by Pannu *et al.* [B6]. Rieger *et al.* [B1] studied inward melting of n-octadecane in a horizontal cylinder using a co-ordinate transformation technique and obtained experimental and numerical results for Rayleigh numbers in the range $10^5 \leq Ra \leq 10^6$. They observed three-dimensional Benard convection in the bottom region of the melt layer, which was unsteady in their time wise behavior. Their simulations using the body-fitted curvilinear co-ordinate approach also predicted the three vortex circulation zones observed in experiments.

Melting inside a horizontal cylinder was also investigated both experimentally and numerically by Ho and Viskanta [B3]; they reported the presence of secondary vortices induced by thermal instability in the bottom of the melt region for larger Rayleigh numbers, but failed to predict numerically the existence of the vortices. This may be due to the relatively coarse computational grid they used in their simulation. Park and Chang [B10] studied numerically the same problem and found that at low Rayleigh number (1.0×10^6) the natural convection flow in the melt region was unicellular. For a higher Rayleigh number (8.0×10^6) they obtained both flow patterns reported by both Saitoh and Hirose [B7] and Rieger *et al.* [B1] by applying a small perturbation to the vorticity field during the initial stage of the melting. However they did not observe secondary flows at the top of the melted annular as did Pannu *et al.* [B6]. They concluded that there existed a bifurcation phenomenon in certain Rayleigh number range of the melting process. Prasad and Sengupta [B8, B9] investigated the effects of variation in the Rayleigh, Stefan and Prandtl numbers on melting inside a horizontal cylinder using a numerical model and obtained useful correlations for the melt time and Nusselt number.

Nicholas and Bayazitoglu [B12] studied numerically the melting of an unrestrained solid in a horizontal cylinder Moreover an extensive investigation concerning melting of an unfixed solid in a horizontal cylinder was performed by Bareiss and Beer [B13] . Sparrow and Geiger [B4] provided a definitive comparison between melting in a horizontal tube in which the solid is either constrained to be stationary or may freely fall to the bottom of the tube due to its higher density than the melt phase. They observed that the amount of mass melted in the unconstrained mode exceeds that melted in the constrained mode by 50 to 100% , depending on the operating conditions. Their numerical solutions also showed that about 90% of the melting in an unconstrained mode occurs at the lower portion of the solid, which is in quite close proximity to the lower portion of the tube wall. Recently Chen *et al.* [B16] obtained theoretical formulae of the melting rate, thickness of the liquid layer, elapsed time of solid PCM and Nusselt number during the close-contact melting of a PCM inside a horizontal cylinder.

2.1.3 Melting around a Horizontal Cylinder

Melting characteristics around (i.e. external to) a horizontal heated cylinder immersed in a PCM provide some of the most fundamental information concerning the latent heat-of-fusion thermal energy storage systems. This configuration was extensively studied both experimentally and theoretically; a comprehensive review is available in Yao and Prusa [A29].

It has been established both experimentally and theoretically that free convection during melting around a horizontal cylinder proceeds as follows. Conduction heat transfer predominates only during an initial brief period after which free convection becomes the dominant mode of heat transfer. Recirculation of the melt produces a "pear- shaped" solid-liquid surface. Moreover, melt volume against time can be well correlated as a function of Rayleigh and Stefan numbers both experimentally and theoretically.

Table 2.2 Summary of Literature for Melting around a Horizontal Cylinder

<table>
<tr><th>Author(s)</th><th colspan="2">Configuration</th></tr>
<tr><td>Goldstein, R. J. & Ramsey, J. W. (1978) [C3]
Sparrow, E. M. et al. (1978) [C1]
Bathelt, A. G. et al. (1979)[C2]
Abdel-Wahed, R. M. et al (1979) [C4]
Bathelt, A.G. & Viskanta, R. (1980) [C5]
White, D. A. et al. (1986) [C6]</td><td colspan="2">• Experimental investigation of natural convection in the melting of PCM around heated horizontal cylinder.</td></tr>
<tr><td>Sparrow, E. M. et al. (1978) [C1]
Rieger, H. et al. (1982) [C7]
Prusa, J. & Yao, L. S. (1984) Part I and II [C8, C9]
Ho, C. J. and Chen, S. (1986) [C10]</td><td colspan="2">• Theoretical / Numerical study of the melting around a heated horizontal cylinder embedded in a PCM.</td></tr>
<tr><td>Ramsey, J. W. et al. (1979) [C11]
Bathelt, A. G. et al. (1979)[C15]
Sasaguchi, K. & Viskanta, R. (1989) [C12]
Sasaguchi, K et al. (1994) [C13]</td><td>• Experimental Study</td><td rowspan="2">• Convection – dominated melting and freezing around multiple horizontal cylinders.</td></tr>
<tr><td>Lacroix, M (1993) [C16]
Sasaguchi, K & Kusano, K. (1995) [C14]</td><td>• Numerical Analysis</td></tr>
</table>

Sparrow *et al.* [C1] carried out experiments to investigate the role of natural convection in the melting of a PCM around a horizontal cylinder. Bathelt *et al.* [C2] visualized the solid-liquid interface photographically and measured the local heat transfer coefficients using a shadowgraph technique for the experimental investigation of melting around a heated horizontal cylinder. Their experimental results provided conclusive evidence of the important role played by natural convection in melting of a solid due to an embedded cylindrical heat source. Goldstein and Ramsey [C3] did a similar experiment to that of Bathelt *et al.* [C2] and found that the shape of the melt region could vary considerably, being symmetrical about the vertical plane, pear- shaped or even keyhole-shaped depending on the conditions as the plume begins to develop.

Melting around a heated horizontal horizontal cylinder embedded in a PCM was first modeled by Rieger *et al.* [C7] using a body-fitted co-ordinate transformation technique. Numerical solutions were obtained for Rayleigh number up to 1.5×10^5, Stefan number in the range $0.005 \leq St \leq 0.08$ and Prandtl number of 50. Prusa and Yao [C8, C9] developed a numerical model to investigate melting around a horizontal cylinder with constant heat flux and constant temperature boundary conditions using a co-ordinate transformation technique. Ho and Chen [C10] simulated the melting of ice around a horizontal isothermal cylinder and found that the melting process was strongly affected by altering the re-circulation flow developed in the molten area due to the density anomaly. It was also found that the melt shape and the predicted flow pattern were in good agreement with the experimental results of White *et al.* [C6].

Additional research results on convection–dominated melting around multiple horizontal cylinders can be found in [C11, C13-C16]. Most of this work deals with two dimensional configurations and restrained solid (unmelted) zones, as is the case in the present work.

2.1.4 Melting in a Horizontal Concentric Annulus

Melting of a PCM in a horizontal concentric annulus is not only a basic thermal engineering problem but also of potential interest to many practical applications. This configuration has been extensively adopted for heat exchanger in refrigeration systems and low-temperature storage systems utilizing PCM. No work has been reported for melting of PCMs in vertical or inclined annuli.

Betzel & Beer [D1-D3] studied experimentally and theoretically the melting process of an unconstrained PCM between two horizontal concentric cylinders. They reported an interesting process that owing to gravitational forces the solid moves downward to contact with the lower part of the outer tube as well as with the upper part of the inner tube, and pointed out that in this process thin liquid films form between the solid and the walls and conduction heat transfer is the dominating mechanism during melting.

Heat transfer characteristics during melting of a PCM in an concentric annulus with fins has been extensively determined by Sasaguchi *et al.*, (1986) [D4];Sasaguchi & Sakamoto, 1990 [D5]; Sasaguchi, (1990) [D6]; Sasaguchi *et al.*, (1990) [D7]; Sasaguchi, (1992) [D8]. Sasaguchi *et al.* (1986) [D4] observed the melting behavior from a heated inner tube in a concentric annulus and found that the heat flux for the finned tube is markedly greater than that for the bare tube, and that the melt fraction is a function of Biot number and Stefan number as well as the number of transfer units.

Ng, Devahastin and Mujumdar [D9] studied the free convective melting of a phase change material in a horizontal cylindrical annulus. They employed the same finite element method as employed in this work to simulate the free convection-dominated melting of a pure paraffin wax in a cylindrical annulus heated isothermally from the inside wall. A multiple cellular pattern was observed at high Rayleigh numbers ($>10^6$). Their results reveal that an increase in the Rayleigh number promotes the heat transfer rate. However no numerical simulation has been carried out for melting of a phase change material in horizontal annuli of arbitrary cross-section.

2.2 NUMERICAL METHODS FOR PHASE CHANGE PROBLEMS

A simulation of the phase change phenomenon requires the solution of the conservation equations accounting for the convection and conduction in the fluid zone and the conduction in the solid zone. In addition an interface equation to couple both phases is needed. The analytical approach is only possible for very limited cases when several restrictive assumptions can be assumed. On the other hand, parametric studies of experimental designs covering real situations are usually prohibitively expensive. Therefore, the numerical techniques are recognized as a convenient way of obtaining accurate solutions and identifying configurations of practical interest

Two classes of solution methods have been developed to handle phase change problems numerically: front-tracking and fixed grid methods to allow for the moving interface.

In the front tracking methods, the discrete phase change front is tracked continuously and the latent heat release is treated as a moving boundary condition. This requires either deforming meshes [E1-E5], or transformation of variables or coordinate [E6-E10], or using changing time step (for one-dimensional problem) so that the interface coincides with the grid nodes. The front-tracking methods are not suitable for problems in which phase change takes place over a temperature interval although they are accurate for isothermal phase change problems. Also, for problems involving complex geometry and/or large geometry change in the molten zone, the implementation of these methods is extremely difficult, sometimes is impossible, e.g. for multi-dimensional problems with multi-interface in the phase change processes.

Fixed grid methods removes the need to explicitly satisfy interface boundary conditions at the phase front and therefore are able to utilize standard solution procedures for the fluid flow and energy equations, without resorting to mathematical manipulations and transformations. They are amenable to physical interpretation and easy to implement, especially for multi-dimensional problems and for multi-interface problems.

Three methods have been developed for fixed grid methods. They are the effective heat capacity method, the enthalpy method, and the source-based method. The enthalpy method and the source-based method are outlined briefly in the following section.

2.2.1 Enthalpy Method

Shamsundar and Sparrow [E11] in 1975 first proposed the enthalpy method which includes both enthalpy and temperature as the dependant variables in the field equation.

Therefore, the final discrete algebraic equation system requires non-simultaneous iterative solvers. The enthalpy model has been widely used in the finite difference techniques since finite difference is always associated with non-simultaneous iterative solvers. On the other hand the enthalpy method has seldom been implemented in the finite element technique. This is because of the feature of the enthalpy model which requires non-simultaneous iterative solver makes the solution procedure of the finite element method both inefficient and difficult to implement due to the fact that the existing finite element programs are always equipped with direct solvers. Recently Gong and Mujumdar [E12] developed a simultaneous iterative procedure for the finite element analysis of the enthalpy model. Gong and Mujumdar [E13] also developed a non-iterative procedure in the context of the finite element method for conduction phase change problems. This makes the implementation of the enthalpy method very easy and straightforward in the finite element method.

2.2.2 Source-Based Method

A source based method was proposed by Rolphe and Bathe [E14] which is completely conservative. However, it appears to be inefficient computationally. To improve the computational efficiency, new schemes were developed by Voller [E15] and Swaminathan and Voller [E16]. The improved versions are effective in solving a wide range of phase change problems including conduction-convection controlled phase change problems.

2.2.3 Fixed Grid Methods for Convection-Controlled Melting

The examples of fixed grid solutions of convection-diffusion phase change can be found in Morgan[E18], Gartling[E17] and Voller *et al.*[E19].

A major problem with fixed grids is in accounting for the zero velocity condition as the liquid region turns to solid. Two methods were developed for modeling the development of free convection during the melting and freezing processes. One is the viscosity approach proposed by Gartling [E17] and Morgan [E18] and the other is the enthalpy-porosity approach proposed by Voller and Prakash [E19] and Brent *et al.* [E20]. Morgan [E18] employed a simple approach of fixing the velocities to zero n a computational cell whenever the mean latent heat content reaches some predetermined value between 0 and λ, where λ is the latent heat of phase change. Gartling [E17] employed a more subtle approach in making the viscosity a function of ΔH such that as ΔH decreases from λ to 0 the value of the viscosity increases to a large value thus simulating the liquid-solid phase change.

Voller and Prakash [E19] investigated various ways of dealing with the zero solid velocities in fixed grid enthalpy solutions of freezing in a thermal cavity. They proposed a pseudo porous medium model with the porosity decreasing from 1 to 0 as ΔH decreases from λ to 0. In this way, on prescribing a "Darcy" source term, velocities arising from the solution of the momentum equations are inhibited, reaching values close to zero on complete solid formation.

REFERENCES

A. Melting along a Horizontal and Vertical Wall.

1. Hale, N. W. and Viskanta, R., 1978, "Photographic Observation of the Solid-Liquid Interface Motion during Melting of a Solid Heated from an Isothermal Vertical Wall," *Lett. Heat Mass Transfer*, Vol. 5, pp. 329-337.
2. Bareiss, M. and Beer, H., 1984, "Experimental Investigation of Melting Heat transfer with Regard to Different Geometry Arrangements," *Int. Commun. Heat Mass Transfer*, Vol. 106, pp. 12-19.
3. Benard, C., Gobin, D. and Martinez, F., 1985, "Melting in Rectangular Enclosures: Experiments and Numerical Simulations," *J. Heat Transfer*. Vol. 107, pp. 794-803
4. Ho, C. J. and Viskanta, R., 1984, "Heat Transfer during Melting from an isothermal Vertical Wall," *J. Heat Transfer*, Vol. 106, pp. 12-19.
5. Gau, C. and Viskanta, R., 1986, "Melting and Solidification of a Pure Metal on a Vertical Wall," *J. Heat Transfer*, Vol. 108, pp. 174-181.

6. Wolf, F. and Viskanta, R., 1987, "Melting of a Pure Metal from a Vertical Wall," *Exper. Heat Transfer*, Vol. 1, pp. 17-30.

7. Gadgil, A. and Gobin, D., (1985), " Analysis of Two-Dimensional Melting in Rectangular Enclosures in Presence of Convection," *J. Heat Transfer*, Vol. 106, pp. 20-26.

8. Webb, B. W. and Viskanta, R., 1986, "Analysis of Heat transfer during Melting of a Pure Metal from an Isothermal Vertical Wall," *Numerical Heat Transfer*, Vol. 9, pp. 539-558.

9. Lacroix, M. 1992, "Predictions of Natural-Convection-Dominated Phase-Change Problems by the Vorticity-velocity Formulation of the Navier-Stokes Equations," *Numerical Heat Transfer*, Part B, Vol. 22, pp. 79-93.

10. Costa, M., Oliva, A., Perez Segarra, C.D. and Alba, R., 1991, " Numerical Simulation of Solid-Liquid Phase Change Phenomena," *Comput. Meth. Appl. Mech. Eng.*, Vol. 91, pp. 1123-1134.

11. Usmani, A.S., Lewis, R.W. and Seetharamu, K.N., 1992, "Finite Element Modeling of Natural-Convection-Controlled Change of Phase" *Int. J. Num. Meth. Eng.*, Vol. 14, pp. 1019-1036

12. Rady, M.A. and Mohanty, A.K., 1996, " Natural Convection during Melting and Solidification of Pure Metals in a Cavity," *Num. Heat. Transfer*, Part A, Vol. 29, pp. 49-63.

13. Keller, J.R. and Bergman, T.L., 1989, "Prediction of Conjugated Heat Transfer in Solid-Liquid System: Inclusion of Buoyancy and Surface Tension Forces in the Liquid Phase," *J. Heat. Transfer*, Vol.111, pp. 690-698.

14. Liu, A., Voth, T.E. and Bergman, T.L., 1993, "Pure Metal Melting and Solidification with Liquid Phase Buoyancy and Surface tension Forces," *Int. J. Heat Mass Transfer*, Vol. 36, pp. 411-422.

15. Ho, C.J. and Chu, C.H., 1993, "Periodic Melting within a Square Enclosure with an Oscillatory Temperature, ," *Int. J. Heat Mass Transfer*, Vol. 36, pp. 725-733

16. Ho, C.J. and Chu, C.H., 1993, " The Melting Process of Ice from a Vertical Wall with Time-Periodic Temperature Perturbation inside a Rectangular Enclosure," *Int. J. Heat Mass Transfer*, Vol. 36, pp. 3171-3186.

17. Ho, C.J. and Chu, C.H., 1996, "Numerical Simulation of Heat penetration through a Vertical Rectangular Phase Change Material/Air Composite cell," *Int. J. Heat Mass Transfer,* Vol. 39, pp. 1785-1795.

18. Sasaguchi, K., Ishihara, A. and Zhang, H., 1996, "Numerical Study on Utilization of Melting of a Phase Change Material for Cooling of a Heated Surface at a Constant Rate," *Numerical Heat Transfer,* Part A, Vol. 29, pp. 19-31.

19. Benard, H., 1900, "Tourbillions Cellulaires dan une Nappe Liquid," *Revue Generale des Sciences Pures et Appliqees,* Vol. 11, pp. 1309-1328.

20. Yen, Y.C. and Galea, F., 1968, "Onset of Convection in a Layer of Water Formed by Melting of Ice from Below," *Phys. Fluids,* Vol. 11, pp. 1263-1269.

21. Yen, Y.C., 1980, "Free Convection Heat Transfer Characteristics in a Melt Water Layer," *Journal of Heat Transfer,* Vol. 103, pp. 550-556.

22. Seki, N., Fukosako, S. and Sugawara, M., 1977, "A Criteria on Onset of Free Convection in a Horizontal Melted Water Layer with Free surface," *Trans. ASME Ser.C, J. Heat Transfer,* Vol. 99, 92-98.

23. Hale, N.W. and Viskanta, R., 1980, "Solid-Liquid Phase Change Heat Transfer and Interface Motion in Materials Cooled or Heated from Above or Below," *Int. J. Heat Mass Transfer,* Vol. 23, pp. 283-292.

24. Gau, C., Viskanta, R. and Ho, C.J., 1983, "Flow Visualization during Solid-Liquid Phase Change Heat Transfer II. Melting in a Rectangular Cavity," *Int. Comm. Heat Mass Transfer,* Vol 10, pp. 183-190.

25. Diaz, L.A. and Viskanta, R., 1984, "Visualization of the Solid-Liquid Interface Morphology Formed by Natural Convection during melting of a Solid from Below," *Int. Comm. Heat Mass transfer,* Vol. 11, pp. 35-43.

26. Lacroix, M. and Benmadda, M., 1998, "Analysis of natural Convection Melting from a Heated Wall with Vertically Oriented Fins," *Int. J. Num. Meth. For Heat and Fluid Flow,* Vol. 8, pp 465

27. Lacroix, M. and Binet, B., 1998, "Numerical Study of Natural Convection-Dominated Melting inside Uniformly and Discretely heated Rectangular Cavities," *Numerical Heat Transfer, Part A- Applications,* Vol. 33, pp 207-224.

28. Gong, Z.X. and Mujumdar, A.S., 1998, "Flow and Heat Transfer in Convection-Dominated Melting in a Rectangular Cavity Heated from below," *Int. J. Heat Mass Transfer*, Vol. 14, No. 17, pp. 2573-2580

29. Yao, L.S. and Prusa, J., 1989, "Melting and Freezing," *Advances in Heat Transfer*, Vol. 19, pp. 1-95.

30. Viskanta, R., 1983, "Phase Change Heat transfer," in *Solar Heat Storage: Latent Heat Material*, G.A. Lane, ed., CRC Press, Boca Raton, Chapter 5.

31. Viskanta, R., 1985, "Natural Convection in Melting and Solidification," *Natural Convection Fundamentals and Applications*, eds., S. Kakac, W. Aung and R. Viskanta, Hemisphere Publishing Corp., Washington, D.C., pp. 845-877.

32. Viskanta, R., 1988, "Heat Transfer during melting and Solidification of Metal," *J. Heat Transfer*, Vol. 110, pp. 1205-1219.

33. Samarskii, A.A., Vabishchevich, P.N., Iliev, O.P. and Churbanov, A.G., 1993, "Numerical Simulation of Convection/Diffusion Phase Change Problems-a Review," *Int. J. Heat Mass Transfer*, Vol. 36, pp. 4095-4106.

34. Fukusako, S. and Yamada, M., 1994, "Recent Advances in Research on Melting Heat Transfer Problems." *Proceedings of the 10th Int. Heat Transfer Conference*, Vol. 1, pp. 313-331.

B. Melting Inside a Horizontal Cylinder

1. Rieger, H., Projahn, U., Bareiss, M. and Beer, H., 1983, "Heat Transfer during Melting inside a Horizontal Tube," *J. Heat Transfer*, Vol. 105, pp.226-234.

2. Bareiss, M. and Beer, H. 1984, "Experimental Investigation of Melting Heat Transfer with regard to Different Geometric arrangements." *Int. Commun. Heat Mass Transfer*, Vol. 11, pp 323-333

3. Ho, C.J. and Viskanta, R, 1984, " Heat Transfer during inward Melting in a Horizontal tube," *Int. J. Heat Mass Transfer*, Vol. 27, pp. 705-716.

4. Sparrow, E.M. and Geiger, G.T., 1986, "Melting in a Horizontal Tube with the Solid either Constrained or Free to Fall under Gravity," *Int. J. Heat Mass Transfer*, Vol. 29, pp. 1007-1019.

5. Hirata, T. and Nishida, K., 1989, "An Analysis of Heat Transfer Using Equivalent Thermal Conductivity of Liquid Phase during melting inside an isothermally Heated Horizontal Cylinder," *Int. J. Heat Mass Transfer*, Vol. 33, pp. 1663-1670.

6. Pannu, J., Joglekar, G. and Rice, P., 1980, " Natural Convection Heat transfer to Cylinders of Phase Change Material Used for Thermal Storage," *AICHE Symposium Series*, No. 198. Vol. 76. pp. 47-55.

7. Saitoh, T. and Hirose, K., 1982, "High Rayleigh Number solution to Problems of Latent Heat Thermal Heat storage in a Horizontal Cylinder Capsule," *J. Heat Transfer*, Vol. 104, pp. 545-553.

8. Prasad, A. and Sengupta, S., 1987, "Numerical Investigation of Melting inside a Horizontal Cylinder including the Effects of Natural Convection" *J. Heat Transfer*, Vol. 109, pp. 803-806.

9. Prasad, A. and Sengupta, S., 1988, "Nusselt Number and Melt time Correlations for Melting inside a Horizontal Cylinder subjected to an Isothermal Wall Temperature Condition" *Transactions of the ASME*, Vol. 110, pp. 340-345.

10. Park, C.E. and Chang, K.-S., 1992, "Bifurcating Solution of Inward Melting in a Horizontal Tube," in *Transport Phenomena in Heat and mass Transfer*, J.A. Reizes, ed., pp. 704-714.

11. Ro, S.T. and Kim, C.-J., 1994, "Bifurcation Phenomenon during the fixed-solid-mode Melting inside a Horizontal Cylinder," *Int. J. Heat Mass Transfer*, Vol. 37, pp. 1101-1109.

12. Nicholas, D. and Bayazitoglu, Y., 1980, "Heat Transfer and Melting Front within a Horizontal Cylinder," *J. Heat Transfer*, Vol. 102, pp. 229-232.

13. Bareiss, M. and Beer, H. 1984, "An Analytical Solution of the Heat Transfer During Melting of an Unfixed solid Phase Change Material inside a Horizontal Tube," *Int. J. Heat Mass Transfer*, Vol. 27, pp 739-746.

14. Saitoh, T. and Kato, K., 1993 "Experiment on Melting in Heat Storage Capsule with Close Contact and Natural convection," *Exper. Therm. Fluid Sci.*, Vol. 6, pp. 273-281.

15. Saitoh, T., Kato,H. and Maruhara, K., 1992, " Numerical Computation on Combined Natural Convection and Close-Contact Melting in a Cylindrical Energy Storage Capsule," *Proc. Int. Conf. Comput. Sci.*, pp. 1-5.

16. Chen, W.Z., Yang, Q.S., Dai, M.Q. and Cheng, S.M., 1998, " An Analytical Solution of the Heat Transfer Process during Contact Melting of a Phase Change Material inside a Horizontal Elliptical Tube," *Int. J. Energy Research*, Vol. 22, pp. 131-140.

C. Melting around a Horizontal Cylinder.

1. Sparrow, E.M., Schmidt, R.R. and Ramsey, J.W., 1978, "Experiments on the Role of Natural Convection in the Melting of Solids," *J. Heat. Transfer*, Vol. 100, pp.11-16.

2. Bathelt, A.G., Viskanta, R. and Leidenfrost, W., 1979, "An Experimental Investigation of the Natural Convection in the Melt Region around a Heated Horizontal Cylinder," *J. Fluid Mechanics*, Vol. 90, pp. 227-239.

3. Goldstein, R.J. and Ramsey, J.W., 1979, "Heat Transfer to a Melting Solid with Application to Thermal Storage Systems," *Heat Transfer Studies*: Festchrift for E.R.G. Echert," Hemisphere, New York.

4. Abdel-Wahed, R.M., Ramsey, J.W. and Sparrow, E.M., 1979, "Photographic Study of melting about an Embedded Horizontal Heating Cylinder," *Int. J. Heat Mass Transfer*, Vol. 22, pp 171-173.

5. Bathelt, A.G. and Viskanta, R., 1980, "Heat Transfer at the Solid-Liquid Interface during Melting from a Horizontal Cylinder," *Int. J. Heat Mass Transfer*, Vol. 23, pp. 1493-1503.

6. White, D.A., Viskanta,R. and Leidenfrost, W., 1986, "Heat Transfer during Melting of Ice around a Horizontal Isothermal Cylinder," *Exp. Fluids*, Vol. 4, pp. 171.

7. Rieger, H., Projahn, U. and Beer, H., 1982, "Analysis of the Heat Transport Mechanisms during Melting around a Horizontal Circular Cylinder," *Int. J. Heat Mass Transfer*, Vol 25, pp. 137-147.

8. Prusa, J. and Yao, L.S., 1984, "Melting around a Horizontal Heated Cylinder: Part I-Perturbation and Numerical Solution for Constant Heat Flux Boundary condition, " *J. Heat. Transfer*, Vol. 106, pp. 376-384.

9. Prusa, J. and Yao, L.S., 1984, "Melting around a Horizontal Heated Cylinder: Part II-Numerical Solution for Isothermal Boundary condition," *J. Heat. Transfer*, Vol. 106, pp. 469-472.

10. Ho, C.J. and Chen, S., 1986, "Numerical solution of melting of Ice around a Horizontal Cylinder," *Int. J. Heat Mass Transfer*, Vol.29, pp. 1359-1369.

11. Ramsey, J.W., Sparrow, E.M. and Varejao, M.C., 1979, "Melting about Horizontal Row of Heating Cylinders," *J. Heat. Transfer*, Vol. 101, pp. 732-733.

12. Sasaguchi, K. and Viskanta, R., 1989, "Phase Change Heat Transfer during Melting and Resolidification of Melt around Cylindrical Heat Source(s)/Sink(s)," *J. Energy. Re. Tech.*, Vol. 111, pp.43-49.

13. Sasaguchi, K., Kusano, K. and Kitagawa, H., 1994, "Solid/Liquid Phase-Change Heat Transfer around two Horizontal, Vertically Spaced Cylinders-An Experimental Study on the Effect of Density Inversion of water," *Heat Transfer-Japanese Research*, Vol. 23, pp. 645-657.

14. Sasaguchi, K. and Kusano, K., 1995, "A Numerical Analysis of Solid/liquid Phase Change Heat Transfer around two Horizontal, Vertical Spaced Cylinders in Rectangular Cavity," *ASME JSME Thermal Engineering conference*, Vol. 4., pp. 471-476.

15. Bathelt, A.G., Viskanta, R. and Leidenfrost, W., 1979, "Latent Heat-of-Fusion Energy Storage: Experiments on Heat Transfer from Cylinders during Melting," *J. Heat Transfer*, Vol 101, pp 453-458.

16. Lacroix, M., 1993, "Numerical Simulation of Melting and Resolidification of a Phase Change Material around two Cylindrical Heat Exchangers," *Numerical Heat Transfer*, Part A, Vol. 24, pp 143-160.

D. Melting in Horizontal Concentric Annulus.

1. Betzel, T. and Beer, H., 1986, "Experimental Investigation of Heat Transfer during Melting around a Horizontal Tube with and without Axial Fins," *Int. Comm. Heat Mass transfer*, Vol 13, pp. 639-649.

2. Betzel, T. and Beer, H., 1986, "Prediction and Measurement of melting Heat Transfer to an Unfixed Phase Change Material Heated in a Horizontal Concentric Annulus," *Proc. 8th Int. Heat Transf. Conf.*, Vol. 4, pp. 1793-1798.

3. Betzel, T. and Beer, H., 1988, "Solidification and Melting Heat transfer to an Unfixed Phase Change Material (PCM) Encapsulated in a Horizontal Concentric Annulus," *Warme- und Stoffubertrang*, Vol. 22, pp. 335-344.

4. Sasaguchi, K., Imura, H. and Furusho, H., 1986, "Heat Transfer Characteristics of a Latent Heat Storage Unit with a Finned Tube (1st Report: Experimental Studies on Solidification and Melting Process)," *Bull. JSME*, Vol. 29, pp. 2978-2985.

5. Sasaguchi, K. and Sakamoto, Y., 1990, "Effect of Natural Convection on Melting of Phase-Change Material around a Finned Tube," *Heat Transf. Japanese Res.*, Vol. 19, pp. 474-491.

6. Sasaguchi, K., 1990, "An Experimental Study on Melting of Phase-Change Material around Finned Tubes," *Trans. JSME* Vol. 56B, pp.2785-2792.

7. Sasaguchi, K., Yoshida, M. and Nakashima, S., 1990, "Heat Transfer Characteristics of a Latent Heat Thermal Energy Storage Unit with a Finned Tube (Effects of Fin Configuration), " *Heat Transf. Japanese Res.*, Vol. 19, pp. 11-27.

8. Sasaguchi, K., 1992, "Heat transfer Enhancement in Latent heat Thermal Energy Storage Unit Using Finned Tubes," *ASME Paper Solar Engng.*, Vol. 1, pp. 83-87.

9. Ng, K.W., Devahastin, S. and Mujumdar, A.S., 1998, "Free Convective Melting of a Phase Change Material in a Horizontal Cylindrical Annulus," *Transactions TSTU,* Tom 4., No. 1., pp 40-52.

E. Numerical Methods For Phase Change Problems

1. Lynch, D R. and O'Neill, K., 1981, "Continuously Deforming Finite Elements for the Solution of Parabolic Problems, with and without Phase Change," *Int. Numer. Meths. Engrg.*, Vol. 17, pp 81-96.

2. Lynch, D.R., 1982, "Unified approach to Simulation on Deforming Elements with Application to Phase Change Problems," *J. Computational Physics*, Vol. 47, pp. 303-317.

3. Lynch, D.R. and Sullivan, J.M., 1985, "Heat Conservation in Deforming Element Phase Change Simulation," *J. Computational Physics*, Vol. 57, pp. 387-411

4. Albert, M.R. and O'Neill, K., 1986, "Moving Boundary-Moving Mesh Analysis of Phase Change Using Finite elements with Transfinite Mappings," *Int. Numer. Meths. Engrg.*, Vol. 23, pp. 591-607

5. Zabaras, N. and Ruan, Y., 1990, "Moving and Deforming Finite-Element Simulation of Two-dimensional Stefan Problems," *Communication in Appl. Num. Meth.*, Vol. 6, pp. 495-506.

6. Kim, C.J. and Kaviany, M., 1990, "A Numerical Method for Phase Change Problems," *Int. J. Heat Mass Transfer,* Vol. 33, pp. 2721-2734.

7. Kim, C.J. and Kaviany, M., 1992, "A Numerical Method for Phase Change Problems with Convection and Diffusion," *Int. J. Heat Mass Transfer,* Vol. 35, pp. 457-467.

8. Kim, C.J., Ro, S.T. and Lee, J.S., 1993, "An Efficient Computational Technique to Solve the Moving Boundary Problems in the Axisymmetric," *Int. J. Heat Mass Transfer,* Vol. 36, pp. 3759-3764.

9. Shyy, W., Udaykumar, H.S. and Liang, S.J., 1993, "An Interface Tracking Method Applied to Morphological Evolution during Phase Change, *Int. J. Heat Mass Transfer,* Vol. 36, pp. 1833-1844.

10. Saitoh, T.S. and Nakamura, M., 1994, "Time-Space Method for Multidimensional melting and Freezing Problems," *Int. J. Num. Meth. Eng.*, Vol. 37, pp. 1793-1805.

11. Shamsundar, N and Sparrow, E.M., 1975, "Analysis of Multidimensional Conduction Phase Change via Enthalpy Model, " *J. Heat Transfer*, Vol. 97, pp. 333-340.

12. Gong, Z.X. and Mujumdar, A.S., 1995, "A Simultaneous Iteration procedure for the Finite Element Solution of the Enthalpy Model for Phase Change Heat Conduction Problems," *Int. J. Num. Meth. Heat Fluid Flow*, Vol. 5, pp. 580-600.

13. Gong, Z.X. and Mujumdar, A.S., 1995, "Noniterative Procedure for the Finite-Element solution of the Enthalpy Model for the Phase-Change Heat Conduction Problems," *Num. Heat transfer*, Part B, Vol. 27, pp. 437-446.

14. Rolph, W.D. and Bathe, K.J., 1982, "An Efficient Algorithm for Analysis of Nonlinear Heat Transfer with Phase Change," *Int. J. Num. Meth. Eng.*, Vol. 18, pp. 119-134.

15 Voller, V.R., 1990, "Fast Implicit Finite-Difference Method for the Analysis of Phase Change Problems," *Num. Heat Transfer*, Vol. 17, pp. 155-169.

16 Swaminathan, C.R. and Voller, V,R., 1993, "On the Enthalpy Method," *Int. Num. Meth. Heat Fluid Flow*, Vol. 3, 233-244.

17 Gartling, D.K. 1980, "Finite Element Analysis of Convective Heat Transfer Problems with Change of Phase," in *Computer Methods in Fluids*, K. Morgan, C. Taylor and C.A. Brebbia (eds.), Pentech, London, pp. 257-284.

18 Morgan, K, 1981, "Numerical Analysis of Freezing and Melting with Convection," *Comp. Meth. Appl. Mech. Eng.*, Vol. 28, pp. 275-284.

19 Voller, V.R., Prakash, C., 1987, "A Fixed Grid Numerical Modelling Methodology for Convection-Diffusion Mushy Region Phase-Change Problems," *Int. J. Heat Mass Transfer*, Vol. 30, pp. 1709-1719.

20 Brent, A.D., Voller, V.R. and Reid, K.J., 1988, "Enthalpy-Porosity Technique for Modelling Convection-Diffusion Phase Change: Application to the Melting of a Pure Metal," *Numerical Heat Transfer*, Vol. 13, pp. 297-318.

21 Gong, Z. X., 1997, "Time-dependant Melting and Freezing Heat Transfer in Multiple Phase Change Materials," Ph.D Thesis, Department of Chemical Eng., McGill University, Canada

Chapter 3

Numerical Model

3.1 INTRODUCTION

While a major effort has been devoted to the numerical solution of conduction-controlled phase change problems over the last three decades focus has now shifted to convection-dominated problems involving melting of PCMs in containers. The finite element method has been widely applied to solve conduction-controlled phase change problems, and it is now making inroads in problems involving convection-dominated melting and solidification of PCMs, especially in view of the complex flow geometries encountered in such problems.

Gartling [1] was apparently the first to model convection-dominated melting and solidification problems with the standard Galerkin finite element technique. He employed the Boussinesq assumption and effective heat capacity method to solve the Navier-Stokes and energy equations. To account for the zero velocity condition as the liquid turns to solid or the solid becomes liquid he developed an approach which makes the viscosity a function of ΔH where ΔH is the cumulative energy of latent heat of a computational cell. When ΔH decreases from λ (where λ is the latent heat of the phase change) to 0 the value of viscosity increases to a large value thus simulating the liquid-solid phase change. Morgan [2] presented an explicit finite element algorithm for the solution of convection-dominated melting and solidification problems In his model he employed an enhanced heat capacity to treat the latent heat effect. To account for the velocity evolution at the phase change interface he used a simple approach which fixes the velocities to zero in a computational cell whenever the cumulative energy of latent heat of a cell reaches some predetermined value between 0 and λ. Usmani et al. [3] reported an implicit finite element model based on effective heat capacity approach in combination with the standard Galerkin finite element method with a primitive variable formulation. They also employed the varying viscosity approach to model the velocity evolution at the phase change interface.

In the context of the finite volume method Voller and Prakash [4] and Brent *et al.* [5] investigated various ways of dealing with zero solid velocities in fixed grid enthalpy solutions of freezing in a thermal cavity. They assumed the mushy region to be a pseudo porous medium with the porosity decreasing from 1 to 0 as ΔH decreases from λ to 0. In this way, on prescribing a "Darcy" source term the velocity value arising from the solution of the momentum equations are inhibited, reaching values close to zero on complete solid formation. The enthalpy-porosity model has proved to be effective in solving both isothermal and non-isothermal phase change problems.

In this thesis a Streamline Upwind/Petrov Galerkin finite element model in combination with primitive variables is employed for solving convection dominated melting and solidification problems. The computational code used is that based on Gong's [18] early work. The Boussinesq assumption is invoked and two-dimensionality is assumed. The enthalpy-porosity approach is utilized to model the velocity evolution at the phase change interface. A Penalty formulation is employed to treat the incompressibility constraint in the momentum equations. Simulations are carried out for the melting of a phase change material (n-octadecane) in a horizontal annulus of arbitrary cross-section. Gong [18] has verified the validity of the computational model used in this study by extensive numerical experiments including comparison with analytical solutions, comparison with numerical and experimental results of others etc.

3.2 MATHEMATICAL FORMULATION

3.2.1 Governing Equations

For the mathematical description of the melting process the following assumptions are made: (1) heat transfer in the PCM is conduction/convection controlled, and the melt is Newtonian and incompressible; (2) the flow in the melt is laminar and viscous dissipation is negligible; (3) the densities of the solid and liquid are equal; (4) the Boussinesq assumption is valid for free convection, i.e. density variations are considered only insofar as they contribute to buoyancy, but are otherwise neglected; (5) the solid PCM is fixed to the container wall during the melting process. The following follows closely the discussion given by Gong [18].

Based on the above assumptions, the governing equations in tensor form are

Solid region:

$$\rho\frac{\partial h}{\partial t} = (k_s T_{,j})_{,j} + q_s \tag{1}$$

Liquid Melt Region:

Continuity equation

$$u_{i,i} = 0 \tag{2}$$

Momentum equation

$$\rho(\frac{\partial u_i}{\partial t} + u_j u_{i,j}) = -p_{,i} + [\mu(u_{i,j} + u_{j,i})]_{,j} - \rho g_i \beta(T - T_0) \tag{3}$$

Energy equation

$$\rho(\frac{\partial h}{\partial t} + u_j T_{,j}) = (k_l T_{,j})_{,j} + q_s \tag{4}$$

The initial and boundary conditions are

initial conditions

$$\begin{aligned} T(x,0) &= T^0(x) \\ u_i(x,0) &= u_i^0(x) \end{aligned} \tag{5}$$

boundary conditions

$$
\begin{aligned}
&u_i = \bar{u}_i(s,t) && \text{on } \Gamma_u \\
&t_i = \sigma_{ij} n_j(s) = \bar{t}_i(s,t) && \text{on } \Gamma_t \\
&T = \bar{T}(s,t) && \text{on } \Gamma_T \\
&q = -(kT_{,j}) n_j(s) = q_a(s,t) + q_c(s) + q_r(s) && \text{on } \Gamma_q
\end{aligned}
\tag{6}
$$

3.2.2 Enthalpy-Porosity Model

Two methods are available to account for the physics of the evolution of the flow at the solid/liquid phase change interface in fixed-grid methods namely the enthalpy-porosity model [4, 5] and the viscosity model [1, 3]. The enthalpy-porosity is employed in this study.

The enthalpy-porosity model treats the mushy region as a porous medium. The flow in the mush is governed by Darcy's law. According to the enthalpy-porosity model [4, 5] Eqs. (1) through (4) can be rewritten as follows:

$$u_{i,i} = 0 \tag{7}$$

$$\rho(\frac{\partial u_i}{\partial t} + u_j u_{i,j}) = -p_{,i} + [\mu(u_{i,j} + u_{j,i})]_{,j} - \rho g_i \beta (T - T_0) + A u_i \tag{8}$$

$$\rho(\frac{\partial h}{\partial t} + u_j T_{,j}) = (kT_{,j})_{,j} + q_s \tag{9}$$

In Eq. (8)

$$A = -C(1-\lambda)^2 / (\lambda^3 + b) \tag{10}$$

in which b is a small constant introduced to avoid division by zero and C is a constant accounting for the morphology of the mushy region. In general b is assigned a value of 0.001. For isothermal phase change C is assigned a value of 1.6×10^6.

3.2.3 The Penalty Formulation

To treat the incompressibility constraint in the momentum equation two models can be used, one is the penalty formulation [6, 7] and the other is the so-called slightly compressible formulation [7, 8]. In this study the penalty formulation is employed to treat the incompressibility constraint.

In the penalty formulation, the continuity equation is replaced by

$$u_{i,i} = -\frac{1}{\gamma} p \tag{11}$$

where γ is the penalty parameter which is generally assigned a value of 1.0×10^9.

As a result of the utilization of the penalty approximation, the pressure term and the mass conservation equation are eliminated from the system of equations (Eqs. (7) through (9)). The governing equations (Eqs. (7)-(9)) then become

$$\rho(\frac{\partial u_i}{\partial t} + u_j u_{i,j}) = \frac{1}{\gamma}(u_{i,i})_{,i} + [\mu(u_{i,j} + u_{j,i})]_{,j} - \rho g_i \beta(T - T_0) + Au_i \tag{12}$$

$$\rho(\frac{\partial h}{\partial t} + u_j T_{,j}) = (kT_{,j})_{,j} + q_s \tag{13}$$

Once the velocity and temperature fields are known, the pressure variable is calculated a posteriori if desired at any step by solving the Poisson equation [9]

$$-(p_{,j})_{,j} = \rho(u_j u_{i,j})_{,i} + \rho\beta(g_j T_{,j}) \tag{14}$$

subject to homogeneous Neumann conditions along the boundary Γ; i.e.

$$n_j p_{,j} = 0 \tag{15}$$

In order to obtain a unique pressure field it is necessary to set the pressure at one point in the domain equal to a reference pressure.

3.2.4 Finite Element Model

Following the work of Brooks and Hughes [7] and Argyris [10] the streamline upwind/Petrov-Galerkin method was selected by Gong[19] for the convection and source terms of the momentum and energy equations. After spacewise discretization of Eqs. (12) and (13) in two dimensions subject to above mentioned boundary conditions we obtain the following semi-discrete equation as described by Gong *et al.* [19].

$$\begin{bmatrix} M & 0 & 0 \\ 0 & M & 0 \\ 0 & 0 & N \end{bmatrix} \begin{Bmatrix} \dot{u}_x \\ \dot{u}_y \\ \dot{T} \end{Bmatrix} + \begin{bmatrix} K_{11}+K_{22} & K_{12} & B_1 \\ K_{21} & K_{11}+K_{22} & B_2 \\ 0 & 0 & L_{11}+L_{22} \end{bmatrix} \begin{Bmatrix} u_x \\ u_y \\ T \end{Bmatrix} +$$
$$\begin{bmatrix} A_1(u)+A_2(v) & 0 & 0 \\ 0 & A_1(u)+A_2(v) & 0 \\ 0 & 0 & D_1(u)+D_2(v) \end{bmatrix} \begin{Bmatrix} u_x \\ u_y \\ T \end{Bmatrix} + \begin{bmatrix} P_{11} & P_{12} & 0 \\ P_{21} & P_{22} & 0 \\ 0 & 0 & 0 \end{bmatrix} \begin{Bmatrix} u_x \\ u_y \\ T \end{Bmatrix} + \tag{16}$$
$$\begin{bmatrix} A & 0 & 0 \\ 0 & A & 0 \\ 0 & 0 & 0 \end{bmatrix} \begin{Bmatrix} u_x \\ u_y \\ T \end{Bmatrix} = \begin{Bmatrix} F_1 \\ F_2 \\ G \end{Bmatrix}$$

Typical elements in these matrices are

$$M = \int_\Omega \rho\varphi\varphi^T \, d\Omega \tag{17}$$

$$N = \int_\Omega \rho c_t \, \vartheta\vartheta^T d\Omega \tag{18}$$

$$K_{ij} = \int_\Omega \mu \frac{\partial\varphi}{\partial x_i}\frac{\partial\varphi}{\partial x_j} d\Omega \tag{19}$$

$$L_{ij} = \int_\Omega k \frac{\partial\vartheta}{\partial x_i}\frac{\partial\vartheta}{\partial x_j} d\Omega \tag{20}$$

$$A_i(U_j) = \int_\Omega \rho\tilde{\varphi} u_j \frac{\partial\varphi}{\partial x_i} d\Omega \tag{21}$$

$$D_i(U_j) = \int_\Omega \rho c_t \tilde{\vartheta} u_j \frac{\partial\vartheta}{\partial x_i} d\Omega \tag{22}$$

$$P_{ij} = \int_\Omega \frac{1}{\gamma}\frac{\partial\varphi}{\partial x_i}\frac{\partial\varphi}{\partial x_j} d\Omega \tag{23}$$

$$B_i = \int_\Omega \rho g_i \beta \varphi \vartheta^T d\Omega \tag{24}$$

$$F_i = \int_\Gamma \bar{t}\, \varphi\, d\Gamma + \int_\Omega \rho g_i \beta T_0 \varphi\, d\Omega \tag{25}$$

$$G = \int_\Gamma (q_a + q_c + q_r)\vartheta\, d\Gamma + \int_\Omega q_s \vartheta\, d\Omega \tag{26}$$

in which

$$\bar{\varphi} = \varphi + \bar{k}_1 u_j \varphi_{,j} \tag{27}$$

$$\bar{\vartheta} = \vartheta + \bar{k}_2 u_j \vartheta_{,j} \tag{28}$$

Following Heinrich and Yu [9]

$$\bar{k}_i = \frac{\xi_i l}{2\|u\|} \tag{29}$$

in which $\|u\|$ is the magnitude of the local velocity $\boldsymbol{u}$,

$$\|u\|^2 = u_i u_i \quad \text{(sum)} \tag{30}$$

and l is an average element length whose definition is given in [9]. The parameters ξ_i are given by

$$\xi_i = \coth\zeta_i - \frac{1}{\zeta_i} \tag{31}$$

$$\zeta_1 = \frac{\|u\| l}{2\mu/\rho} \tag{32}$$

$$\zeta_2 = \Pr\zeta_1 \tag{33}$$

It should be noted that the numerical integration of the pressure term (Eq. (23)) must be one order lower than that of the velocity terms.

Using the aforementioned numerical scheme the instantaneous temperature distributions in the PCM are obtained and the magnitude of the cumulative energy charged per unit length Q, is calculated as a function of time. The calculation is made by computing the enthalpy of the PCM at each time increment using the solid PCM at its fusion temperature as the reference state and subtracting the enthalpy of the PCM at the beginning of the melting process. The value of Q is zero at the beginning and increases over the melting process toward Q_T, the cumulative energy charged for a melting process.

The maximum amount of energy which can be charged during the melting process is

$$Q_M = \rho A_{xy} \left[f_H (T_w) - f_H (T_m) \right]$$

In this work, bilinear quadrilateral elements are used to perform all computations. Grid-dependence experiments indicated that the maximum difference of the temperature at an identical location is within 0.16 % between using 20×20 elements and 30×30 elements with dimensionless time step of 4.32×10^{-5} .

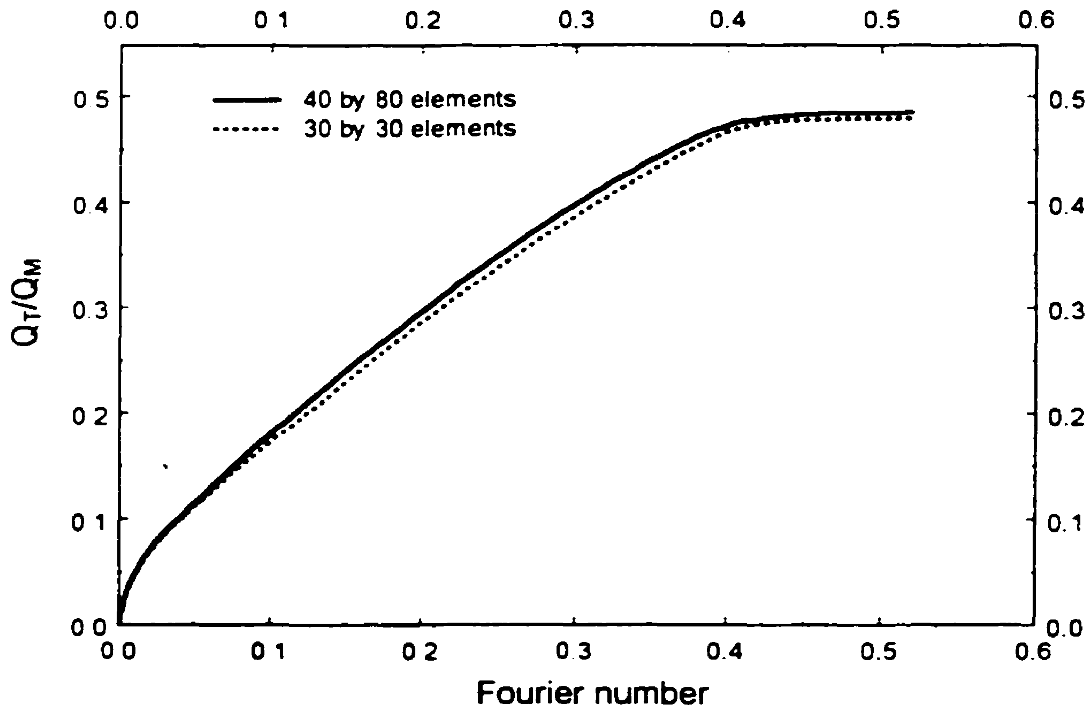

Fig. 3.1 Comparison of Dimensionless Cumulative Energy Charge as a function of the Fourier number for 30 by 30 elements and 40 by 80 elements

Fig. 3.1 compares the results obtained in this work for the dimensionless cumulative energy charged for heating from outside in a horizontal annulus of type A (square external tube with a circular tube inside) for 30×30 elements and 40×80 elements. There is hardly any difference in the results obtained for both the grids. But, in order to achieve a higher resolution of the flow patterns, 40×80 elements are employed in this work. The domain is discretized into 40 elements in the radial direction and 80 elements in the ϕ direction. A source-based scheme [11, 12] is used to treat the phase change effects. A backward Euler scheme is employed to accomplish the time discretization of Eq. (16).

3.2.5 Dimensionless Form of the Governing Equations in two dimensions

For convection-dominated two-dimensional melting or freezing problems subjected to the Dirichlet boundary condition (first kind boundary condition) the dimensionless governing equations are:

Solid region:

$$\frac{\partial H}{\partial Fo} = \frac{k_s}{k_l} Ste(\frac{\partial^2 \theta}{\partial X^2} + \frac{\partial^2 \theta}{\partial Y^2}) \tag{34}$$

Liquid region:

$$\frac{\partial U}{\partial X} + \frac{\partial V}{\partial Y} = 0 \tag{35}$$

$$\frac{\partial U}{\partial Fo} + U\frac{\partial U}{\partial X} + V\frac{\partial U}{\partial Y} = -\frac{\partial P}{\partial X} + \Pr(\frac{\partial^2 U}{\partial X^2} + \frac{\partial^2 U}{\partial Y^2}) + Ra \Pr \sin\omega + A^* U \tag{36}$$

$$\frac{\partial V}{\partial Fo} + U\frac{\partial V}{\partial X} + V\frac{\partial V}{\partial Y} = -\frac{\partial P}{\partial Y} + \Pr(\frac{\partial^2 V}{\partial X^2} + \frac{\partial^2 V}{\partial Y^2}) + Ra \Pr \cos\omega + A^* V \tag{37}$$

$$\frac{\partial H}{\partial Fo} + U\frac{\partial H}{\partial X} + V\frac{\partial H}{\partial Y} = Ste(\frac{\partial^2 \theta}{\partial X^2} + \frac{\partial^2 \theta}{\partial Y^2}) \tag{38}$$

in which

$$\begin{cases} H = \frac{c_s}{c_l} Ste\theta, & \theta < 0 \\ H = Ste\theta + 1 & \theta > 0 \end{cases} \tag{39}$$

and

$$U = \frac{u_x L_y}{\alpha_l}, \quad V = \frac{u_y L_y}{\alpha_l}, \quad \theta = \frac{T - T_m}{T_w - T_m}, \quad H = \frac{h - c_s T_m}{\Delta h}, \quad P = \frac{p L_y^2}{\rho \alpha_l^2},$$
$$X = \frac{x}{L_y}, \quad Y = \frac{y}{L_y}, \quad A^{\bullet} = \frac{A L_y^2}{\rho \alpha_l}, \quad Fo = \frac{t\alpha_l}{L_y^2}, \quad \Pr = \frac{c_l \mu}{k_l}, \tag{40}$$
$$Ra = \frac{\rho^2 c_l g \beta L_y^3 (T_w - T_m)}{\mu k_l}, \quad Ste = \frac{c_l (T_w - T_m)}{\Delta h}$$

It is clear that melting and freezing phase change heat transfer including free convection is determined by the following five dimensionless parameters, Rayleigh number (Ra), Prandtl number (Pr), Stefan number (Ste), the ratio of solid/liquid specific heat (c_s/c_l), as well as the ratio of solid/liquid heat conductivity (k_s/k_l). These are defined for our configuration as follows:

$$\theta = \frac{T - T_m}{T_w - T_m}, \quad Fo = \frac{t\alpha_l}{d^2}, \quad \Pr = \frac{c_l \mu}{k_l},$$
$$Ra = \frac{\rho^2 c_l g \beta d^3 (T_w - T_m)}{\mu k_l}, \quad Ste = \frac{c_l (T_w - T_m)}{\Delta h}$$

3.3 TEST OF THE NUMERICAL MODEL

The above-mentioned numerical model as obtained by Gong [18] is verified by comparison with the experimental results of Gau and Viskanta [13] and the implicit finite difference results of Lacroix [14] for the melting of a pure metal (gallium) inside a two-dimensional rectangular cavity (height L_y=0.0445 m; width L_x=0.089 m). The gallium is assumed to be initially at its fusion temperature. The top and bottom boundaries are adiabatic. At time t=0, the temperature of the left vertical wall is suddenly raised to a prescribed temperature above the melting point. The values of the governing dimensionless numbers and aspect ratio are listed in Table 3.1 for the test problem.

Table 3.1 Parameters Used in the Accuracy Test Runs

R	Aspect ratio L_y/L_x	*0.5*
Ra	Rayleigh number	2.2×10^5
Pr	Prandtl number	*0.021*
Ste	Stefan Number	*0.042*
c_s/c_l	Ratio of solid/liquid specific heat	*1*
k_s/k_l	Ratio of solid/liquid heat conductivity	*1*

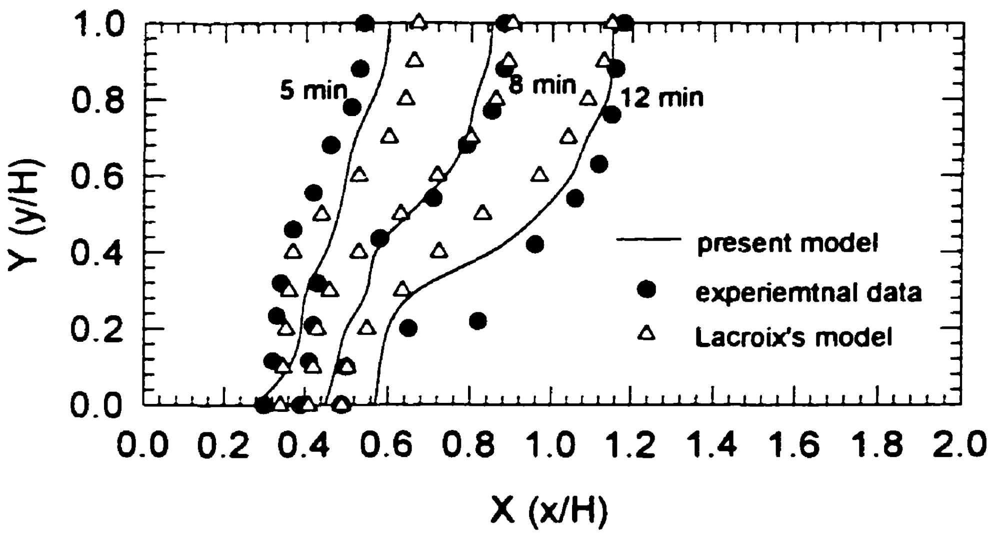

Fig. 3.2 Comparison of the Predicted Phase Front with Experimental Data

Fig. 3.2 compares the predicted phase front by Gong [18] with both the experimental results of Gau and Viskanta [13] and the finite difference prediction of Lacroix [14]. It is seen from this figure that the present model is in good agreement with the results of the above mentioned references. Experimental uncertainty values are not available. It is believed that the computer code is sufficiently accurate for the work presented here.

The discrepancy between the predicted phase front of the present model and the experimental results is due to two possible reasons. First, in the experiment, the solid showed an initial subcooling of approximately 2 °C. This degree of subcooling is significant in the light of the fact the heated wall was at only 8 °C higher than the melting temperature of gallium. The second reason is that it is difficult to impulsively heat the vertical wall to a desired temperature in reality due to its finite thermal inertia. The discrepancy of predicted phase front between the present model and Lacroix's model is due to the difference of the numerical methods used. Lacroix used a front-tracking method while this model uses a fixed-grid enthalpy-porosity approach to model the phase change effects.

REFERENCES

1. Gartling, D.K. 1980, "Finite Element Analysis of Convective Heat Transfer Problems with Change of Phase," in *Computer Methods in Fluids*, K. Morgan, C. Taylor and C.A. Brebbia (eds.), Pentech, London, pp. 257-284.
2. Morgan, K, 1981, "Numerical Analysis of Freezing and Melting with Convection," *Comp. Meth. Appl. Mech. Eng.*, Vol. 28, pp. 275-284.
3. Usmani, A.S., Lewis, R.W. and Seetharamu, K.N., 1992, "Finite Element Modeling of Natural-Convection-Controlled Change of Phase" *Int. J. Num. Meth. Eng.*, Vo.14, pp. 1019-1036.
4. Voller, V.R., Prakash, C., 1987, "A Fixed Grid Numerical Modelling Methodology for Convection-Diffusion Mushy Region Phase-Change Problems," *Int. J. Heat Mass Transfer*, Vol. 30, pp 1709-1719.
5. Brent, A.D., Voller, V.R. and Reid, K.J., 1988, "Enthalpy-Porosity Technique for Modelling Convection-Diffusion Phase Change: Application to the Melting of a Pure Metal," *Numerical Heat Transfer*, Vol. 13, pp. 297-318.
6. Hughes, T.J.R., Liu, W.K. and Brooks, A., 1979, "Review of Finite Element Analysis of Incompressible Viscous Flows by the Penalty Function Formulation," *Journal of Computational Physics*, Vol. 30, pp 1-60.
7. Brooks, A.N. and Hughes, T.J.R, 1982, "Streamline Upwind/Petrov-Galerkin Formulations for Convection Dominated Flows with Particular Emphasis on the Incompressible Navier-Stokes Equations" *Comp. Meth. Appl. Mech. Eng.*, Vol. 32, pp. 199-259.

8. Dyne, B.R. and Heinrich, J.C., 1993, "Physically Correct Penalty-like Formulations for Accurate Pressure Calculation in Finite Element Algorithms of the Navier-Stokes Equations," *Int. J. Num. Meth. Eng.*, Vol. 36, pp. 3883-3902.

9. Heinrich, J.C. and Yu C.C., 1988, "Finite Element Simulation of Buoyancy-Driven Flows with Emphasis on Natural Convection in a Horizontal Circular Cylinder," *Comp. Meth. Appl. Mech. Eng.*, Vol. 69, pp. 1-27.

10. Argyris, J., 1992, " Petrov-Galerkin Finite Element Approach to Coupled Heat and Fluid Flow," *Comp. Meth. Appl. Mech. Eng.*, Vol. 94, pp. 181-200.

11. Voller, V.R., 1990, "Fast Implicit Finite-Difference Method for the Analysis of Phase Change Problems," *Num. Heat Transfer*, Vol. 17, pp. 155-169.

12. Swaminathan, C.R. and Voller, V,R., 1993, "On the Enthalpy Method," *Int. Num. Meth. Heat Fluid Flow*, Vol. 3, 233-244.

13. Gau, C. and Viskanta, R., 1986, "Melting and Solidification of a Pure Metal on a Vertical Wall.," *J. Heat Transfer*, Vol. 174, pp. 174-181.

14. Lacroix, M., 1992, "Predictions of Natural-Convection-Dominated Phase-Change Problems by the Vorticity-Velocity Formulation of the Navier-Stokes Equations," *Numerical Heat Transfer*, Part B, Vol. 22. pp. 79-93.

15. Benard, H. 1990, "Tourbillions Cellulaires dan une Nappe Liquid," *Revue Generale des Sciences Pures et Appliqees*, Vol. 11, pp. 1309-1328, 1900.

16. Hale, N.W., Viskanta, R, 1980, "Solid-Liquid Phase Change Heat Transfer and Interface Motion in Materials Cooled or Heated from Above or Below," *Int., J. Heat Mass Transfer*, Vol 23, pp 283-292

17. Gau, C, Viskanta, R and Ho, C J , 1983, "Flow Visulization during Solid-Liquid Phase Change Heat Transfer II. Melting in a Rectangular Cavity," *Int. Comm. Heat Mass Transfer*, Vol 10, pp 183-190.

18. Gong, Z. X., 1997, "Time-dependant Melting and Freezing Heat Transfer in Multiple Phase Change Materials," Ph.D Thesis, Department of Chemical Eng., McGill University, Canada

19. Gong, Z. X. and Mujumdar, A.S., 1998, "Flow and Heat Transfer in Convection-Dominated Melting in a Rectangular Cavity Heated from Below," *Int. J. Heat Mass Transfer*, Vol. 41, No 17, pp. 2573-2580.

NOMENCLATURE

A porosity function for the momentum equation

A^* dimensionless form of A

A_{xy} area of a computational domain

b a small constant

c specific heat

d diameter of the inner cylinder

C constant

f_H enthalpy-temperature function

Fo Fourier number, $Fo = \dfrac{t\alpha_l}{L_y^2}$

g_i gravitational force vector

h enthalpy

H dimensionless enthalpy

k heat conductivity

$\bar{k}_i$ artificial diffusion coefficient

l average element length

L_x length of rectangular enclosure in x direction

L_y length of rectangular enclosure in y direction

n_i surface unit normal vector

p fluid pressure

P dimensionless fluid pressure

Pr Prandtl number, $\mathrm{Pr} = \dfrac{c_l \mu}{k_l}$

q heat flux

q_a prescribed heat flux

q_c convective heat flux

q_r radiative heat flux

q_s heat source

Q instantaneous energy charged

Q_T total energy charged

Q_M maximum energy charged

r radial co-ordinate

r_s radius of inner cylinder

r_b radius of outer cylinder

Ra Rayleigh number, $Ra = \dfrac{\rho^2 c_l g \beta L_y^3 (T_w - T_m)}{\mu k_l}$

s boundary surface coordinate

Ste Stefan number, $Ste = \dfrac{c_l (T_w - T_m)}{\Delta h}$

t time

T temperature

T_0 reference temperature

T_m melting point of PCM

T_w isothermal wall temperature

u_i velocity component

u_x velocity in x direction

u_y velocity in y direction

U dimensionless velocity of x direction

V dimensionless velocity of y direction

x, y coordinate

X, Y dimensionless coodinate

Greek symbols:

α diffusivity

β expansion coefficient

θ dimensionless temperature, $\theta = \dfrac{T - T_m}{T_w - T_m}$

Δh latent heat

Δt time step

λ porosity of a mush zone

φ shape function of velocity

$\bar{\varphi}$ weighting function for momentum equation

ϑ shape function of temperature

$\bar{\vartheta}$ weighting function for energy equation

γ penalty parameter

Γ boundary

μ viscosity

Ω integration domain

ρ density

ω the angle horizontal direction to x axis

σ_{ij} stress tensor

Superscript:

- over bar, boundary value of the variable

0 initial value

Subscripts:

l liquid

n nth time step

s solid

x component of x direction

y component of y direction

Chapter 4

Results and Discussion

Numerical experiments were carried out to examine effects of PCM container geometry for more efficient thermal energy storage. Using the numerical model described in Chapter 3., simulations were carried out for the melting of a PCM (n-octadecane (99% pure)) in horizontal annuli of the following configurations:

(a) Square external tube with a circular tube inside - Annulus Type A

(b) Circular external tube with a square tube inside - Annulus Type B

Innovative passive methods for enhancement of the melting heat transfer rate such as flipping and introducing eccentricity for the internal tube for the horizontal annuli were identified – a principal objective of this thesis.

4.1 MELTING HEAT TRANSFER IN TYPE A ANNULUS

4.1.1 Effect of Heating inside wall, outside wall and both walls

For heating from inside, the inner wall of the tube is maintained at a constant temperature higher than the melting point of the PCM. The outer wall is adiabatic. The thermo-physical properties of the PCM used i.e n-octadecane (99% pure) are enumerated in Table 4.1. The parameters for the computed problem are listed in Table 4.2. A schematic diagram of the physical model simulated is shown in Fig. 4.1.

TABLE 4.1

Thermo-physical properties of n-octadecane (99% pure)

Property	Solid Phase	Liquid Phase
Density (ρ) kg/m^3	768	768
Thermal Conductivity (K) W/mK	0.358	0.148
Specific Heat (c) $J/kg\,K$	2150	2230
Viscosity $kg/m\,s$	3.06×10^{-3}	
Coefficient of thermal Expansion (β) $1/K$	0.0008	
Latent Heat (L) J/kg	243500	

The various dimensionless numbers used are defined as follows:

$$\theta = \frac{T - T_m}{T_w - T_m}, \quad Fo = \frac{t\alpha_l}{d^2}, \quad \Pr = \frac{c_l \mu}{k_l},$$
$$Ra = \frac{\rho^2 c_l g \beta d^3 (T_w - T_m)}{\mu k_l}, \quad Ste = \frac{c_l (T_w - T_m)}{\Delta h} \qquad (1)$$

The Rayleigh and Prandtl number are based on the inside diameter of the annulus.

TABLE 4.2

Parameters used in the Simulation Runs

Pr	Prandtl number	*46.1*
Ste	Stefan Number	*0.138*
c_s/c_l	Ratio of solid/liquid specific heat	*0.964*
k_s/k_l	Ratio of solid/liquid heat conductivity	*2.419*
θ_I	Initial dimensionless temperature	*-0.0256*

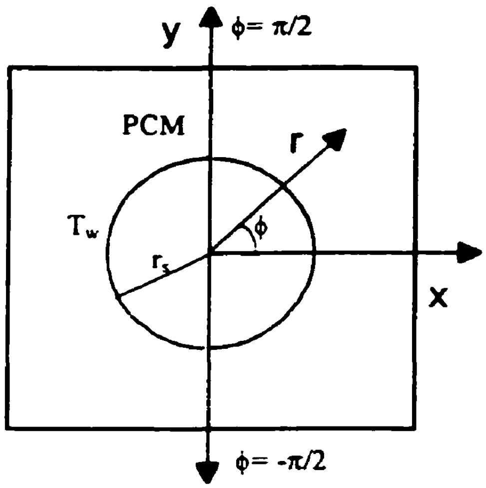

Fig. 4.1 Schematic diagram of the physical model for type A annulus

Fig. 4.2 shows the predicted distribution of isotherms (left) and streamlines (right) at various Fourier numbers for Ra=2.844×10^{6}. At this Rayleigh number, in the early stage of melting (Fo<0.043) no flow is detected in the melt region with only one convection cell formed in the melt zone. The heat transfer rate is controlled by conduction at short times. The single convection cell splits into two cells at Fo=0.043. The size of the second convection cell formed along the top of the heated cylinder increases with elapsed time. The direction of the flow of the second convection cell is anti-clockwise while the original cell flows in the clockwise direction. The melt is heated up to the highest temperature at the junction of the two cells and then floats up due to its lower density. The two cells recombine at a later stage for Fo > 0.26 and thereafter remain unicellular for the rest of the melt period.

The local dimensionless heat flux along the heated wall is given as $\partial\theta/\partial R$, where

$$\theta = \frac{T - T_m}{T_w - T_m} \quad \text{is dimensionless temperature, and} \qquad (2)$$

$$R = \frac{r - r_s}{r_b - r} \quad \text{normalized polar angle } \Phi = \phi / \pi$$

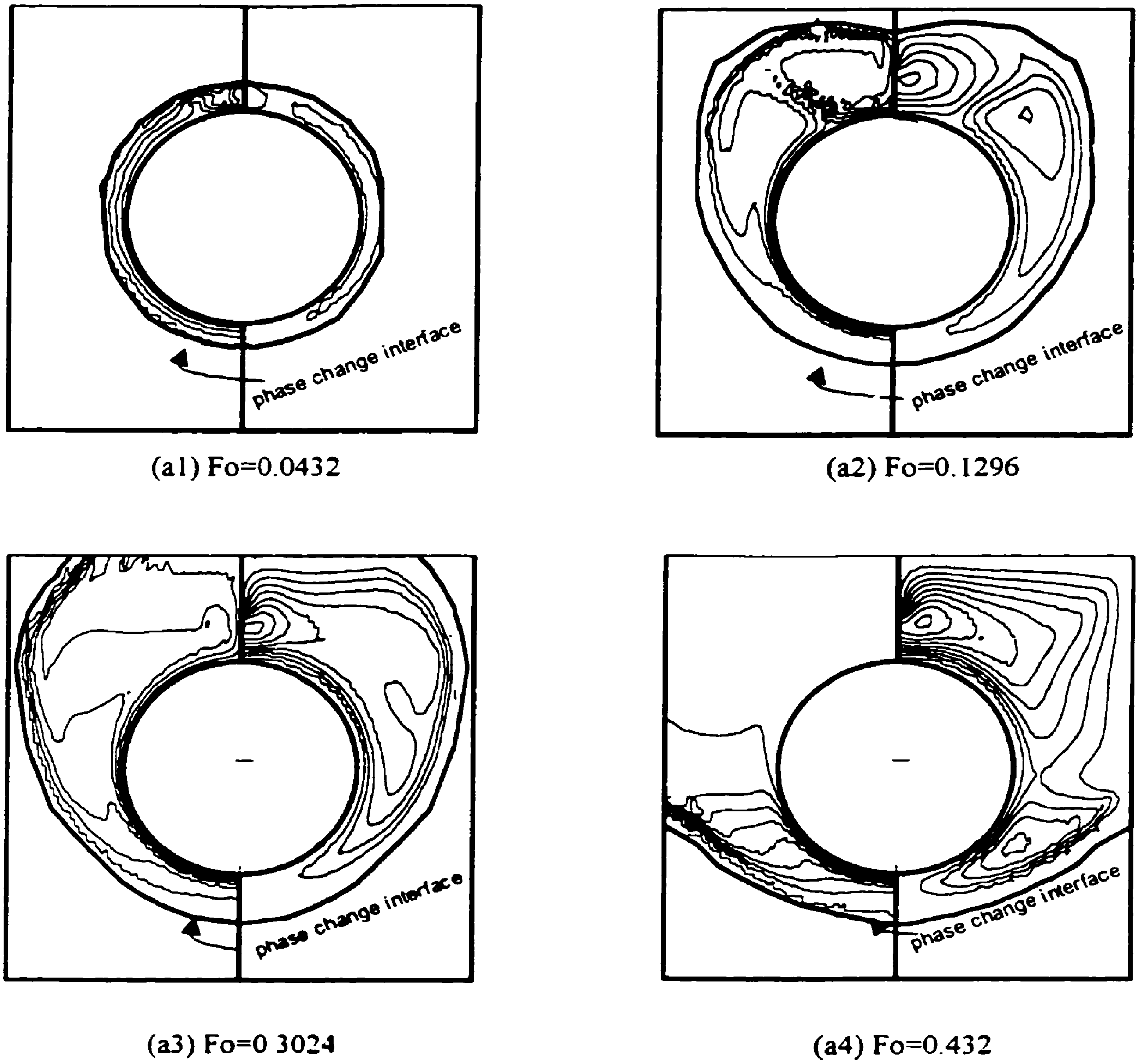

Fig. 4.2 Streamlines(right) and isotherms(left) in the melt zone with Ra=2.844×10^6 for heating from inside

Fig. 4.3 displays the dimensionless heat flux distribution $\partial\theta/\partial R$, corresponding to the flow pattern given in Fig 4.2. Moving from the bottom to the top of the inner cylinder the heat flux decreases smoothly except for the troughs at the junction of the two convection cells. This is due to the fact that the melt has the lowest temperature at the bottom of the cylinder. Since the inner cylinder wall is isothermal, the larger temperature difference between the melt and the heating surface results in a higher heat flux. As the melt front moves upward along the inner cylinder, the melt is being heated up. Hence the temperature difference between the melt and the heating surface is reduced and so is the heat flux. Now the melt at the junction between the two cells is at the highest temperature. Hence the temperature difference is lowest at the junction of the two cells which results in a sudden drop for the heat flux. Moreover the position of the trough is time-dependant. This is a result of the changing size of the second convection cell with time. It can be seen from the dimensionless heat flux distribution curve (Fig. 4.3) that at Fo=0.302, the two convection cells coalesce into a singe cell. Thermal stratification is observed in the upper part of the liquid melt region. The temperature gradient decreases significantly in this region. This results in the predicted smaller heat flux in the upper half of the melt region.

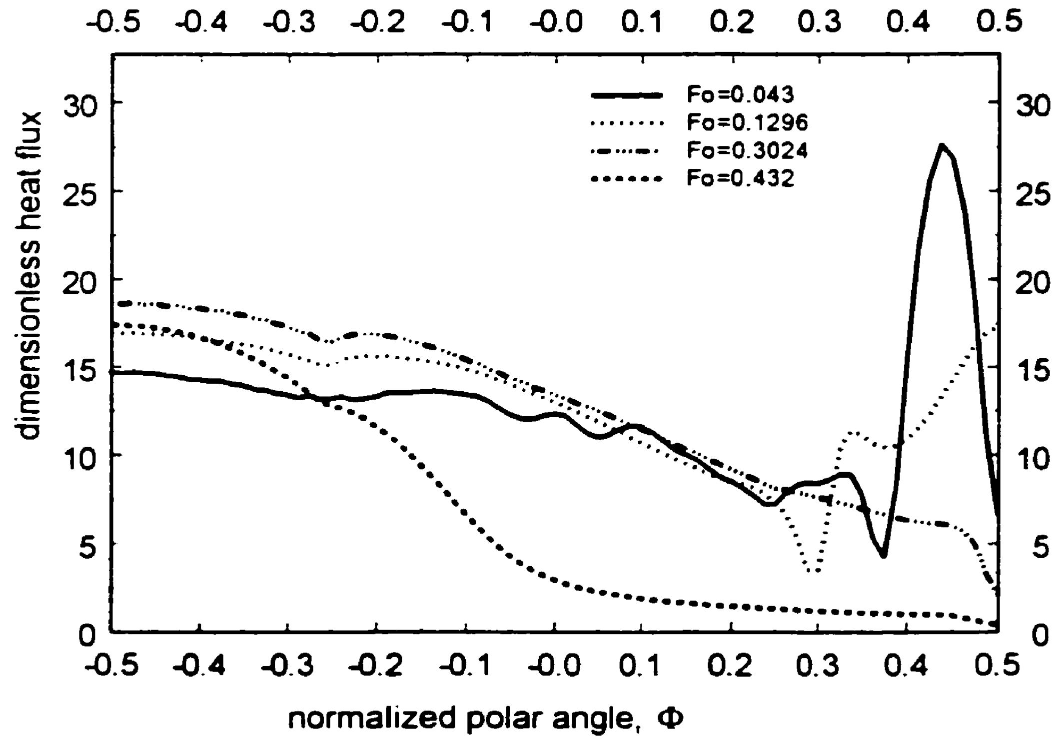

Fig. 4.3 Local Dimensionless heat flux distribution along the heated surface ($Ra=2.844\times10^{6}$)

Fig. 4.4 presents the variations of the dimensionless cumulative energy charged with the dimensionless time (Fourier number). The value of Q i.e, the cumulative energy charged per unit length is zero at the beginning and increases over the melting process toward Q_T, the cumulative energy charged in the melting process.

The maximum amount of energy which can be charged during the melting process is

$$Q_M = \rho A_{xy} \left[f_H(T_w) - f_H(T_m) \right] \qquad (3)$$

This figure shows that the dimensionless cumulative energy charged increases linearly during the first half of the melting process. But, later on the charge rate begins to slow down. This can be attributed to the thermal stratification mentioned earlier. At the last stage of the melting process only a small part of the solid remains at the bottom of the container. Thermal stratification occurs and significantly decreases the temperature gradient at the phase change interface, and therefore the phase change heat transfer rate. Note that in the present model we have assumed that the solid zone is constrained i.e. not free to move.

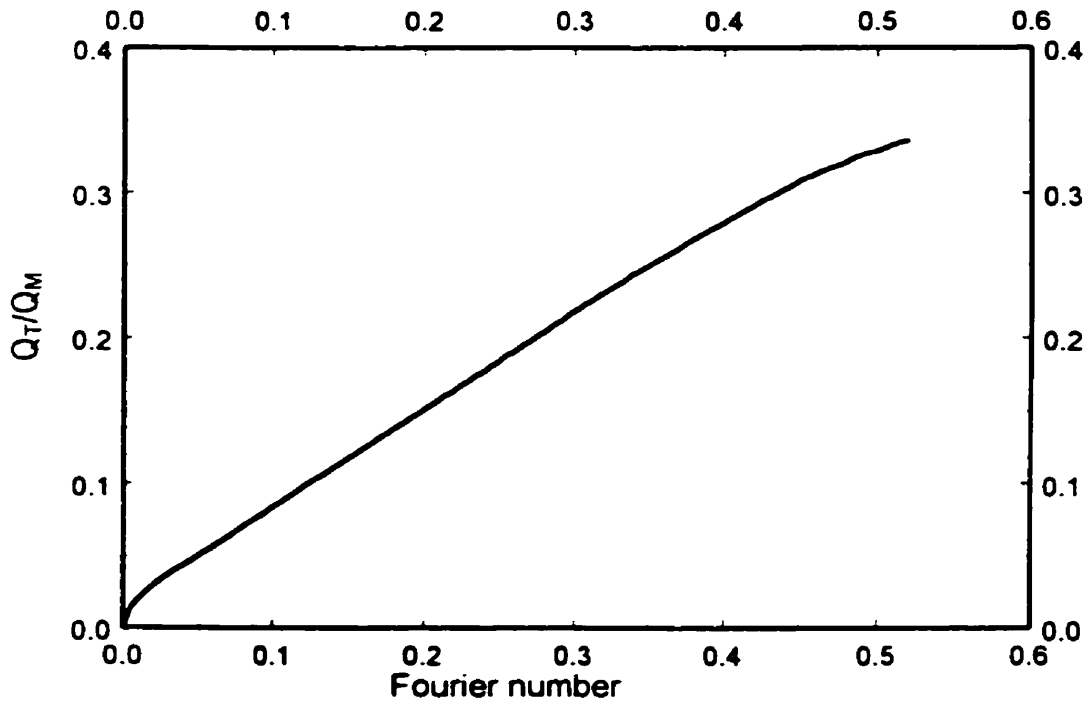

Fig. 4.4 Dimensionless energy charge curve for heating inside wall

(Ra=2.844×10^6)

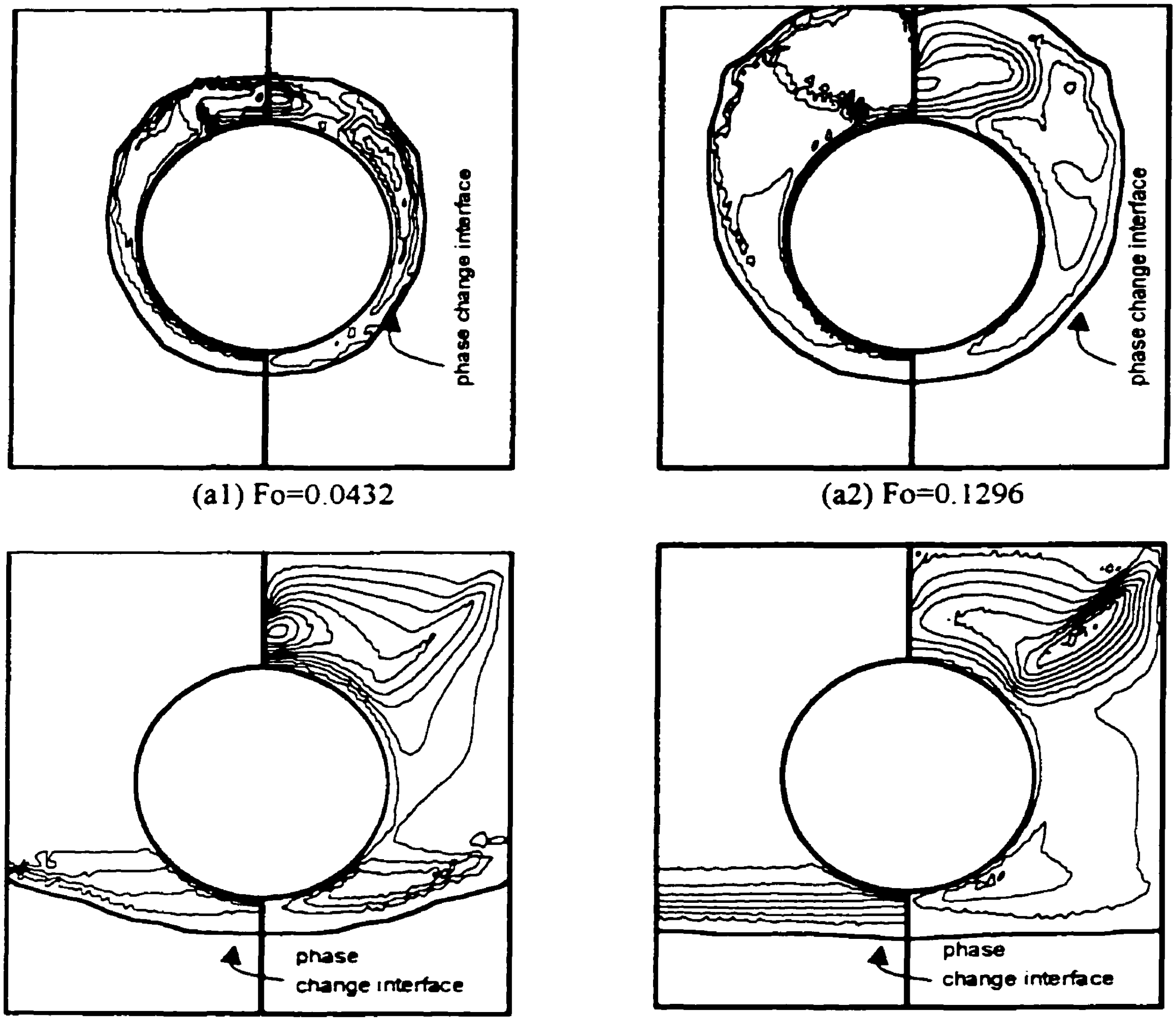

(a1) Fo=0.0432 (a2) Fo=0.1296

(a3) Fo=0 3024 (a4) Fo=0.432

Fig. 4.5 Streamlines(right) and isotherms(left) in the melt zone with Ra=2.844×10^7 for heating from inside

Fig. 4.5 presents the predicted distribution of isotherms and streamlines at different Fourier numbers for Ra=2.844×10^7. The convection cells form much earlier as compared to the earlier case of heating from inside in annulus type A for Ra=2.844×10^6. At an early stage, Fo=0 022, four convection cells are formed. The duration of the four convection cells is short. However the evolution of streamlines and isotherms is similar to the case of Ra=2.844×10^6. As melting progresses, the cells at the top of the inner cylinder combine together. Bicellular flow is observed in the intermediate stage for Fo < 0.238 and thereafter the two cells combine and the flow in the melt remains unicellular throughout the rest of the process. Another important observation that can be made is that the shapes of the cells are quite irregular. No physical explanation can be offered for this observation, however.

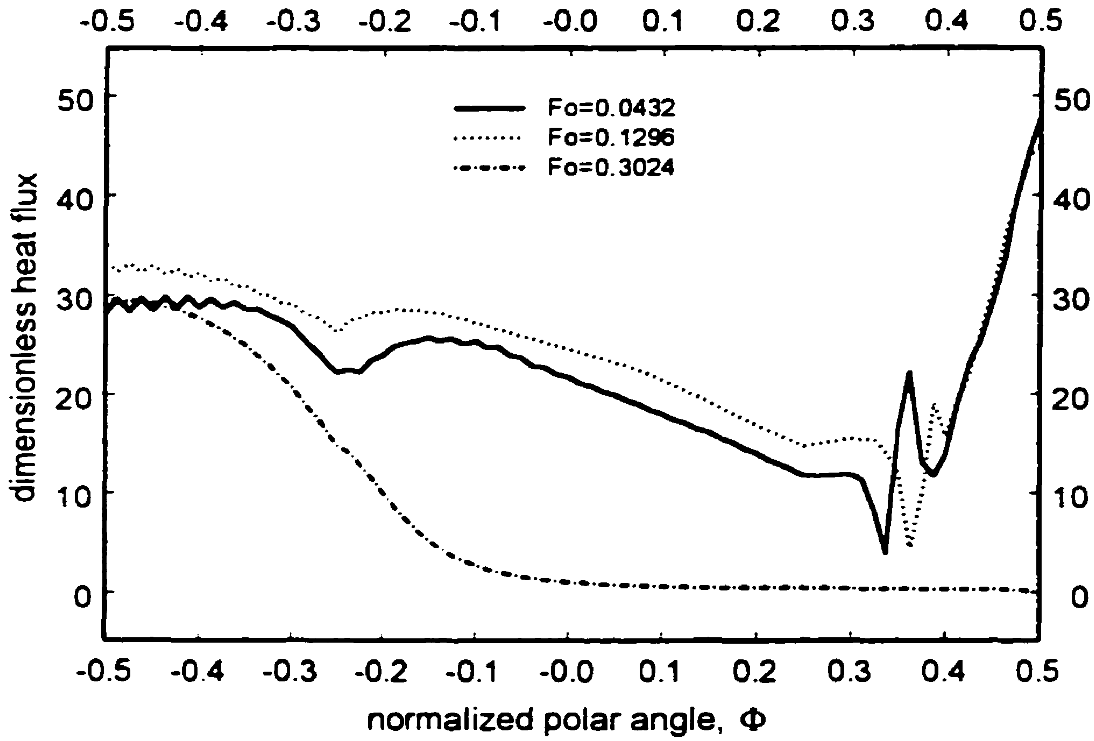

Fig. 4.6 Local Dimensionless heat flux distribution along the heated surface (Ra=2.844×10^7)

Fig. 4.6 displays the local dimensionless heat flux distribution corresponding to the flow pattern given in Fig. 4.5. As stated earlier, the troughs in the curves correspond to the junctions of the convection cells. The single trough in the curve for Fo=0.1296 is a result of bicellular melt flow during this period. For Fo=0.302 the low heat flux in the upper part of the cylinder is due to thermal stratification i.e. high temperature fluid rises to the upper region.

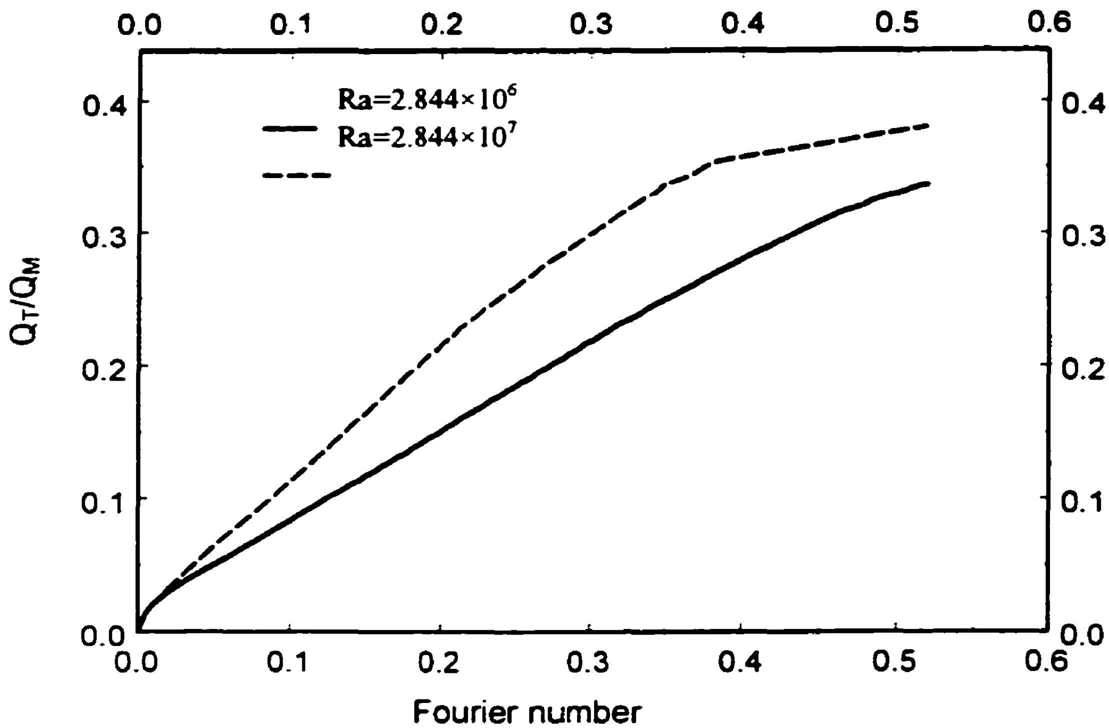

Fig. 4.7 Comparison of dimensionless cumulative energy charge curve for heating from inside

Fig. 4.7 shows a comparison between the dimensionless cumulative energy charged in type A horizontal annulus for heating from inside for two Rayleigh numbers. As in the early stage heat transfer is mainly due to conduction, the cumulative energy charged is identical in both cases Now as the Rayleigh number increases natural convection develops earlier and increases the melting rate due to increased heat charge. This is due to the free convective flow in high Rayleigh number case being much stronger than the one in the low Rayleigh number case.

A comparison of the fraction melted as a function of time for the two Rayleigh numbers is presented in Fig. 4.8. The rate of energy charged to the system is enhanced by the convective flow in the melt which is dominant for high Rayleigh number. Hence the fraction melted is more for higher Rayleigh number as compared to the lower Rayleigh number.

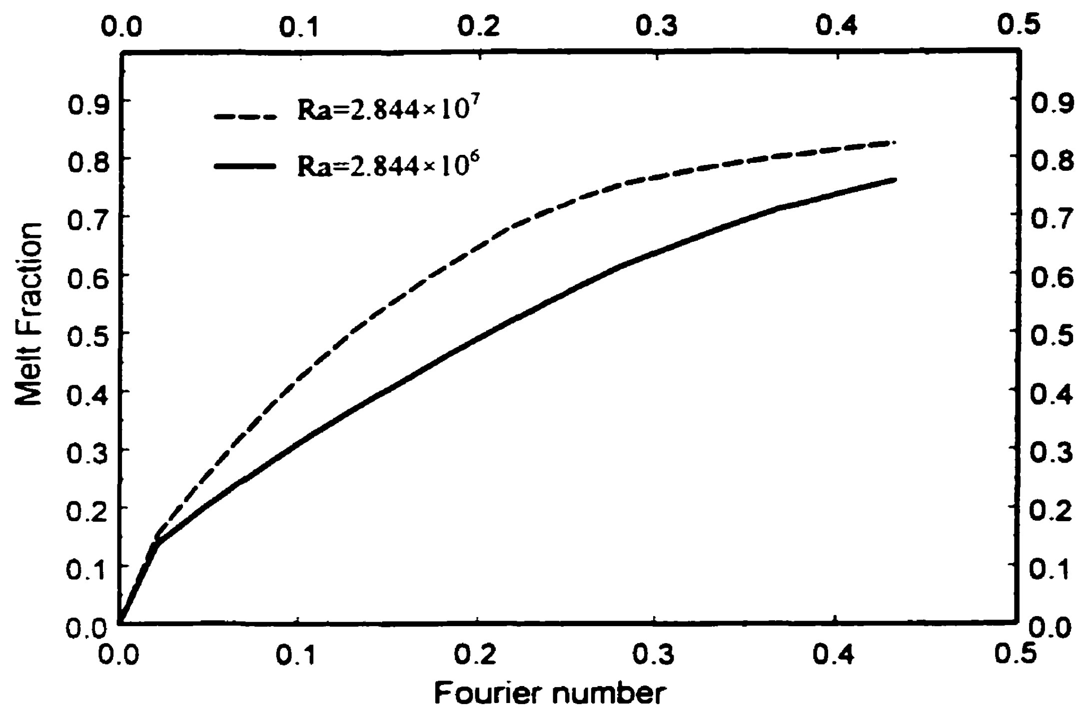

Fig. 4.8 Comparison of melt fraction as a function of Fourier number for type A annulus for heating inside wall

The melting of a PCM in a type A annulus when heated from outside was studied using the numerical model described in Chapter 3. The inside wall of the tube is assumed to be adiabatic. The parameters used for the simulated problem are identical to those in Table 4.1.

For two dimensional melting of a PCM in a rectangular container heated from below, it is known from experiments that three-dimensional convection cells develop and last for a short period of time during the early stage[1]. In this study three-dimensional effects on melting are not considered since a two-dimensional model is employed. However, the duration of the three-dimensional convection is very short [1,2] compared with the whole melting process so that the two dimensional results are believed to be close to reality for long aspect ratio containers. No experimental data are available for direct validation of the predicted results at this time.

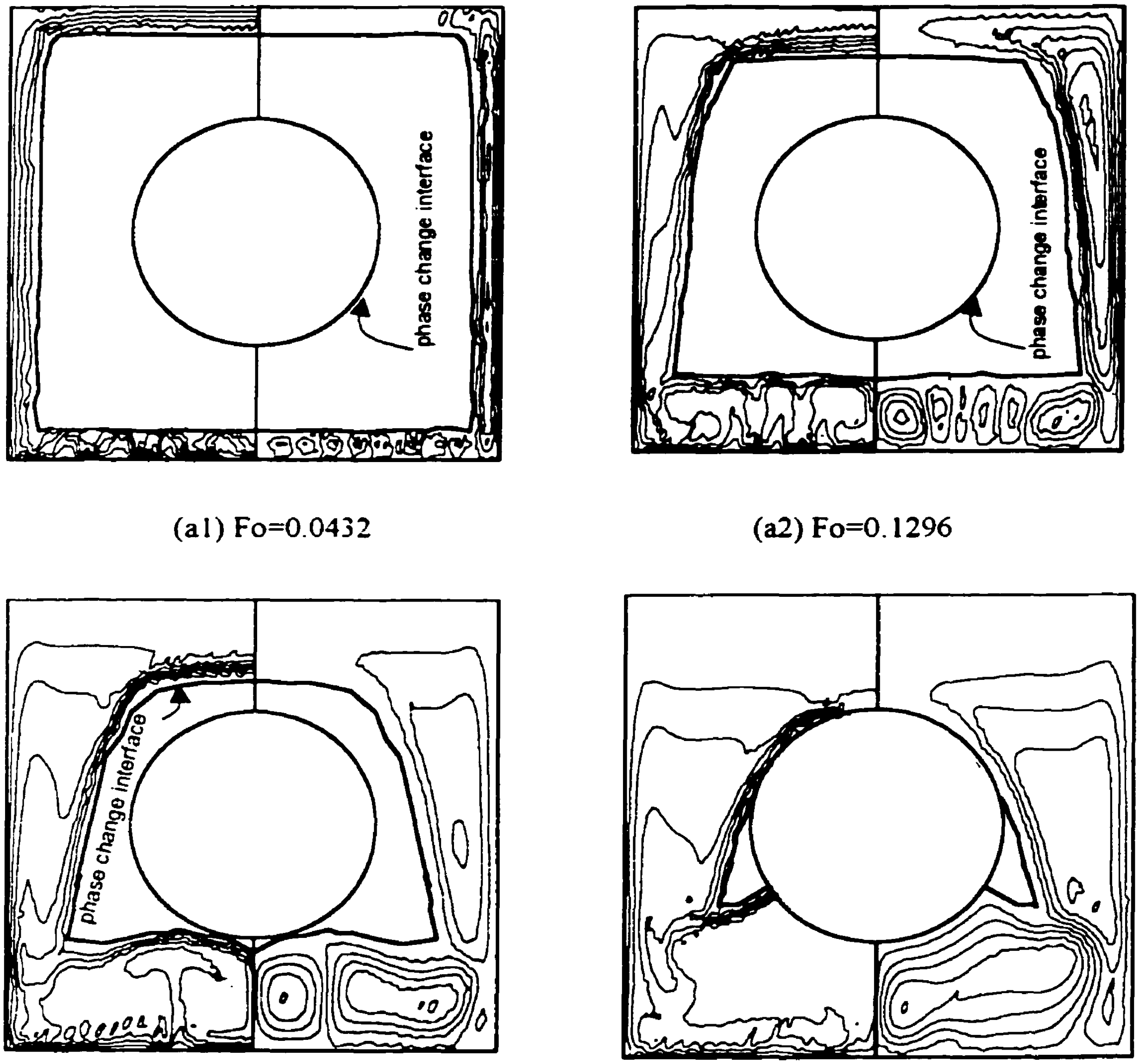

(a1) Fo=0.0432

(a2) Fo=0.1296

(a3) Fo=0 3024

(a4) Fo=0.432

Fig. 4.9 Streamlines(right) and isotherms(left) in the melt zone with Ra=2.844×10^6 for heating from outside

Fig. 4.9 displays the predicted streamlines and isotherms at different Fo values for the computed problem (Ra=2.844×10^6). It can be seen that at Fo=0.0432 a total of nine convection cells develop. The predicted phenomena are consistent with the results obtained by Devahastin *et al* [3] for heating from two adjacent walls in a rectangular enclosure. With the increase in the melt depth, the size of the convection cells increases and the number of cells decreases. The rightmost cell in Fig.4.9 has a large portion at the top of the cavity as the hot melt drifts up resulting in faster melting rate near the top. Moreover, the circulation along the vertical wall intensifies and embraces larger part of the melt zone as time progresses on. This results in the appearance of an upward melting pattern. The size and number of cells is a function of time and as melting proceeds, the cells merge with the neighboring ones and grow in size.

The isotherm contours reveal a concave curvature at the junction of the cells which can be explained as follows. At Fo=0.129, the circulation of the leftmost cell with a clockwise motion and its neighboring cell with an anti-clockwise direction deliver the hot melt to the interface resulting in the formation of high temperature zone near the bottom of the junction. On the other hand, since the third cell is clockwise and the second cell is anti-clockwise, a low temperature junction is observed at the junction of the second and third cells from the right.

Corresponding to the flow patterns and isotherms in Fig. 4.9, Fig 4.10 and Fig. 4.11 illustrates the local dimensionless heat flux $\partial\theta/\partial X$, $\partial\theta/\partial Y$ along the heated isothermal vertical wall and the bottom wall, respectively. The occurrence of each trough and crest corresponds to the junctions of the cells in Fig.4.9. The first crest represents the junction of the leftmost cell and its neighbors Since the first cell is clockwise and the second one is anti-clockwise a low temperature zone is found near the bottom. A high temperature gradient leads to a high heat flux

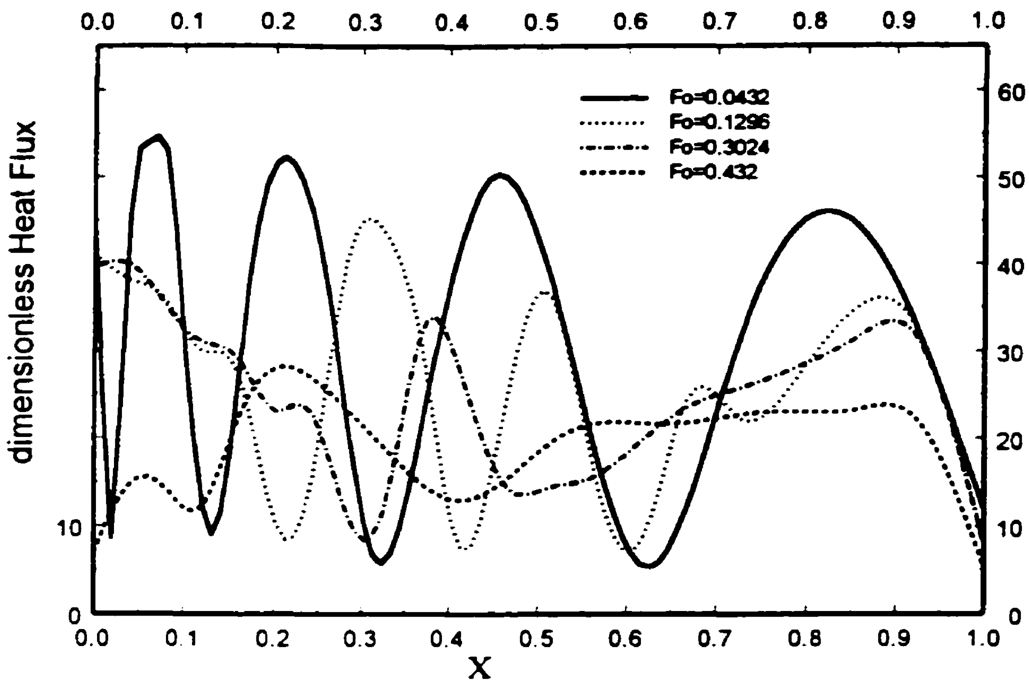

Fig. 4.10 Dimensionless heat flux $\partial\theta/\partial Y$ along the heated bottom wall at different dimensionless times

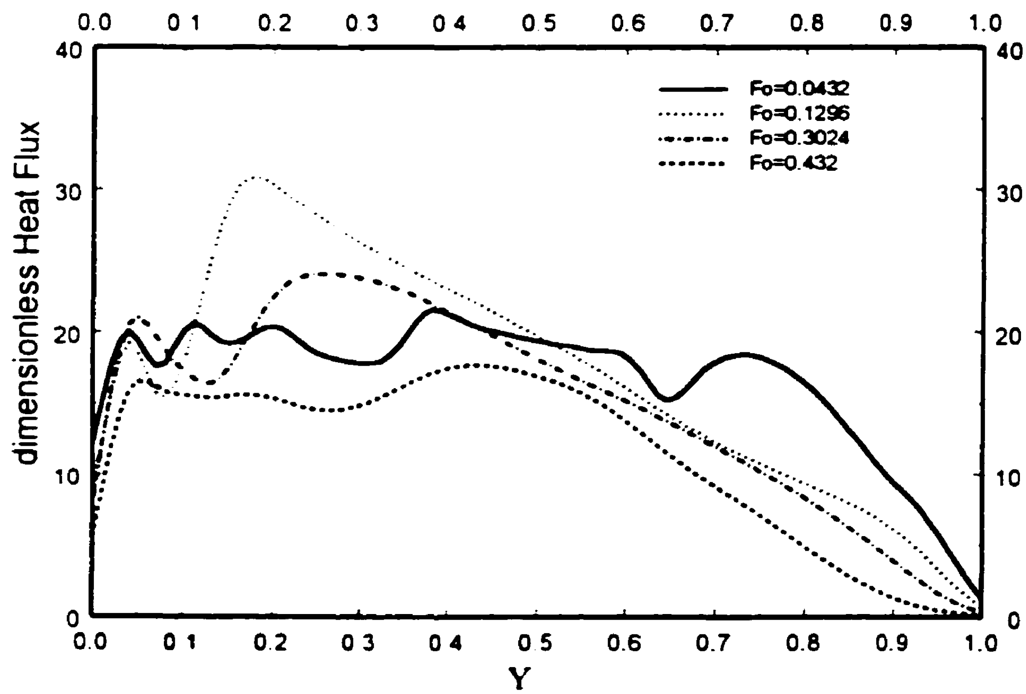

Fig. 4.11 Dimensionless heat Flux $\partial\theta/\partial X$, along the heated vertical wall at different dimensionless times

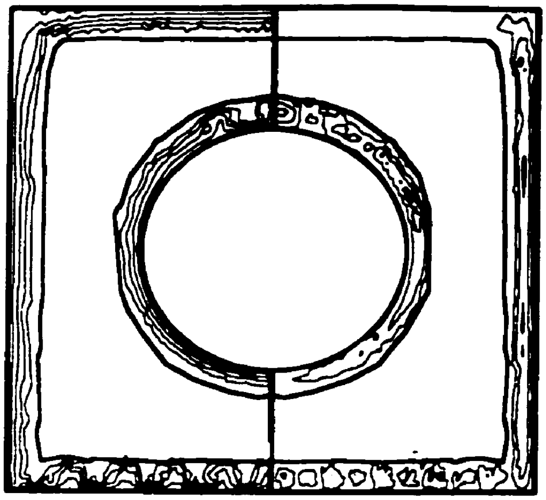

(a1) Fo=0.0432

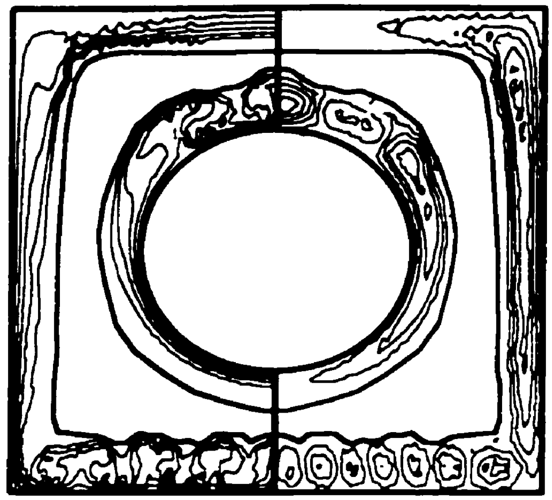

(a2) Fo=0.1296

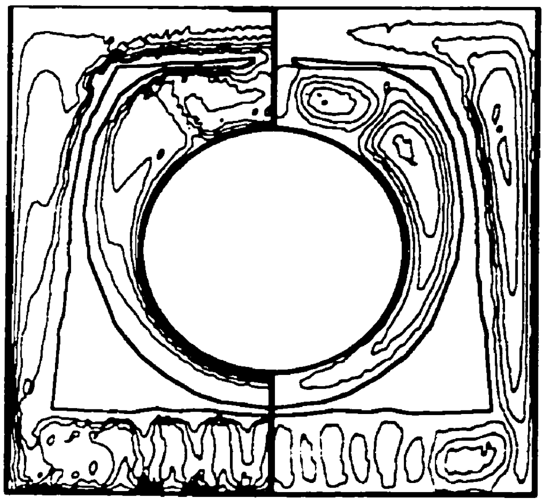

(a3) Fo=0 3024

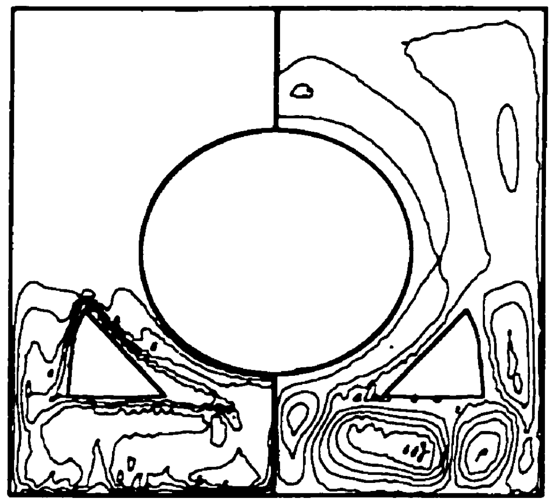

(a4) Fo=0.432

Fig. 4.12 Streamlines(right) and isotherms(left) in the melt zone with Ra=2.844×10^6 for heating from both walls

In addition to heating the inside wall and outside wall numerical simulations were carried out to study the effect of heating both inner and outer walls in a type A annulus. Both the walls of the tube are maintained at a temperature higher than the melting point of the PCM. The parameters are identical to those listed in Table 4.1.

Displayed in Fig. 4.12 are the predicted distributions of isotherms(left) and streamlines(right) at various Fourier numbers for Ra=2.844×10^6. For Fourier number less than or equal to 0.13 it is observed that the distribution of the streamlines and isotherms is similar to that for heating inside wall and outside wall separately. However for Fo=0.173, only a small triangular solid region exists and for the rest there is flow in the melt zone due to convection currents. As time progresses the remaining part of the solid PCM also melts. The dominant role played by convection is clearly noticeable for whole of the melting process.

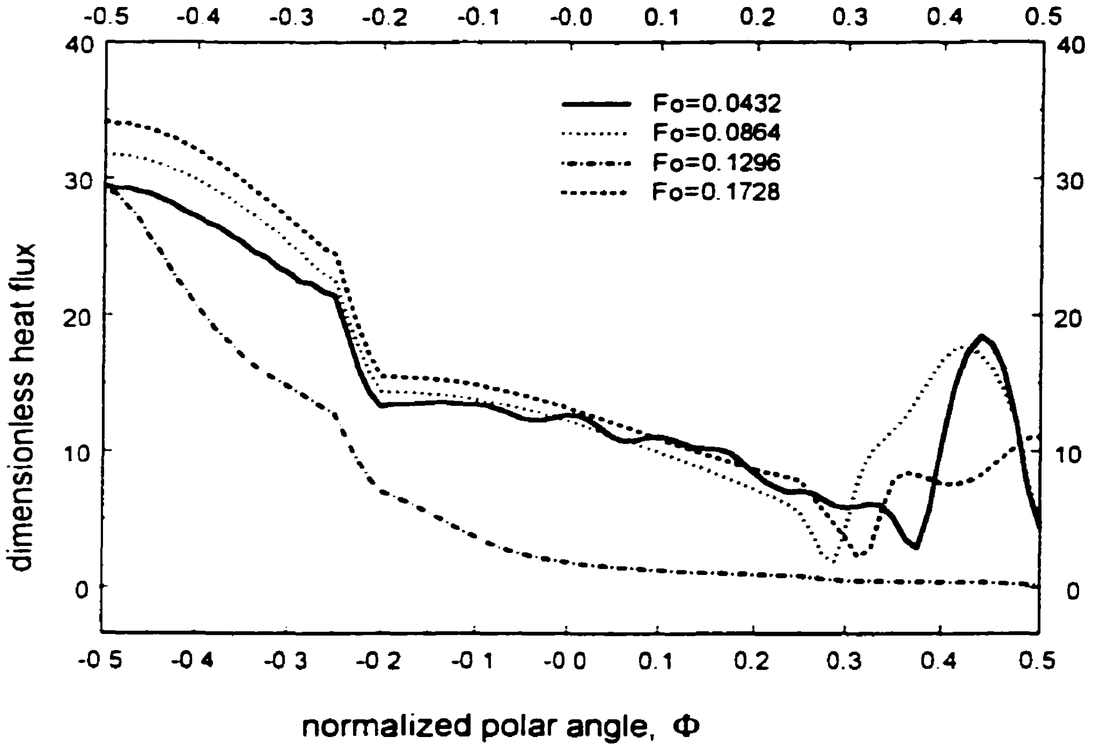

Fig. 4 13 Local Dimensionless heat flux distribution along the heated inside wall (Ra=2.844×10^6)

Displayed in Fig 4 13 is the local dimensionless heat flux along the inside wall corresponding to the flow pattern in Fig. 4.13. Also Fig. 4.14 and Fig. 4.15 illustrates the local dimensionless heat flux $\partial\theta/\partial Y$. $\partial\theta/XY$ along the heated isothermal vertical wall and bottom wall respectively

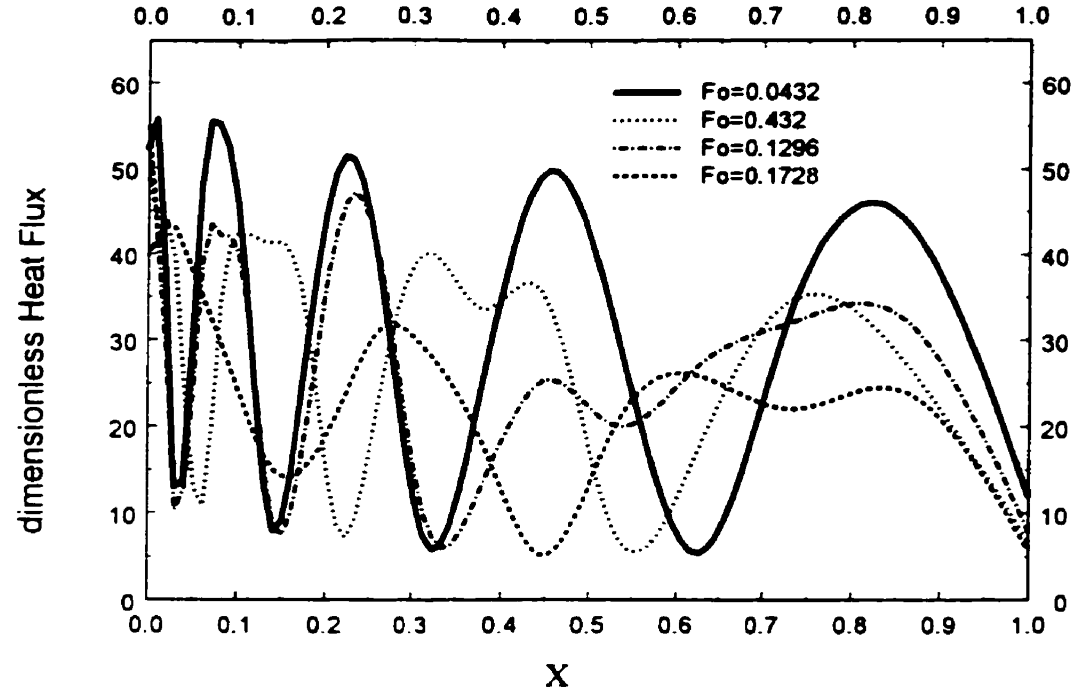

Fig. 4.14 Dimensionless heat flux $\partial\theta/\partial Y$ along the heated bottom wall at different dimensionless times

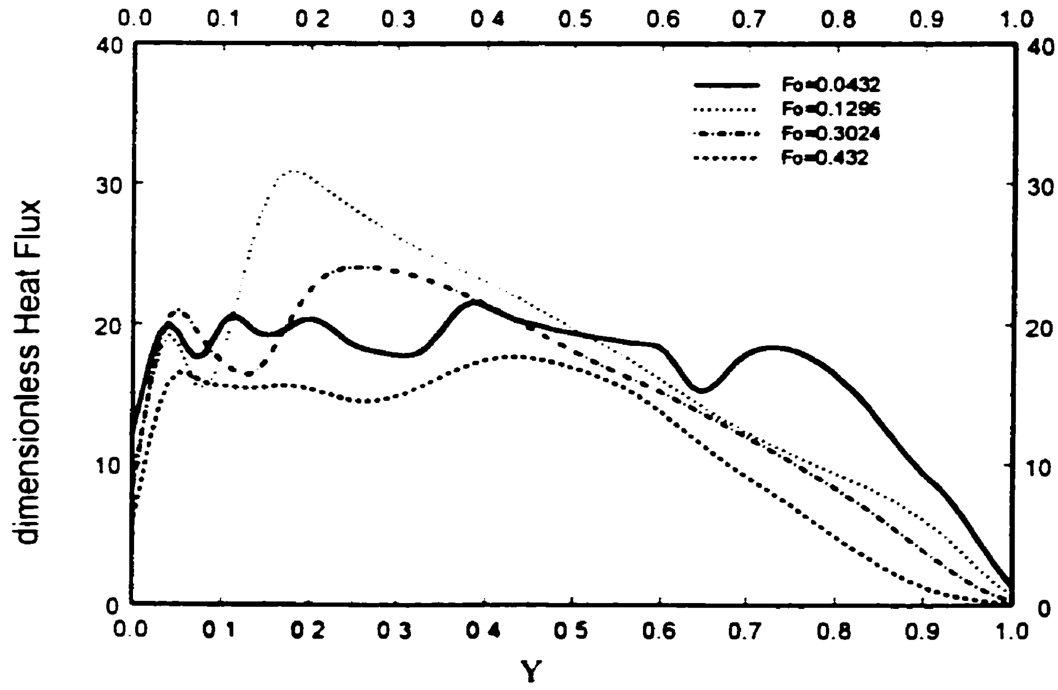

Fig. 4.15 Dimensionless heat Flux $\partial\theta/\partial X$, along the heated vertical wall at different dimensionless times

With the same explanation stated earlier, the occurrence of each trough and crest corresponds to the junctions of the cells in Fig.4.12.

From the results of the numerical experiments, it is observed that the effect of heating both walls on the cumulative heat stored is same as the sum of heating inside wall and outside wall separately until there is interaction between the two melt zones. This can be easily deduced by observing the streamline and isotherm contours in Figures 4.2, 4.9 and 4.12 for either of the cases during the first stage of the melting before the interaction begins of the melt zones, formed by heating inside wall and outside wall. Also it is found that an increase in the Rayleigh number results in an earlier onset of convection thereby expediting the melting process. Moreover, another observation that the melting is most inefficient in the bottom of the enclosure when heating inside wall. While thermal stratification is attained at the top part of the cavity, PCM at the bottom part remains in solid state for heating the inside wall of type A horizontal annulus. Thermal stratification can be eliminated in type A annulus by heating the outside wall, which results in faster melting. Thus there is merit in heating outside wall and of course heating both walls gives rise to faster melting and the energy charged to the solid PCM also increases.

4.1.1 Effect of Eccentricity on the Enhancement of Heat Transfer Rate

Fig. 4.2 shows that heating the inside wall of the horizontal type B annulus causes thermal stratification at $Fo \approx 0.432$ which results in lower heat flux and hence reduced melting. To mitigate this problem and to enhance the heat transfer rate an eccentric annulus is identified as a better alternative to the concentric one and simulations were carried out to investigate how much the heat transfer rate can be enhanced and what parameters influence the enhancement of heat transfer rate, if any. Due to limitations of the computing resources no attempt is made to perform a complete parametric study. Only the effect of Rayleigh number (Ra) is investigated. However the trends are expected to hold even for other geometric parameter values. Note that the axis of the inner container is below (not above) that of the outer one.

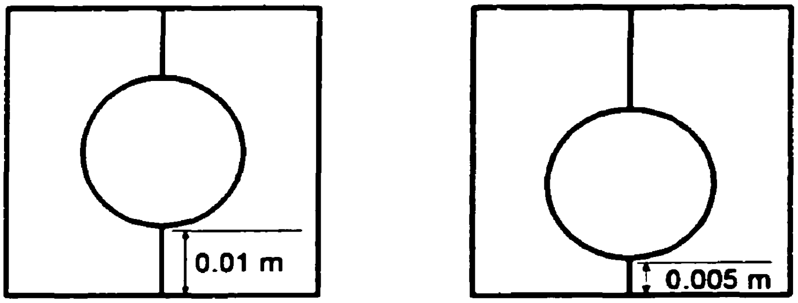

(a) (b)

Fig. 4.16 Concentric and Eccentric annuli

Fig. 4.16 Shows the geometric representation of eccentricity in type A annulus. Displayed in Fig. 4.17 are the predicted streamlines and isotherms at different dimensionless times (Fo numbers) for a Rayleigh number of 2.844×10^6 in an eccentric annulus, when heated from inside. At an early stage the evolution of the streamlines and isotherms is similar to that observed for the concentric annulus in Fig. 4.5 .For Fo > 0.0432 two convection cells are formed in the melt zone. The size of the convection cells increases as time progresses for each case and the flow is bicellular. But at Fo $\geq$ 0.302 for the concentric annulus the two cells merge and become unicellular for the rest of the melting, unlike for the eccentric annuli where the two convection cells persist. The convection cells merge for the eccentric annulus at Fo = 0.454 and thereafter remain unicellular.

Fig. 4.18 presents the local dimensionless heat flux distribution corresponding to the flow pattern shown in Fig 4 17 As mentioned earlier the trough in the heat flux distribution corresponds to the junction of the two convection cells. The single trough in the curves for Fo=0 1296, Fo=0.3024 and Fo=0 432 is a result of bicellular melt flow during this period.

Fig. 4.19 shows a comparison between the dimensionless cumulative energy charged in the system for both concentric as well as eccentric annuli. The cumulative

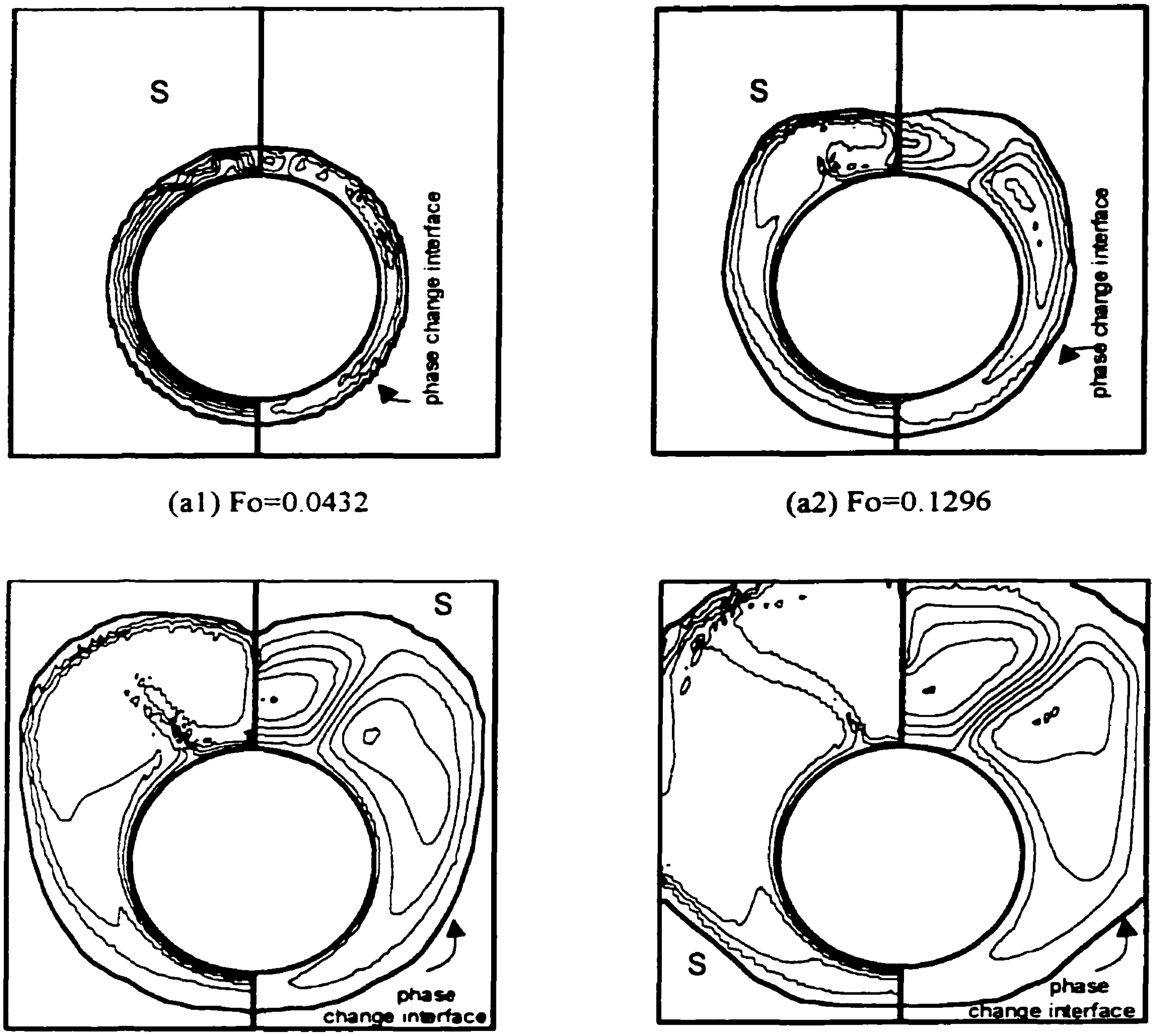

(a1) Fo=0.0432 (a2) Fo=0.1296

(a3) Fo=0 3024 (a4) Fo=0.432

Fig. 4.17 Streamlines(right) and isotherms(left) in the melt zone with Ra=2.844×10^{6} for heating from inside (S = Solid phase)

energy charged to the system is identical for both concentric and eccentric annulus until Fo $\leq$ 0.302. But later on the energy charged to the system is more for eccentric annulus as compared to the concentric annulus. This may be attributed to the fact that a bicellular flow pattern persists for eccentric annuli which results in enhancement of energy charged into the system.

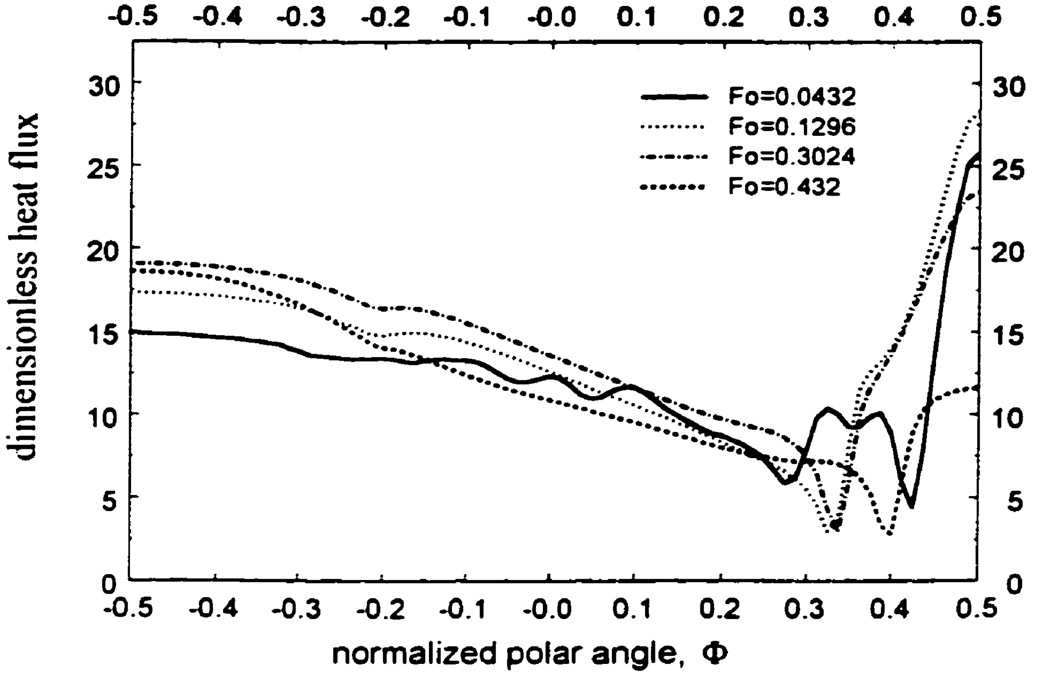

Fig. 4.18 Local Dimensionless Heat Flux Distribution along the Heated Surface ($Ra=2.844\times10^6$)

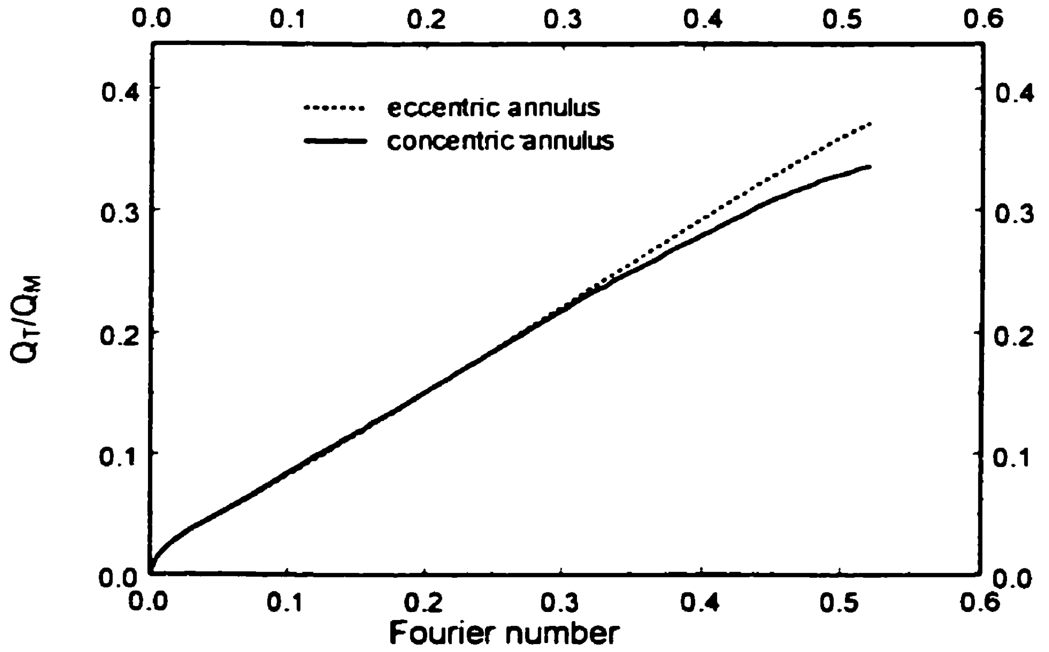

Fig. 4.19 Dimensionless Cumulative Energy Charge as a function of the Fourier number ($Ra=2.844\times10^6$)

A comparison of the fraction melted as a function of time for eccentric and concentric annuli is presented in Fig. 4.20. It can be seen that more melting is achieved with eccentric annulus rather than that with concentric annulus at longer elapsed times. In addition to this, no obvious thermal stratification occurs at the last stage of the melting process for the eccentric annulus. Hence the role played by free convection continues and is not reduced during the last stage of the melting process.

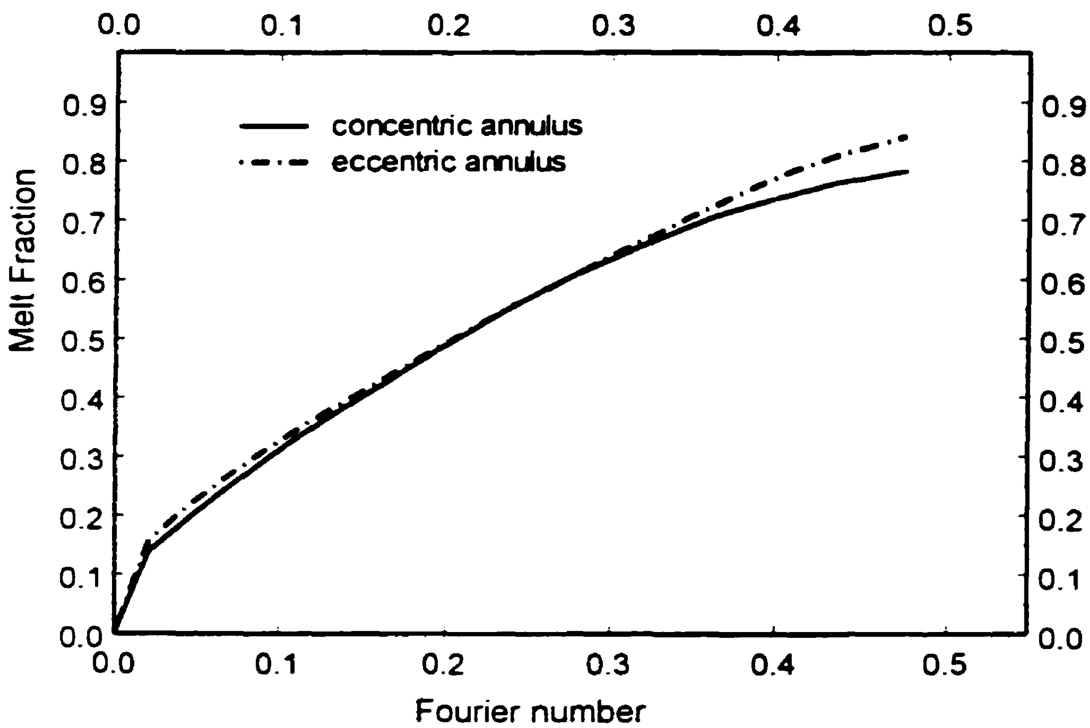

Fig. 4.20 Melt Fraction as a function of Fourier Number ($Ra=2.844\times10^6$)

Fig. 4.21 presents the predicted distribution of isotherms and streamlines at different Fourier numbers for $Ra=2.844\times10^7$ in type A eccentric annulus. The convection cells form much earlier as compared to the earlier case of heating from inside in eccentric annulus type A for $Ra=2.844\times10^6$. However the evolution of streamlines and isotherms is similar to the case of $Ra=2.844\times10^6$. As melting progresses, the cells at the top of the inner cylinder combine together. Bicellular flow is observed in the intermediate stage, thereafter the two cells combine and the flow in the melt remains unicellular throughout the rest of the process. Moreover the shapes of the cells are quite irregular.

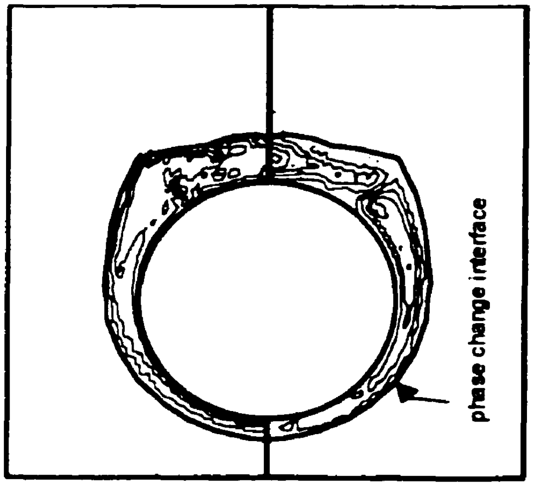

(a1) Fo=0.0432

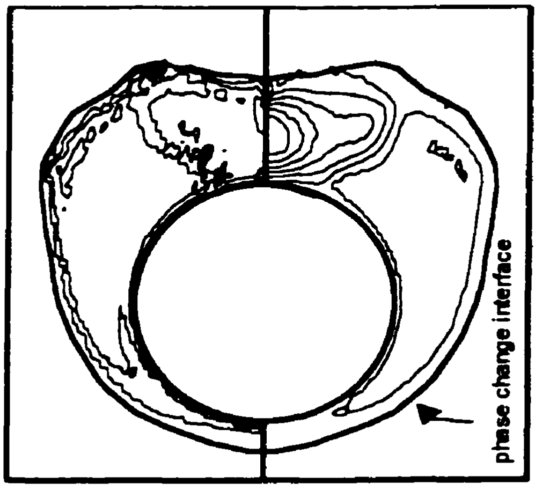

(a2) Fo=0.1296

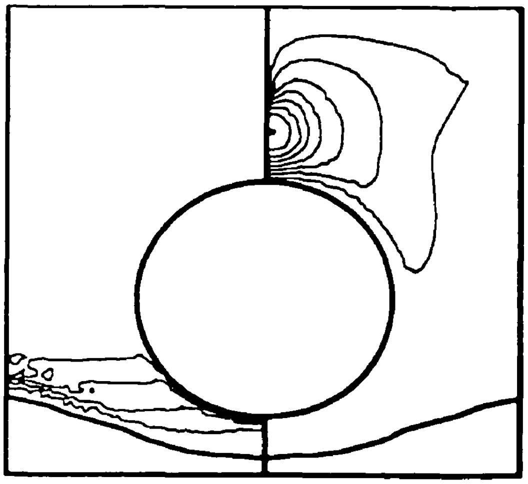

(a3) Fo=0 3024

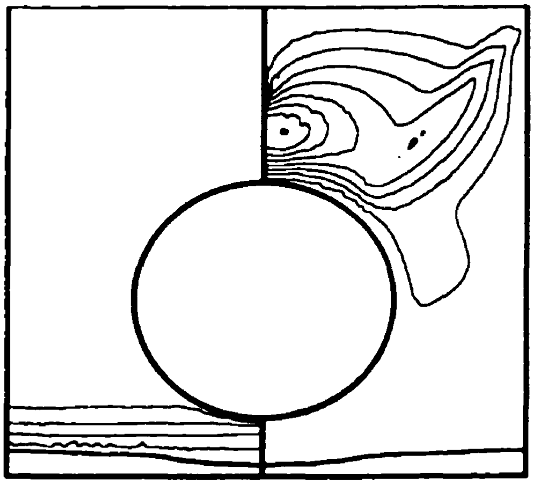

(a4) Fo=0.432

Fig. 4.21 Streamlines(right) and isotherms(left) in the melt zone with Ra=2.844×10^7 for heating from inside

Fig. 4.22 displays the local dimensionless heat flux distribution corresponding to the flow pattern given in Fig. 4.5. As stated earlier, the troughs in the curves correspond to the junction of the convection cells. The single trough in the curve for Fo=0.1296 is a result of bicellular melt flow during this period. Lower heat flux at higher Fourier number results due to thermal stratification which is clearly visible in Fig.4.21 for Fo=0.432.

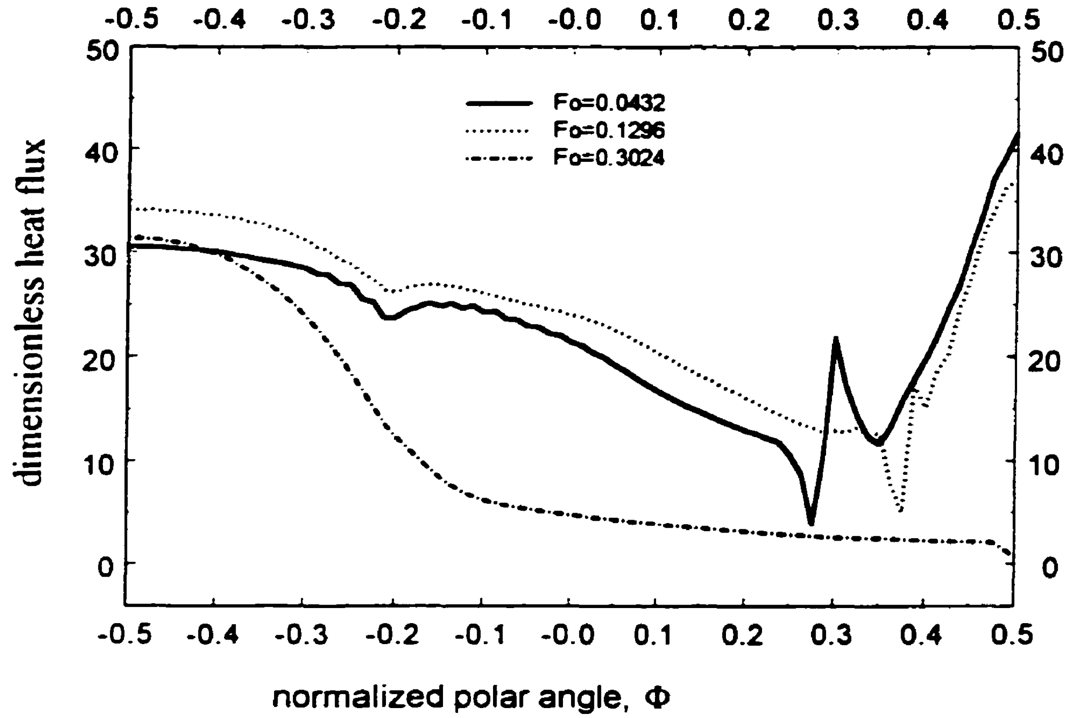

Fig. 4.22 Local Dimensionless Heat Flux Distribution along the Heated Surface ($Ra=2.844\times10^7$)

Fig. 4.23 shows a comparison between the dimensionless cumulative energy charged in the system for both concentric as well as eccentric annuli at the same Rayleigh number of 2.844×10^7. The cumulative energy charged to the system is identical for both concentric and eccentric annuli only during the initial stage. The energy charged to the system is higher for eccentric annulus as compared to the concentric annulus for Fo>0.05 as can be seen in Fig. 4.23. This is due to the fact that more melting occurs in the eccentric annulus as convection continues to play a very important role as opposed to that in concentric annulus.

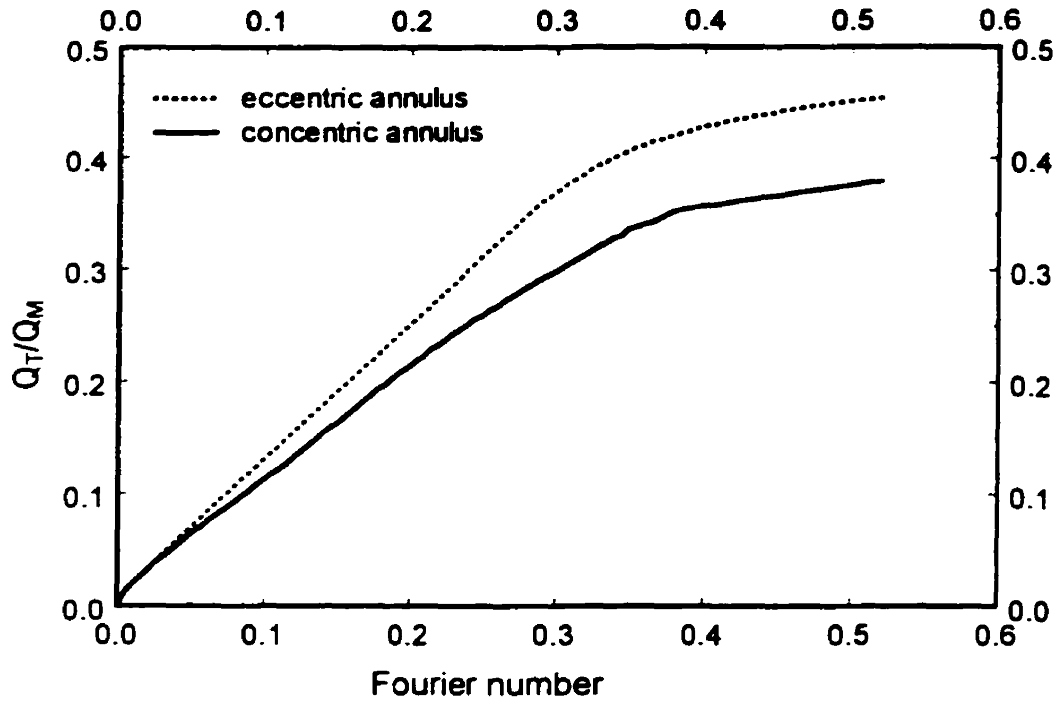

Fig. 4.23 Dimensionless Cumulative Energy Charge as a function of the Fourier number for eccentric and concentric annulus at Ra=2.844×10^7

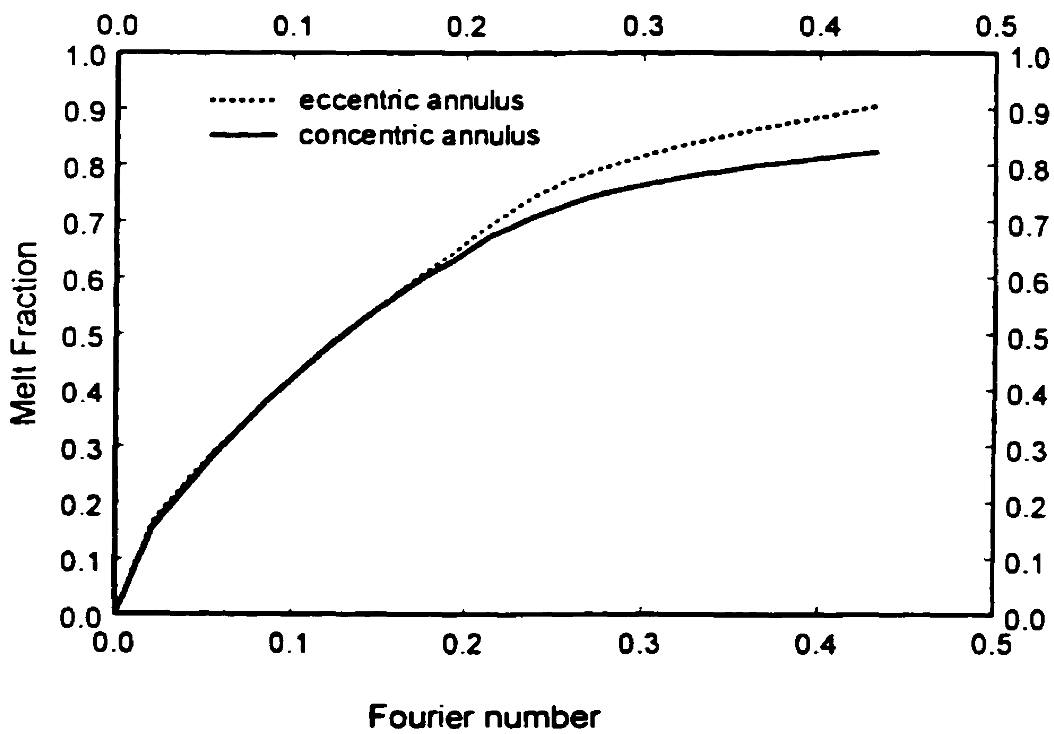

Fig 4 24 Melt Fraction as a function of Fourier Number (Ra=2.844×10^7)

A comparison of the fraction melted as a function of time for eccentric and concentric annuli is presented in Fig. 4.24. More melting is achieved with eccentric annulus rather than that with the concentric annulus.

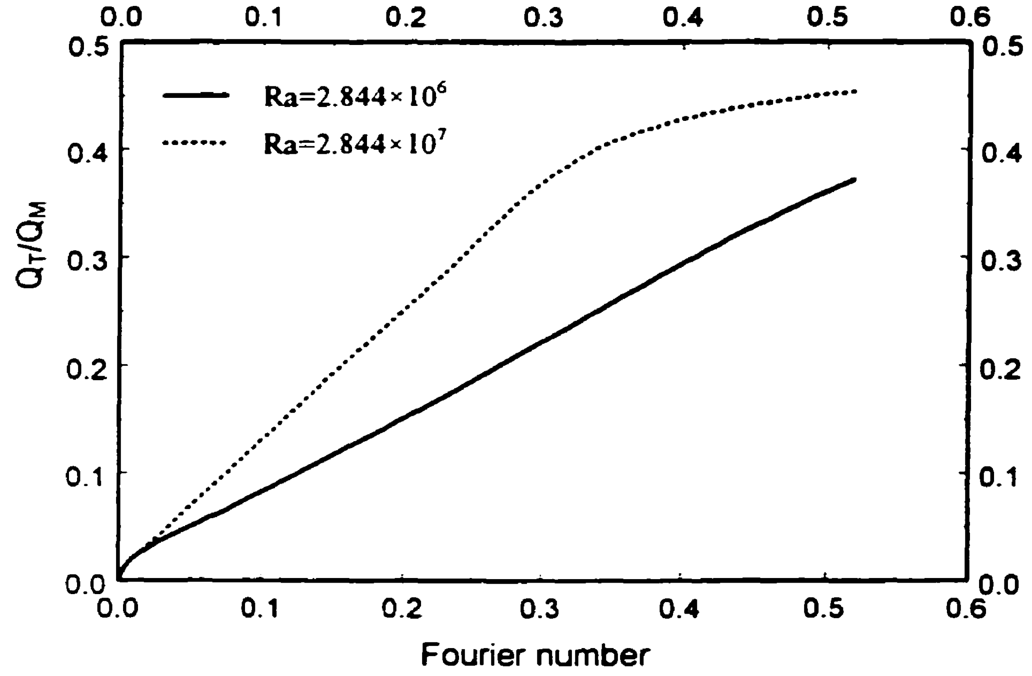

Fig. 4.25 Dimensionless cumulative energy charge curve

Fig. 4.25 shows a comparison between the dimensionless cumulative energy charged in type A horizontal annulus for heating from inside for two Rayleigh numbers. In the early stage heat transfer is mainly due to conduction and the cumulative energy charged is identical in both cases for a short period. Now as the Rayleigh number increases natural convection develops earlier and increases melting due to increased heat charge. This can be attributed to the fact that free convective flow in high Rayleigh number case is much more than the one in the low Rayleigh number case.

A comparison of the fraction melted as a function of time for the two Rayleigh numbers is presented in Fig. 4.26. The rate of energy charged to system is enhanced by the convective flow in the melt which is dominant for high Rayleigh number. Hence the fraction melted is more for higher Rayleigh number as compared to the lower Rayleigh number.

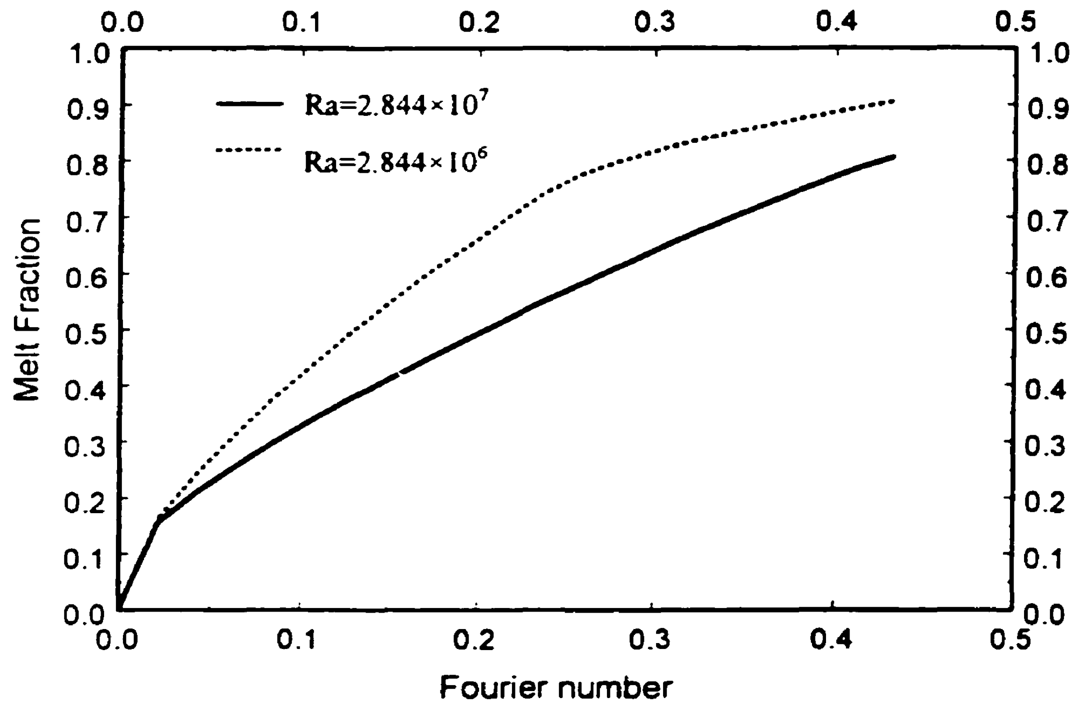

Fig. 4.26 Comparison of melt fraction as a function of Fourier number

From the numerical experiments it can be deduced that eccentric geometry is superior to the concentric one (all other parameters being held constant) due to the vertically upward orientation of the buoyancy force in the melt phase at high Rayleigh numbers. This follows directly from the comparison of the cumulative energy charged and melt fraction (Fig 4.19, 4.20 for Ra=2.844×10^6 and Fig.4.23, 4.24 for Ra=2.844×10^7) for both eccentric and concentric horizontal annuli of type A. An increase in the Rayleigh number results in earlier onset of natural convection adding to the benefit of eccentricity of the annulus increasing the rate of melting. Note that the centerline of the inner container must be below (not above) the axis of the outer cylinder.

4.1.2 Effect of Flipping on the Enhancement of Heat Transfer Rate

Flipping of the PCM container in the type A horizontal annulus is identified as a potential passive means of enhancing the heat transfer rate during the latter stages of the melting process. A schematic representing this idea is represented in Fig.4.27. Numerical experiments were carried out to determine how much the heat transfer rate can be enhanced using this simple procedure.

It is assumed that the liquid phase is well mixed and the melt is stationary after the PCM container is flipped or inverted. However, numerical simulations indicated that as the initial conditions after the PCM container is inverted whether the liquid phase is well mixed and stationary (at pre-flipping conditions) or not has little effect on the heat transfer rates. Therefore, in the subsequent situations the temperature and velocity fields were not modified to the adiabatic mixing cup temperature after the horizontal annulus container is inverted. The solid phase is fixed spatially and not allowed to move as the container is inverted(or flipped).

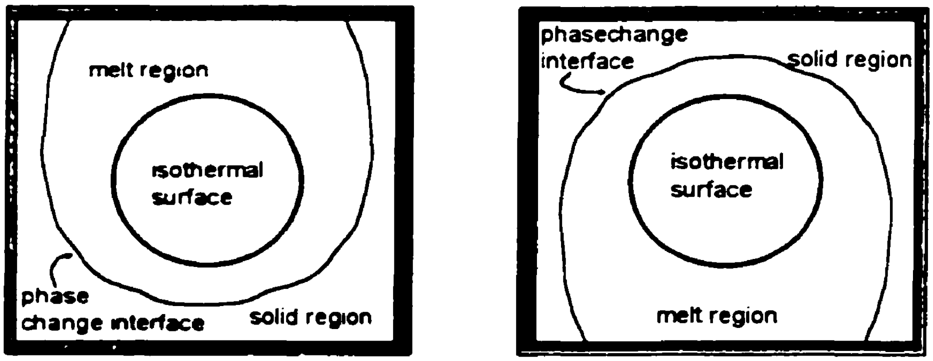

(a) (b)

Fig. 4.27 Schematic of the physical system for annulus type A

Consider the case of heating the inside wall of type A horizontal annulus. The PCM container is flipped at Fo = 0.216 and held in that position for subsequent heating. The effect of flipping on the melting and the heat transfer rate is studied numerically

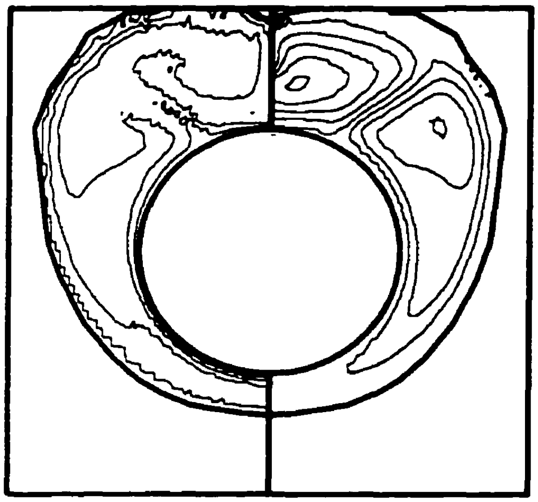

(a1) Fo=0.259

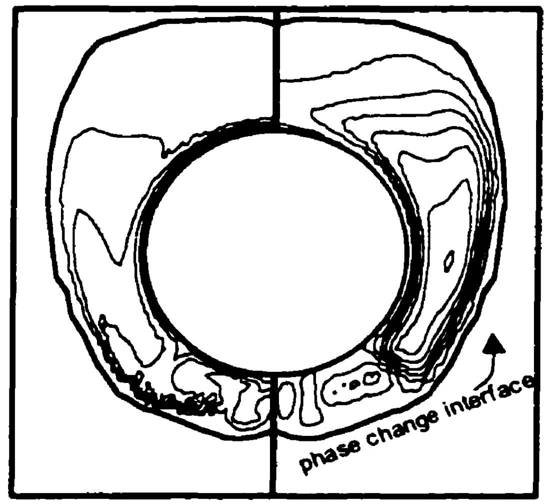

(b1) Fo=0.302

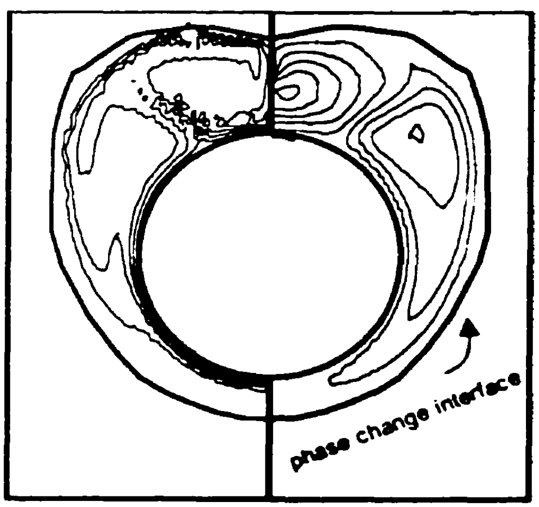

(a2) Fo=0 259

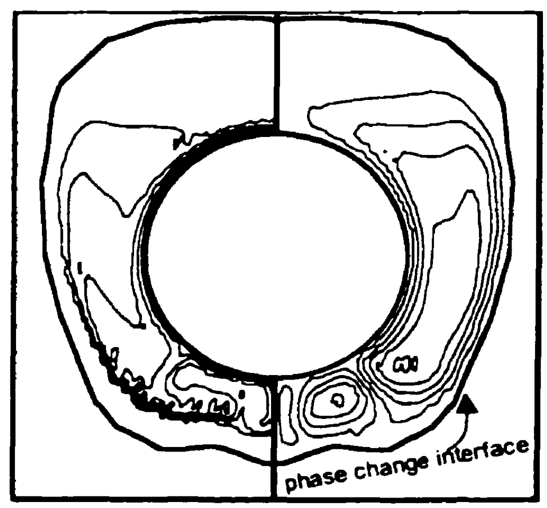

(b2) Fo=0.302

Fig. 4.28x Streamlines(right) and isotherms(left) in the melt zone with Ra=2.844×10^6 for unflipped and flipped horizontal annuli of type A

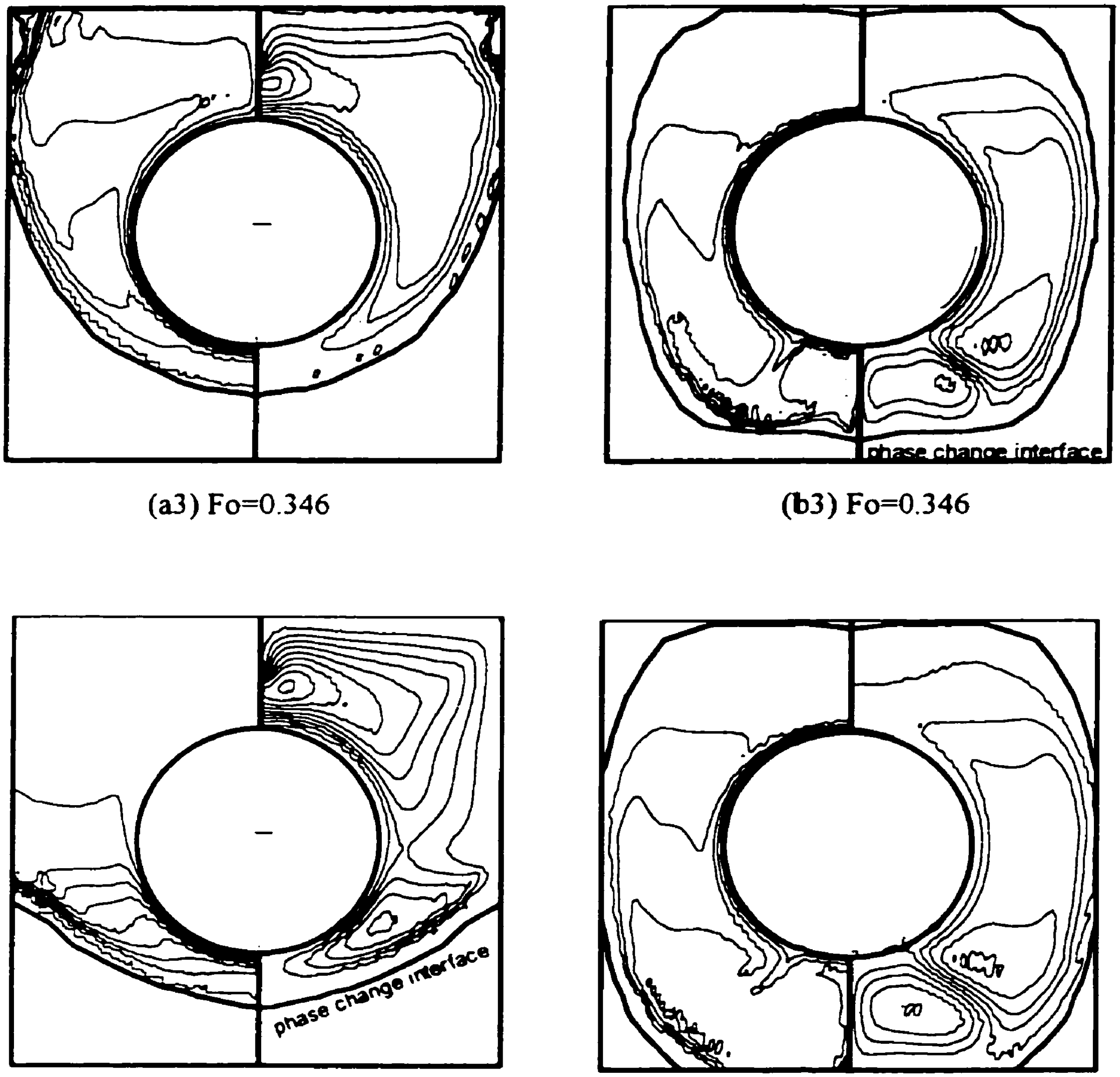

(a3) Fo=0.346 (b3) Fo=0.346

(a4) Fo=0.432 (b4) Fo=0.432

Fig. 4.28y Streamlines(right) and isotherms(left) in the melt zone with Ra=2.844×10^6 for unflipped and flipped horizontal annuli of type A

Fig. 4.28x and 4.28y presents the predicted streamlines and isotherm contours at different dimensionless times (Fourier numbers) for the second period in the case of the flipped horizontal annulus (type A) for a Rayleigh number of 2.84×10^6. No thermal stratification occurs in the flipped container and convection continues to play a significant role; it does not decrease during the last stage of the melting process. This explains why the energy charge rate is enhanced by flipping the horizontal annulus of type A.

Fig. 4.29 displays the local dimensionless heat flux distribution corresponding to the flow pattern shown in Fig.4.28 The crest and the trough in the heat flux distribution curve correspond to the junction of the convection cell. At Fo=0.346 and Fo=0.432 the single trough is a result of bicellular melt flow during this period.

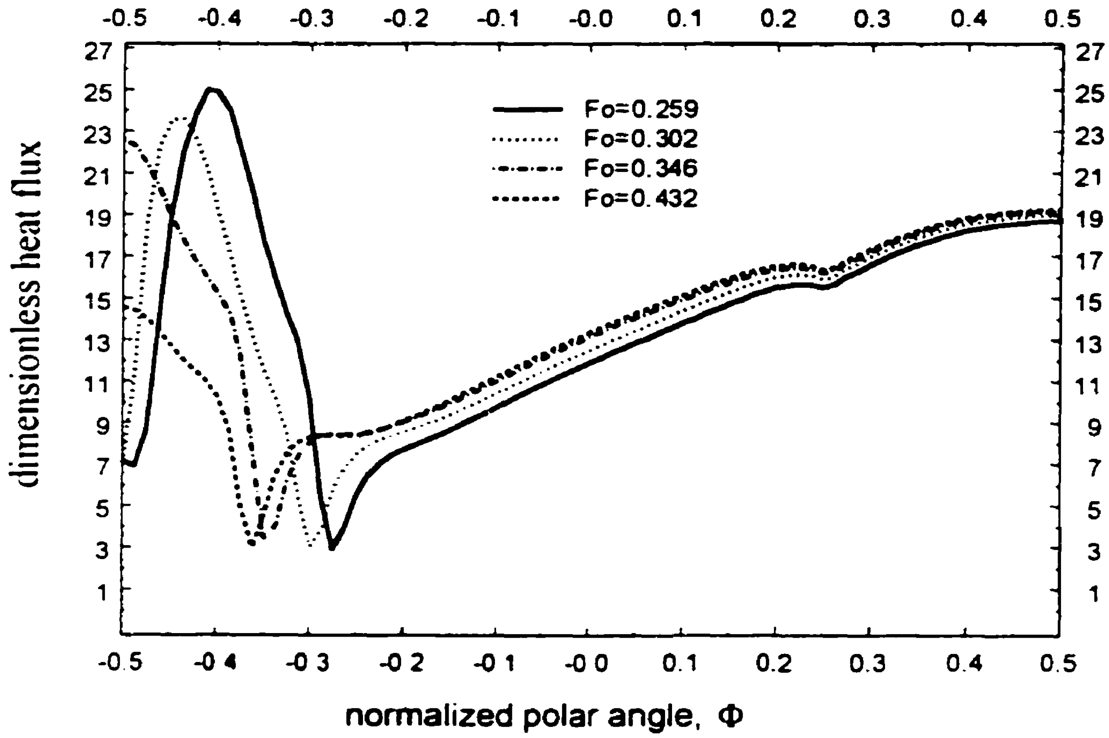

Fig. 4.29 Local Dimensionless Heat Flux Distribution along the Heated Surface ($Ra=2.844\times10^{6}$)

Fig. 4.30 Shows a comparison between the dimensionless cumulative energy charged in the system for both unflipped as well as flipped annuli. As the PCM container is flipped at Fo > 0.216 Fig. 4.31 reveals that the cumulative energy charged for the flipped case is higher than that for the unflipped case. This can be attributed to the fact that for the flipped horizontal annulus bicellular flow continues and hence keeping the

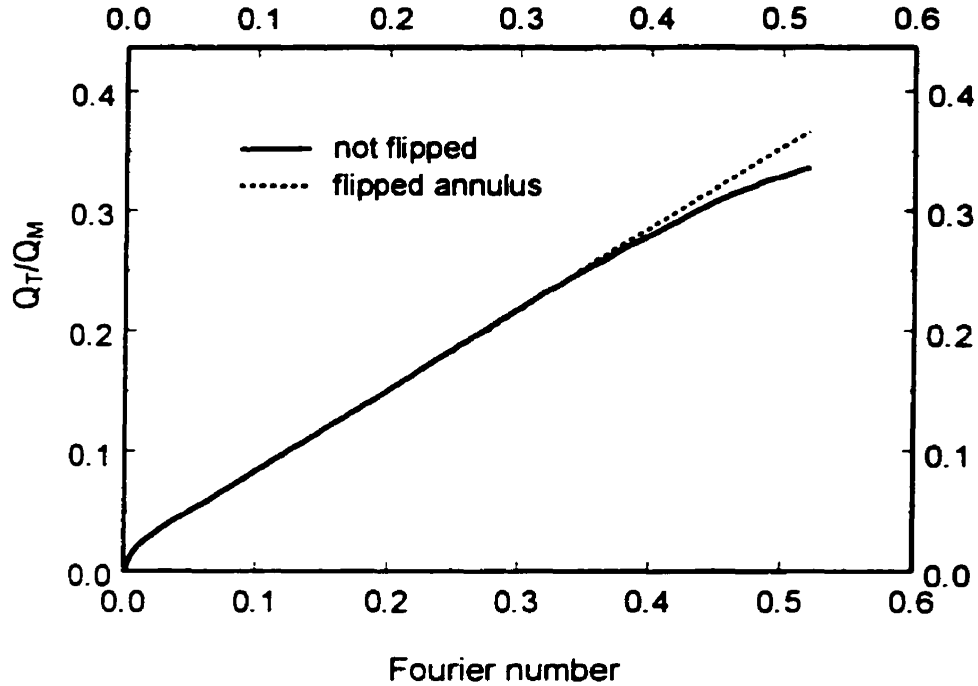

Fig. 4.30 Comparison of Dimensionless Cumulative Energy Charge as a function of the Fourier number(Ra=2.844×10^6)

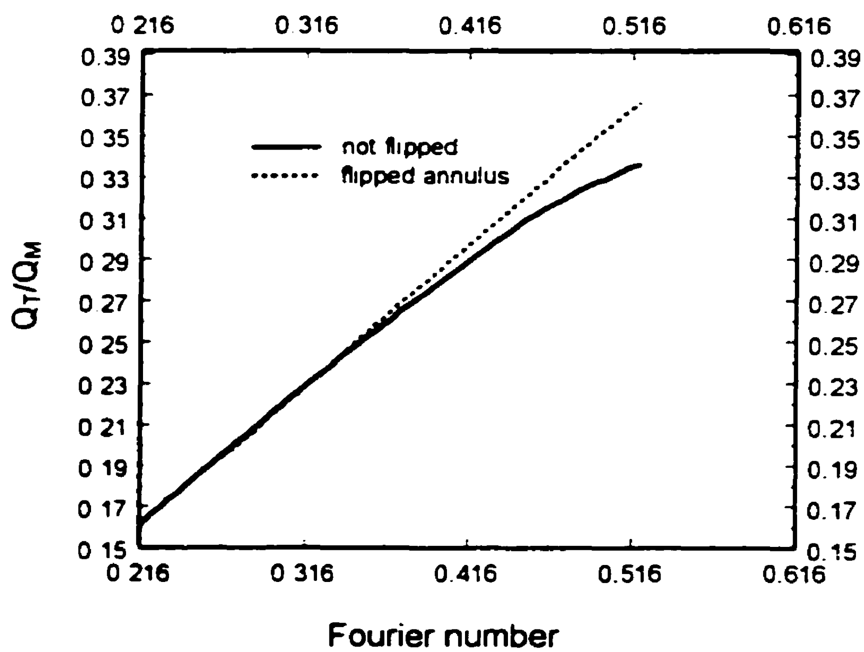

Fig. 4.31 Amplification of Fig.4.30 (Ra=2.844×10^6)

convection flow active thereby increasing the heat transfer rate. But for the unflipped case it is clearly observed in Fig. 4.2 that thermal stratification occurs and reduces the heat transfer rate.

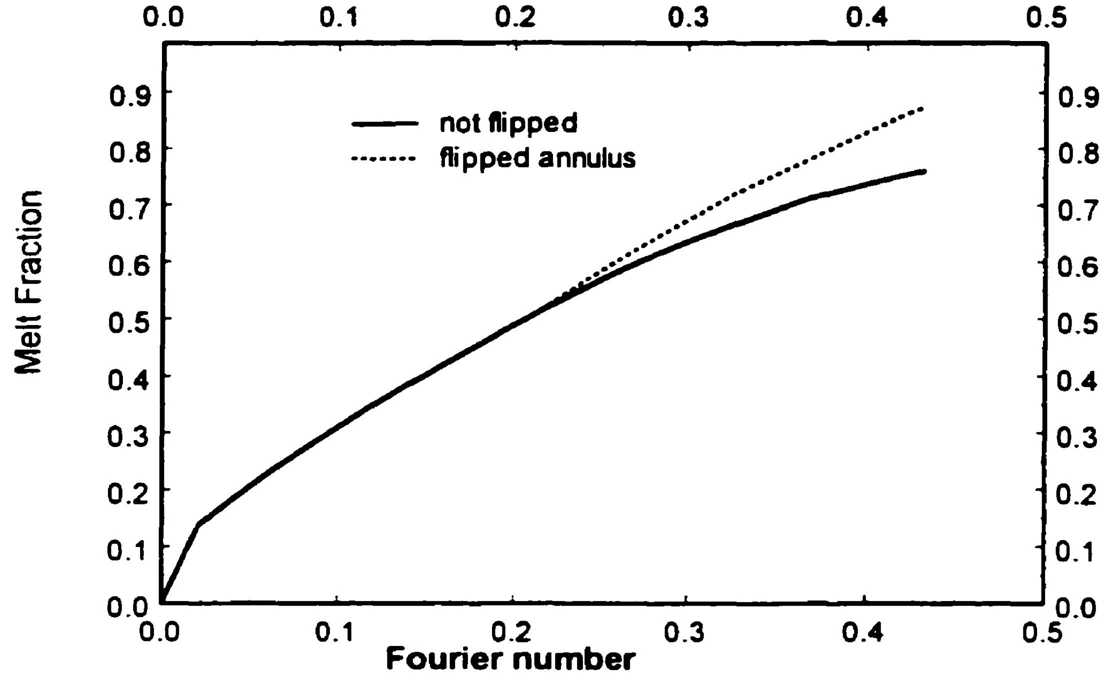

Fig. 4.32 Melt Fraction as a function of Fourier Number (Ra=2.844×10[6])

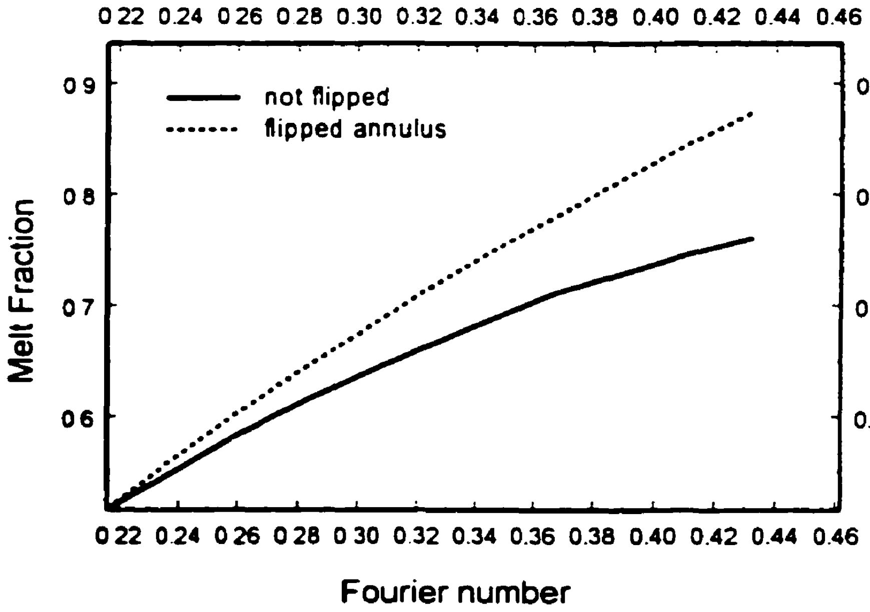

Fig. 4.33 An Amplification of Fig. 4.31(Ra=2.844×10[6])

A comparison of the fraction melted for both the flipped and unflipped horizontal annulus of type A is presented in Fig.4.32. From the figure it is obvious that there is enhancement in the melting rate with the flipped container relative to the conventional unflipped case at long elapsed times.

It should be noted that the concept of flipping at an appropriate time during the melt cycle (storage or charge cycle) may not be feasible for all design configuration of PCM storage type heat exchangers. Also, the beneficial effect of flipping appears only during the late stages of melting. Again, these results assume that the unmelted portion of the PCM is fixed i.e not free to move during melting or upon flipping.

4.2 MELTING HEAT TRANSFER IN TYPE B ANNULUS

4.2.1 Effect of Heating inside wall, outside wall and both walls

For type B annulus, a schematic diagram of the physical model simulated is shown in Fig.4.34. To study the effect of heating only inside wall, the inner wall of the tube is maintained at a constant temperature higher than the melting point of the PCM. The outer wall is adiabatic. The PCM used for the numerical experiments is n-octadecane (99% pure) and the parameters for the computed problem are the same as listed in Table 4.2.

The various dimensionless numbers used are defined as follows:

$$\theta = \frac{T - T_m}{T_w - T_m}, \quad Fo = \frac{t\alpha_l}{d^2}, \quad \Pr = \frac{c_l \mu}{k_l}, Ra = \frac{\rho^2 c_l g \beta d^3 (T_w - T_m)}{\mu k_l}, \quad Ste = \frac{c_l (T_w - T_m)}{\Delta h} \qquad (4)$$

The Rayleigh and Prandtl number are based on the inside diameter of the annulus.

The local dimensionless heat flux along the heated wall is given as $\partial\theta/\partial R$, where

$$\theta = \frac{T - T_m}{T_w - T_m} \quad \text{is dimensionless temperature, and} \qquad (5)$$

$$R = \frac{r - r_i}{r_b - r} \quad \text{normalized polar angle } \Phi = \phi / \pi$$

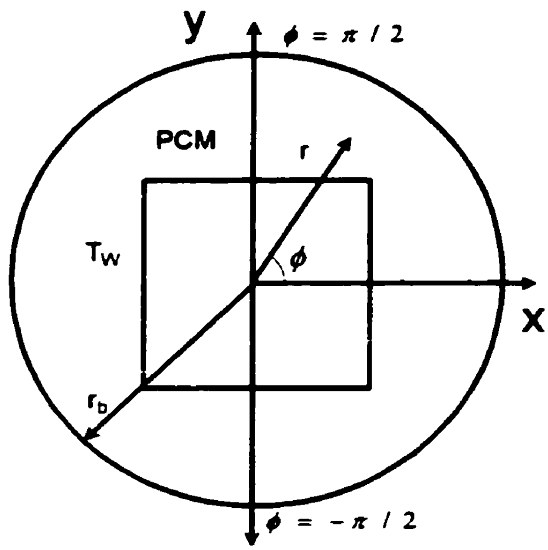

Fig.4.34 Schematic diagram of the physical model for type B annulus

Fig. 4.34 displays the predicted distributions of isotherms (left) and streamlines (right) at various Fourier numbers for Ra=2.844×10^6. It is seen that at Fo=0.0432 a total of six convection cells develop. The predicted phenomena are similar to those obtained by Gong *et al.* [4] for melting in a rectangular cavity heated from below. The size of the convection cells increases and the number of cells decreases with increase in the melt depth. The increase in the melt depth further results in the formation of a single convection cell at the top heated surface of the inner tube. At Fo=0.26 it is found that a bicellular flow exists and that only a small portion of the PCM at the bottom remains to be melted.

Figs. 4.36, 4.37 and 4.38 display the dimensionless heat flux distributions $\partial\theta/\partial Y$, $\partial\theta/\partial X$, $\partial\theta/\partial Y$ along the heated bottom wall, vertical wall and top wall, respectively corresponding to the flow patterns shown in Fig. 4.35. Moving from left to the right along the bottom heated wall the heat flux is almost constant except for the troughs at the junction of the convection cells as displayed in Fig. 4.36. Along the heated vertical wall the heat flux decreases smoothly The melt has the highest temperature difference at the bottom of the inner tube which results in higher heat flux. The dimensionless heat flux distribution along the inner heated top wall is wave like for Fo=0.0432 and 0.086 corresponding to the multiple convection cells. There are 3 crests and 2 troughs on the

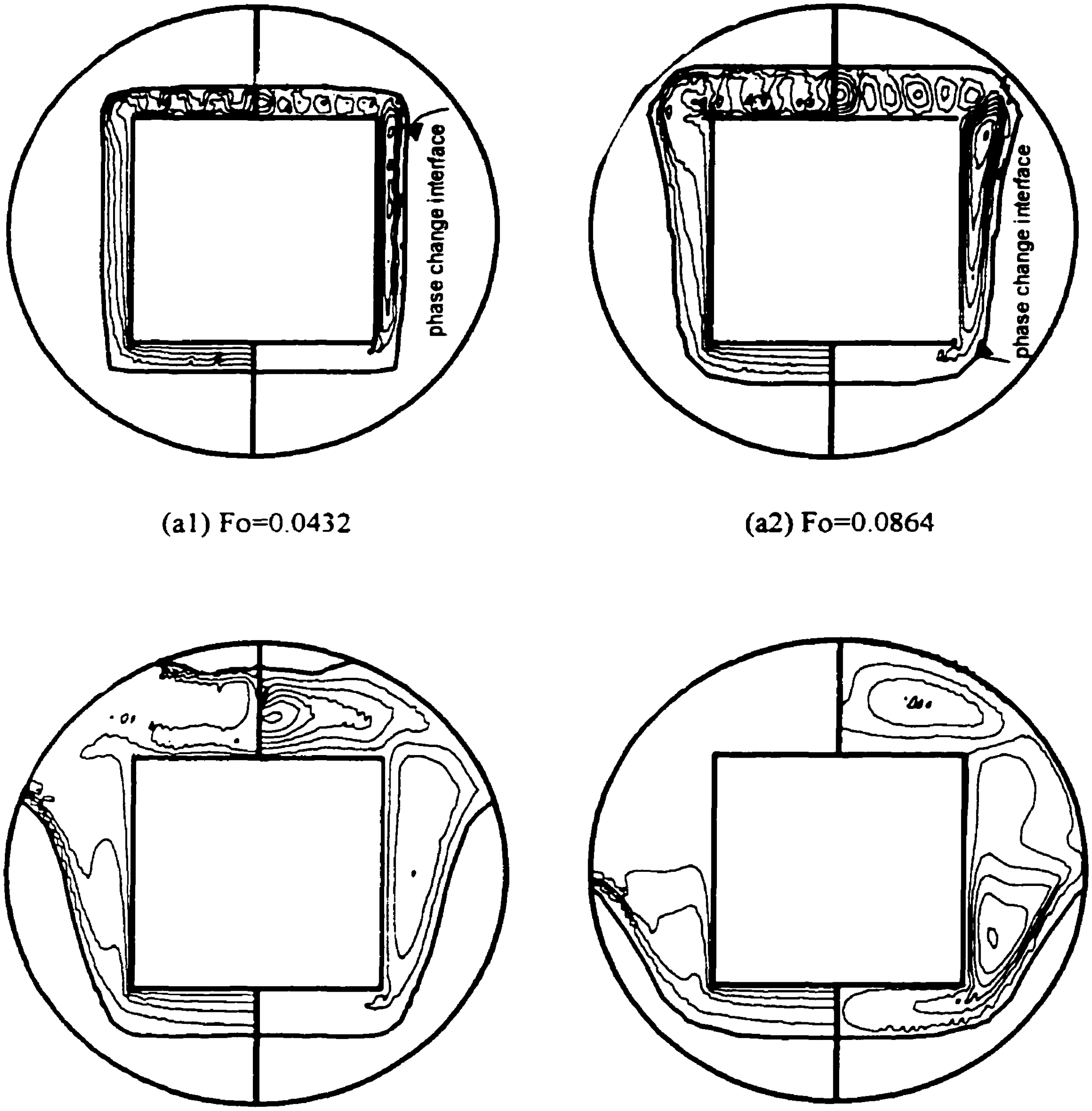

(a1) Fo=0.0432 (a2) Fo=0.0864

(a3) Fo=0.1728 (a4) Fo=0.259

Fig. 4.35 Streamlines (right) and isotherms (left) in the melt zone with Ra=2.844×10^6 for heating from inside

dimensionless heat flux curve of Fo=0.0432 displayed in Fig. 4.38. These crests and troughs correspond to the five junctions of the six convection cells visible in the streamline contours in Fig.4.35(a1). The first crest from left corresponds to the junction of the first and second convection cells. The flow direction of the first circulation is clockwise and the second circulation is anti-clockwise. The liquid layers from the two circulation cells are cooled after passing the phase change interface and then reach the junction of the two circulation zones at the bottom. This causes a low temperature zone to appear near the junction at the bottom of the inner surface of the container. As the bottom surface of the inner wall is isothermal, a low temperature near the bottom isothermal surface means a large temperature difference for heat transfer. This results in a higher heat flux. Similarly the first trough from left corresponds to the junction of the second and third convection cells in Fig. 4.35(a1). At the junction of the two cells a high temperature zone is developed which results in lower temperature difference between the wall and the melt and hence a lower heat flux.

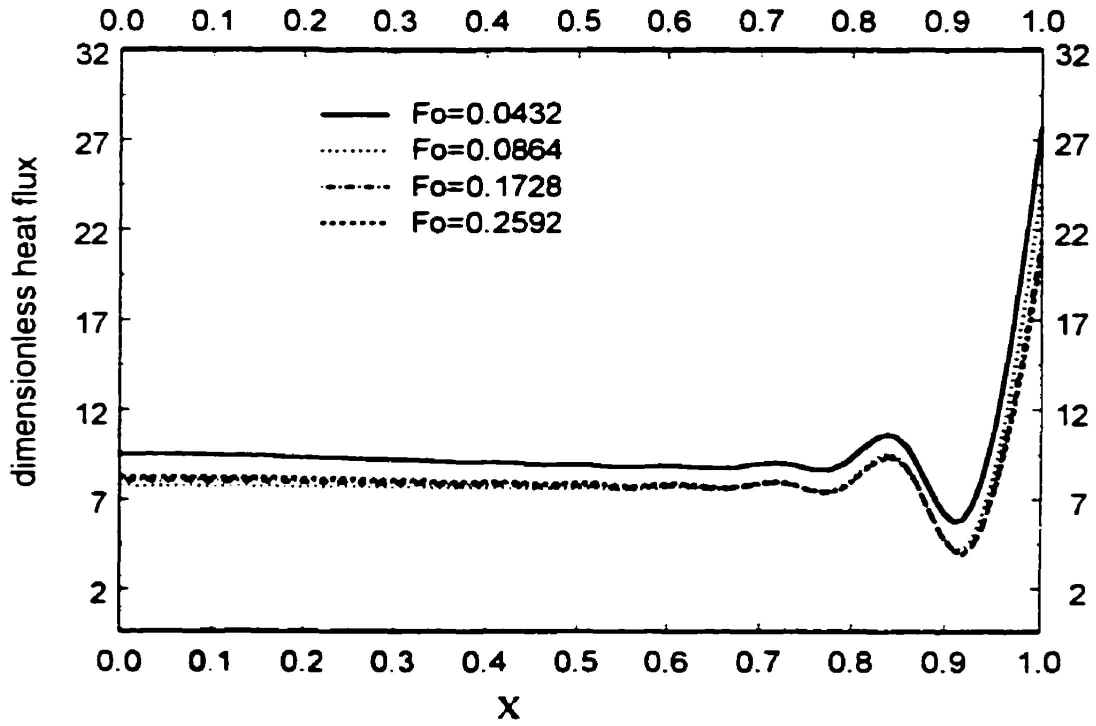

Fig. 4.36 Dimensionless heat flux $\partial\theta/\partial Y$ along the heated bottom wall at different dimensionless times

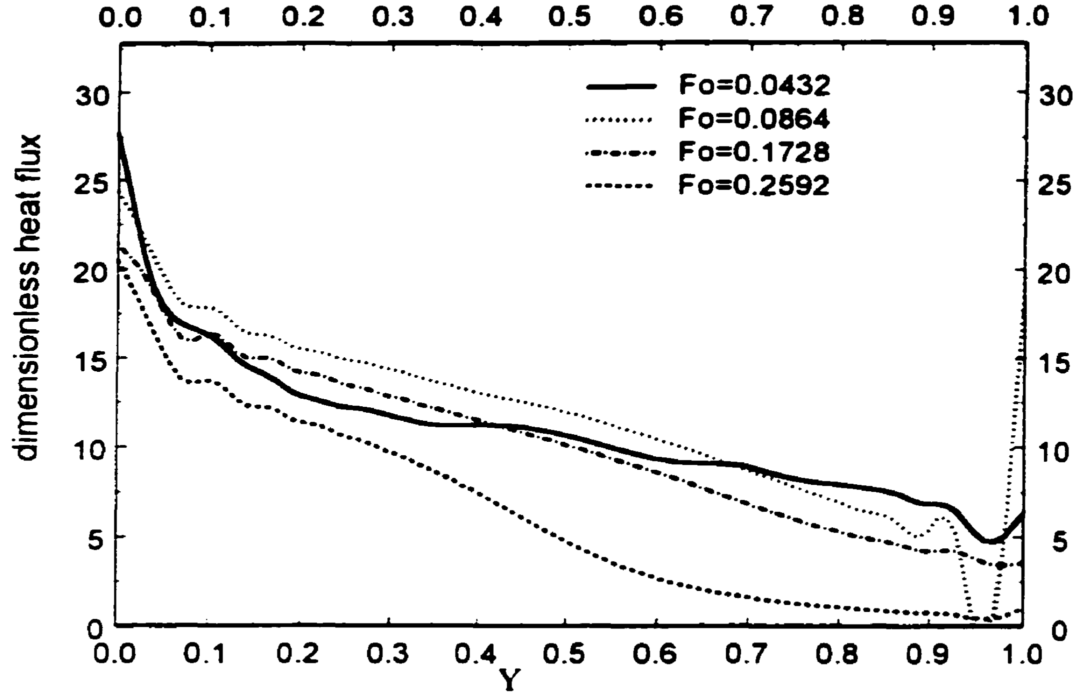

Fig. 4.37 Dimensionless heat Flux $\partial\theta/\partial X$, along the heated vertical wall at different dimensionless times

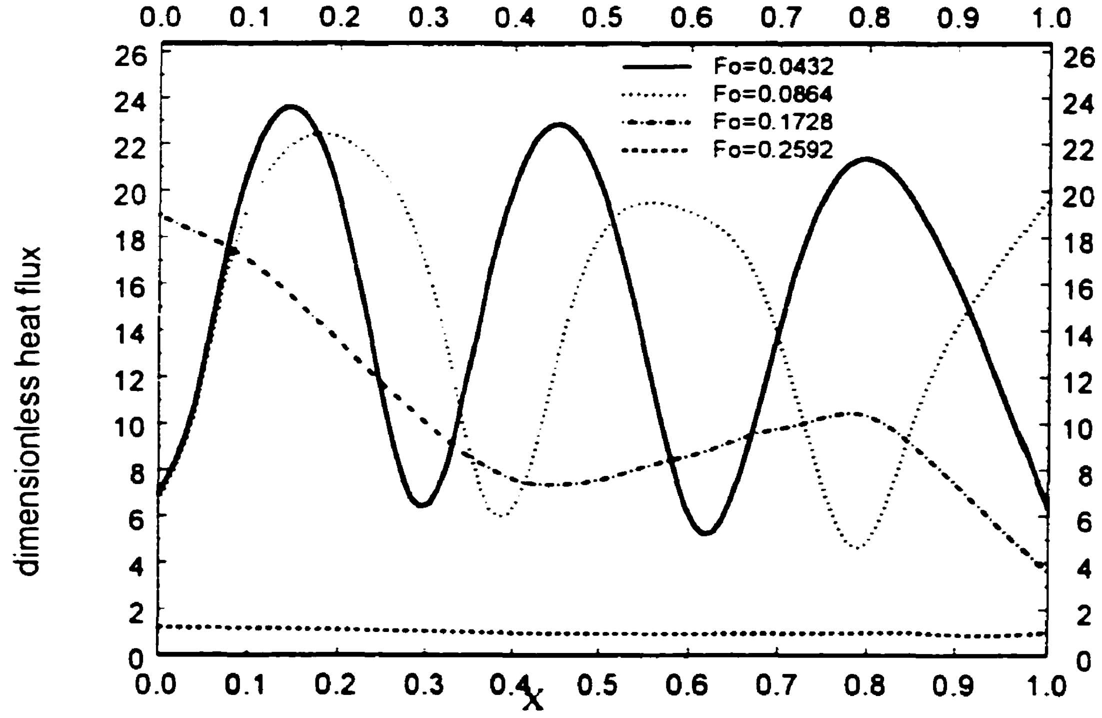

Fig. 4.38 Dimensionless heat flux $\partial\theta/\partial Y$ along the heated top wall at different dimensionless times

Fig. 4.39 presents the variation of the dimensionless cumulative energy charged with the dimensionless time (Fourier number). The value of Q i.e, the cumulative energy charged per unit length is zero at the beginning and increases over the melting process toward Q_T, the cumulative energy charged in the melting process.

The maximum amount of energy which can be charged during the melting process is

$$Q_M = \rho A_{xy} \left[f_H(T_w) - f_H(T_m) \right] \qquad (6)$$

The dimensionless cumulative energy charged increases linearly during the first half of the melting process. Afterwards, the charge rate begins to slow down. This occurs due to thermal stratification during the terminal stage of the melting process leading to a lower heat transfer rate at large Fourier numbers.

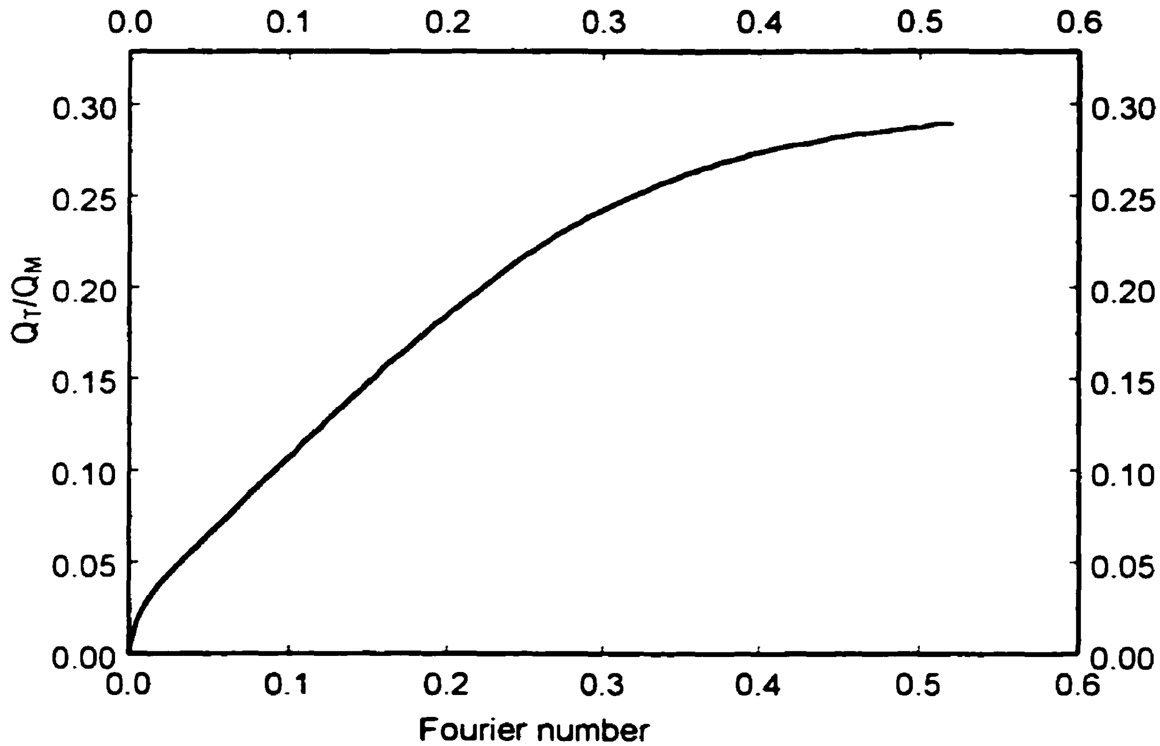

Fig 4.39 Dimensionless energy charge curve

Numerical experiments were carried out to study the effect of heating outside wall of type B annulus. The inside wall is assumed to be adiabatic for this case.

Fig. 4.40 presents the predicted streamlines and isotherms at different Fo values for the computed problem (Ra=2.844×10^6). During the initial stages the heat transfer is controlled mainly by conduction. As time progresses convection cells develop and at Fo=0.0864 four cells are observed. Later on these cells merge to form two large cells and the flow continues to remain bicellular until the whole PCM solid melts. No thermal stratification is observed even at the late stages of melting as good mixing appears to take place, until full melting of the PCM solid occurs.

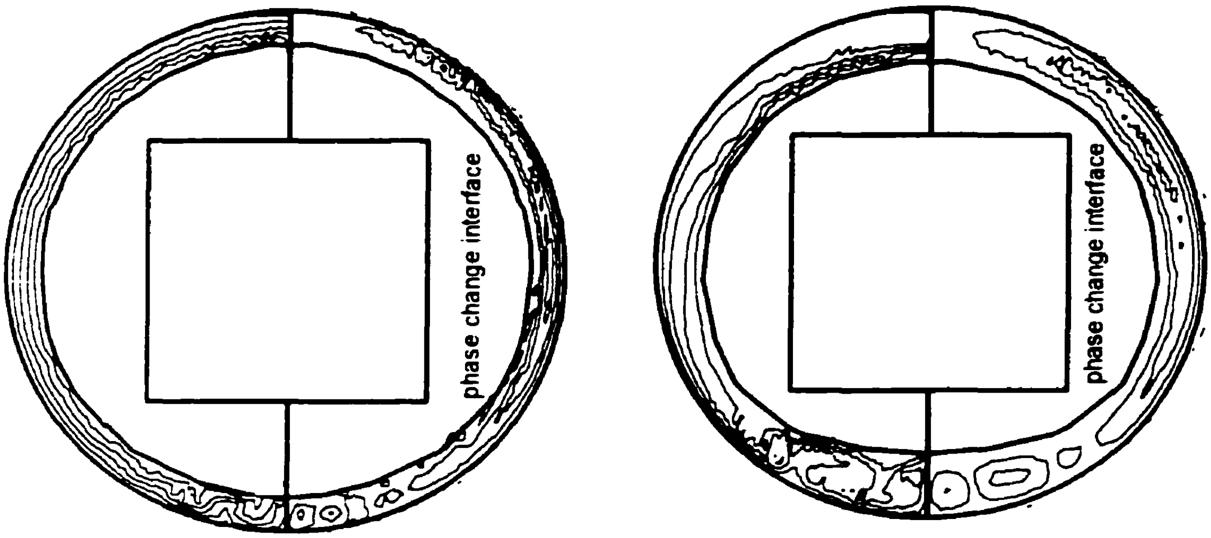

(a1) Fo=0.0432 (a2) Fo=0.0864

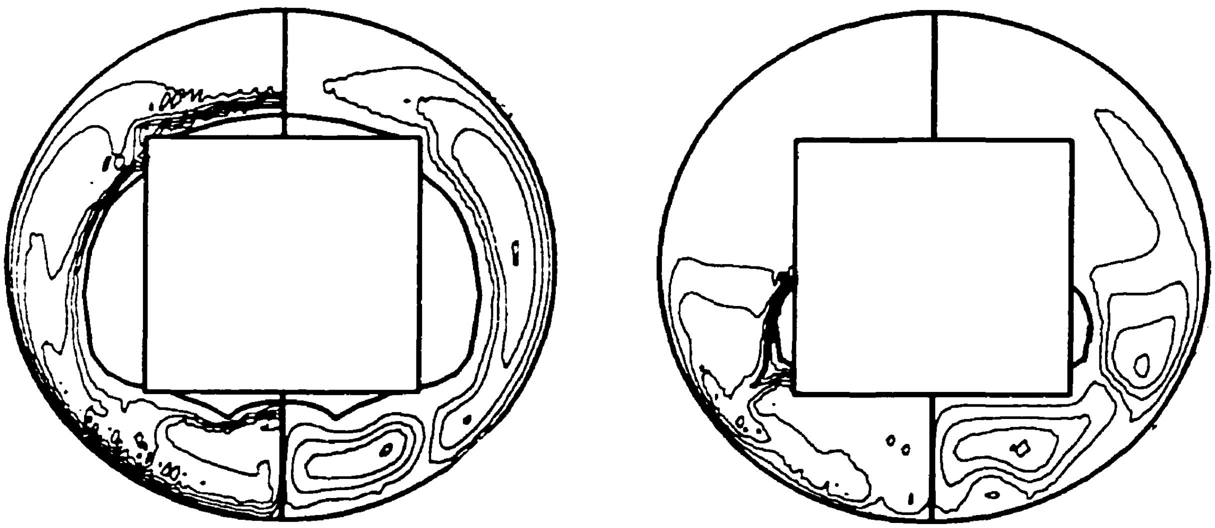

(a3) Fo=0 216 (a4) Fo=0.3024

Fig. 4.40 Streamlines(right) and isotherms(left) in the melt zone with Ra=2.844×10^6 for heating from inside

Displayed in Fig. 4.41 are the local dimensionless heat flux, $\partial\theta/\partial R$, distributions along the heated outer wall corresponding to the flow patterns presented in Fig. 4.40. With the same explanation as noted earlier, the troughs in the curves correspond to the junction of the adjacent convection cells. At Fo=0.086, the two crests and one trough correspond to the junction of the four convection cells shown in Fig4.40 (a2). For Fo=0.3024, the lower heat flux is due to the fact that at this time most of the solid is melted and the difference in temperature between the outer wall and melt is not very high.

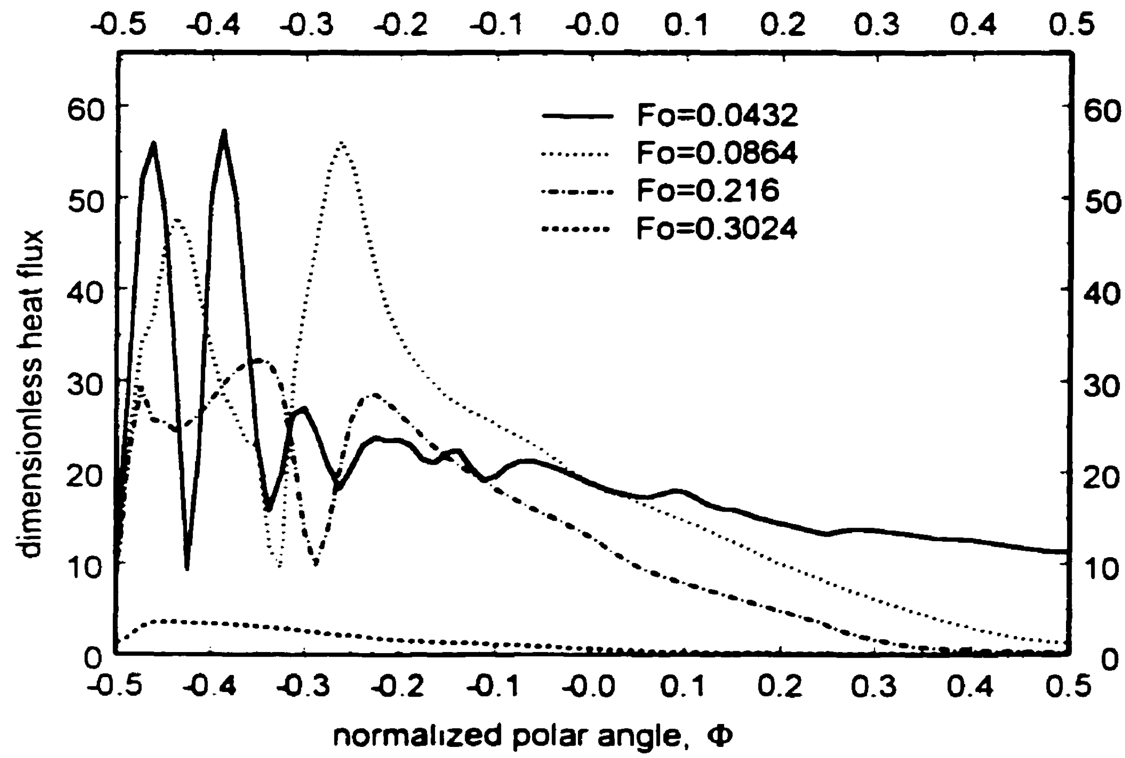

Fig. 4.41 Local Dimensionless heat flux distribution along the heated surface ($Ra=2.844\times10^6$)

Fig.4.42 presents the variation of the dimensionless cumulative energy charged as a function of the Fourier number. As can observed from this figure the energy charge rate increases nearly linearly initially and at the final stage of the melting it is almost constant. Near the outer wall of the tube most of the solid is melted and hence there is no further increase in the energy charge.

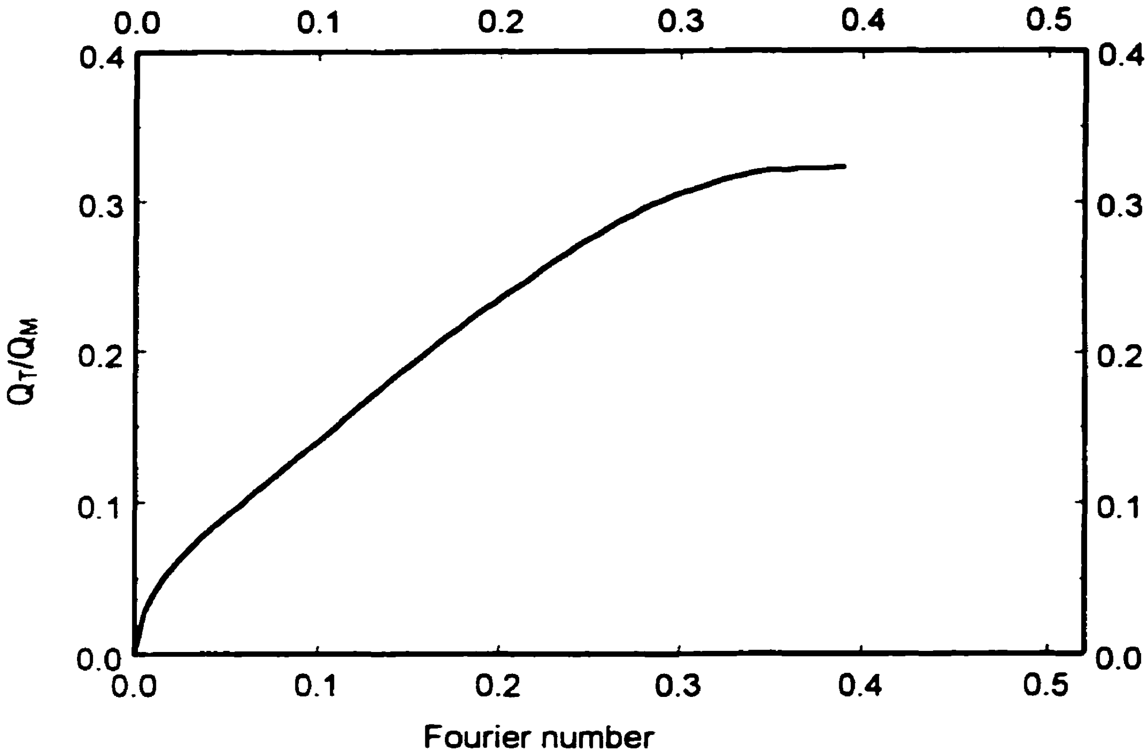

Fig. 4.42 Dimensionless energy charge curve (Ra=2.844×10^{6})

To study the effect of heating the inside wall and outside wall simultaneously numerical simulations were carried out using the numerical model described in Chapter 3. Both walls of the tube are maintained at a temperature higher than the melting point of the PCM. The parameters are identical to those listed in table 4.1.

Displayed in Fig. 4.43 are the predicted distributions of isotherms (left) and streamlines (right) at various dimensionless times for Ra=2.844×10^{6}. At Fo=0.0432 it is observed that the distribution of streamlines and isotherms is the same as the one obtained for heating the inside wall and outside walls separately. This is due to the fact that there is no interaction between the melt zones formed by heating the inside wall and outside wall. However as time progresses interaction between the melt zones leads to more melting and hence at Fo=0.0864 only a small portion of the PCM solid remains. Later on, the entire solid melts. Depending on the location a number of convection cells are observed of different sizes. This increased melting is a result of the dominant effect of convection.

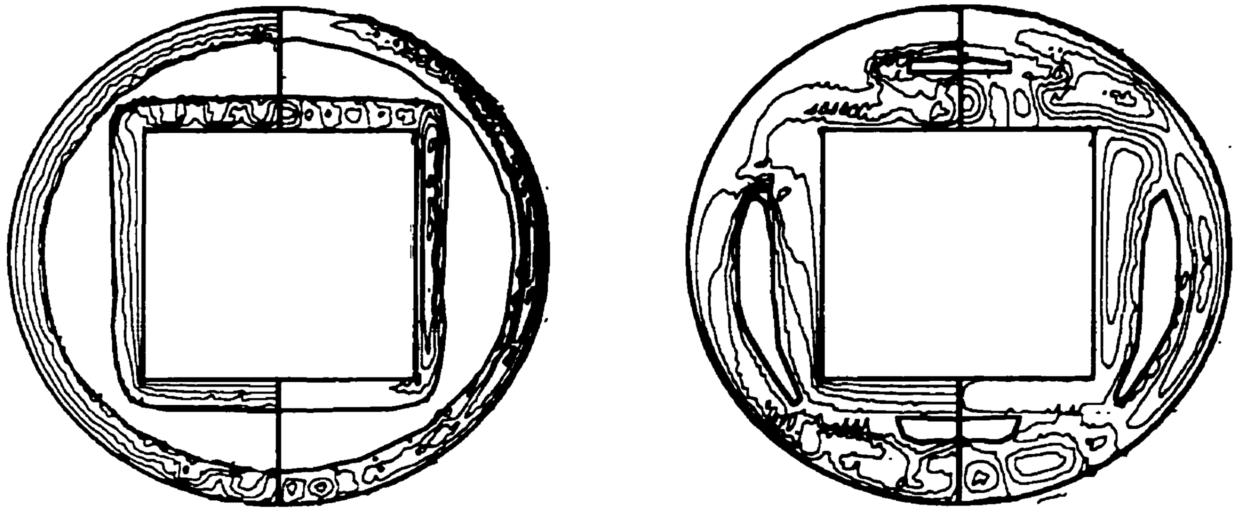

(a1) Fo=0.0432 (a2) Fo=0.0864

Fig. 4.43 Streamlines(right) and isotherms(left) in the melt zone with Ra=2.844×10^{6} when both the inside and outside walls are heated

Figures 4.44,4.45 and 4.46 present the local dimensionless heat flux distributions $\partial\theta/\partial Y$, $\partial\theta/\partial X$, $\partial\theta/\partial Y$ along the heated isothermal bottom wall, vertical wall and top wall of the inner tube, respectively corresponding to the flow patterns shown in Fig. 4.43. Moreover, Fig. 4.47 displays the local dimensionless heat flux $\partial\theta/\partial R$ along the heated outer wall. As shown in Fig.4 44 it is observed that the heat flux is almost uniform except for the troughs at the junction of the convection cells. Similarly along the heated vertical wall of the inner tube the heat flux drops gradually. Moving along the heated top wall of the inner tube it is seen that a wave like pattern is observed which corresponds to the multiple convection cells as displayed in Fig 4 46 With the same explanation applicable here the troughs and crests correspond to the junctions of the convection cells. Fig. 4.47 shows the occurrence of three troughs which represent the four convection cells as observed in Fig. 4.43(a2) at Fo=0 0864

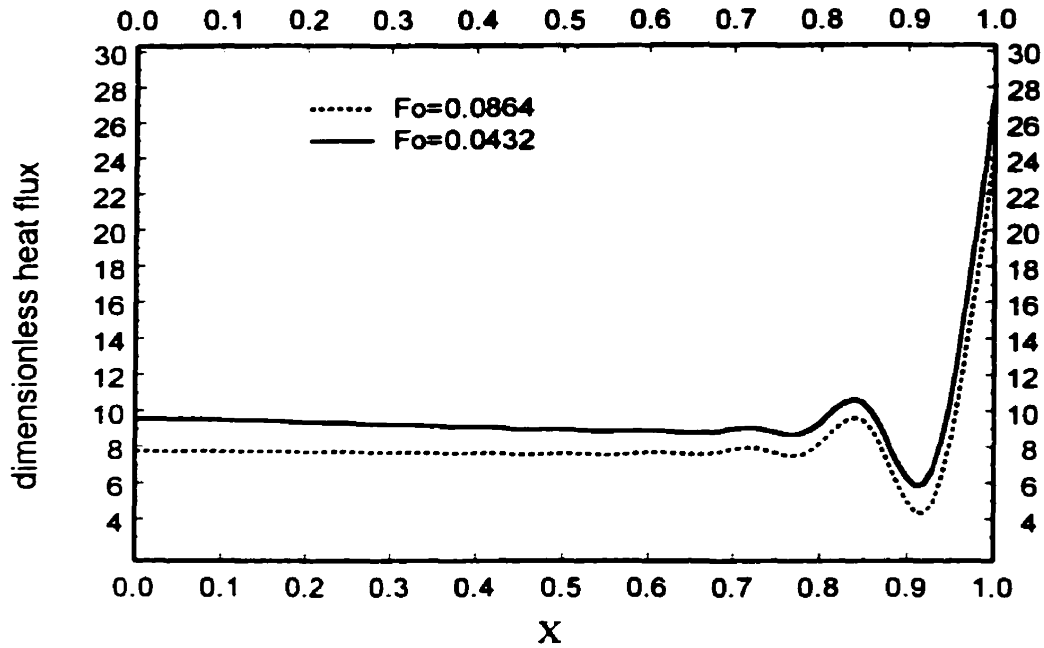

Fig. 4.44 Dimensionless heat flux $\partial\theta/\partial Y$ along the heated bottom wall at different dimensionless times (Ra=2.844×10^{6})

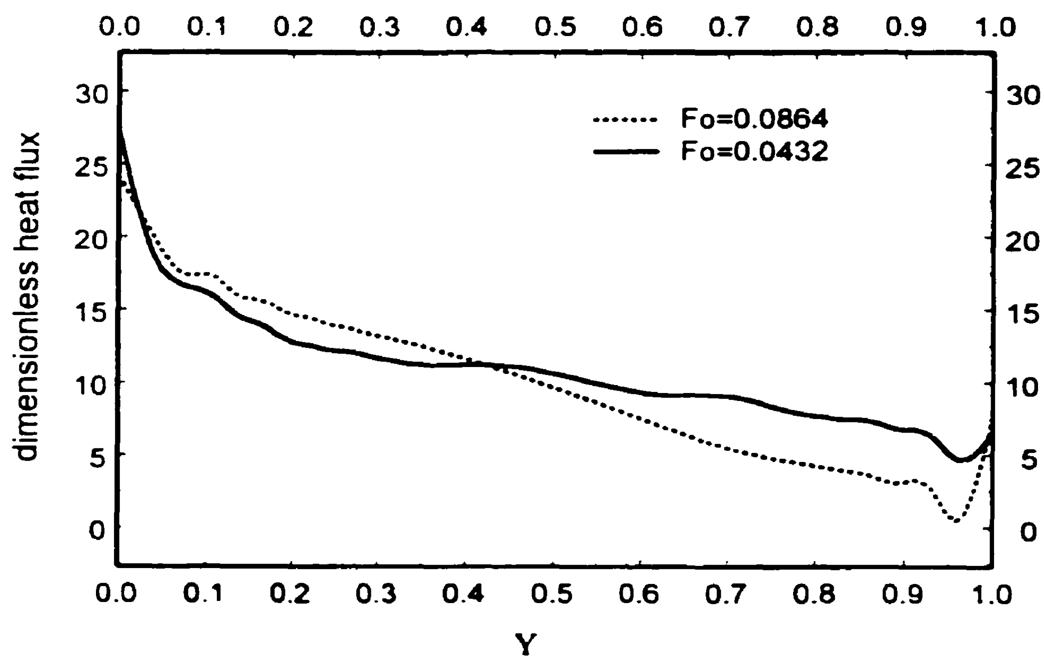

Fig. 4.45 Dimensionless heat Flux $\partial\theta/\partial X$. along the heated vertical wall at different dimensionless times (Ra=2.844×10^{6})

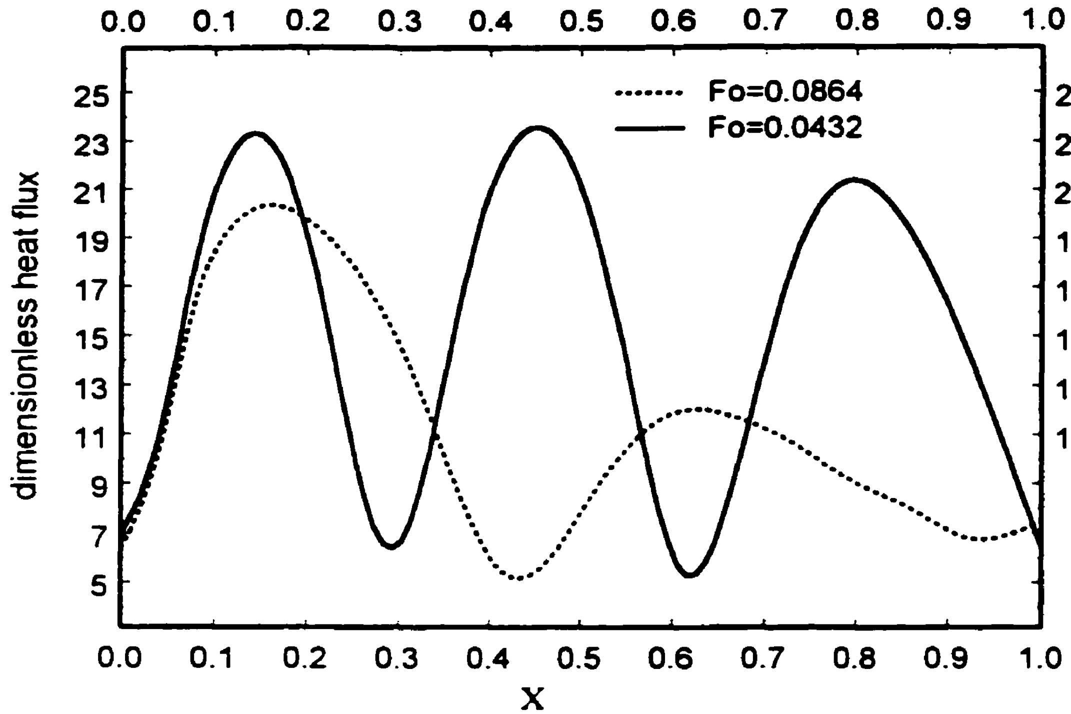

Fig. 4.46 Dimensionless heat flux $\partial\theta/\partial Y$ along the heated top wall at different dimensionless times (Ra=2.844×10^6)

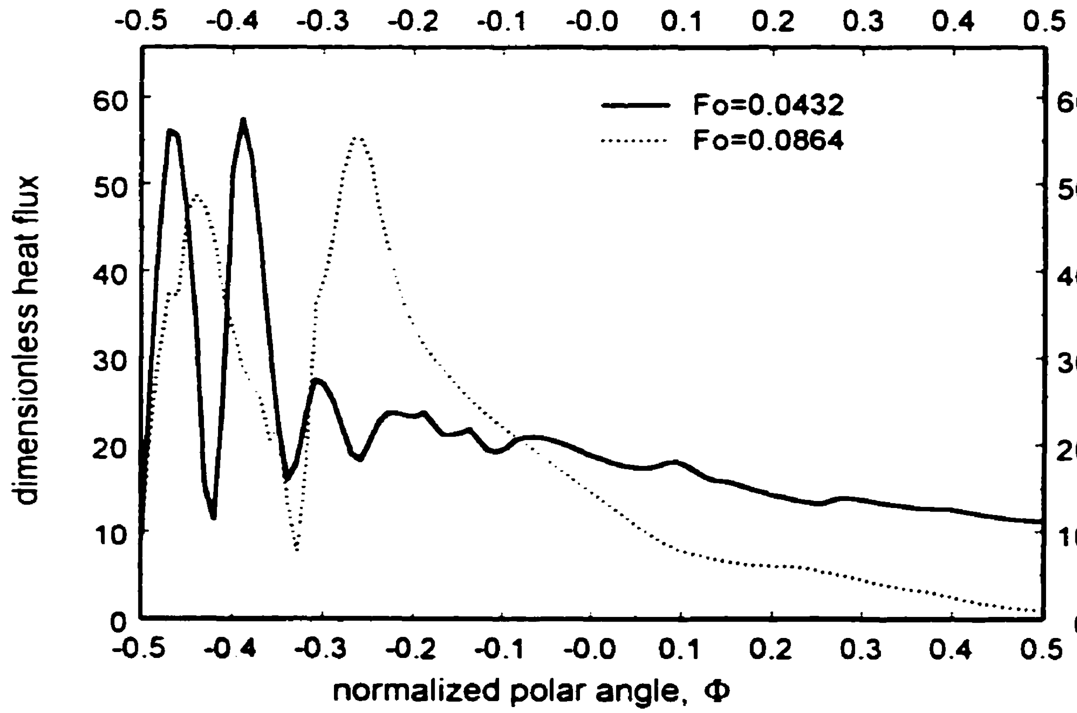

Fig. 4.47 Local Dimensionless heat flux distribution along the heated surface (Ra=2.844×10^6)

Fig.4.48 presents the dimensionless cumulative energy charged as a function of the Fourier number when both walls of the annulus are heated. It can be seen that the energy charged remains almost linear until the final stage of the melting when it remains constant. This can be attributed to the fact that in the final stage almost all the PCM has melted giving rise to lower temperature difference and hence reduced rate of energy charge.

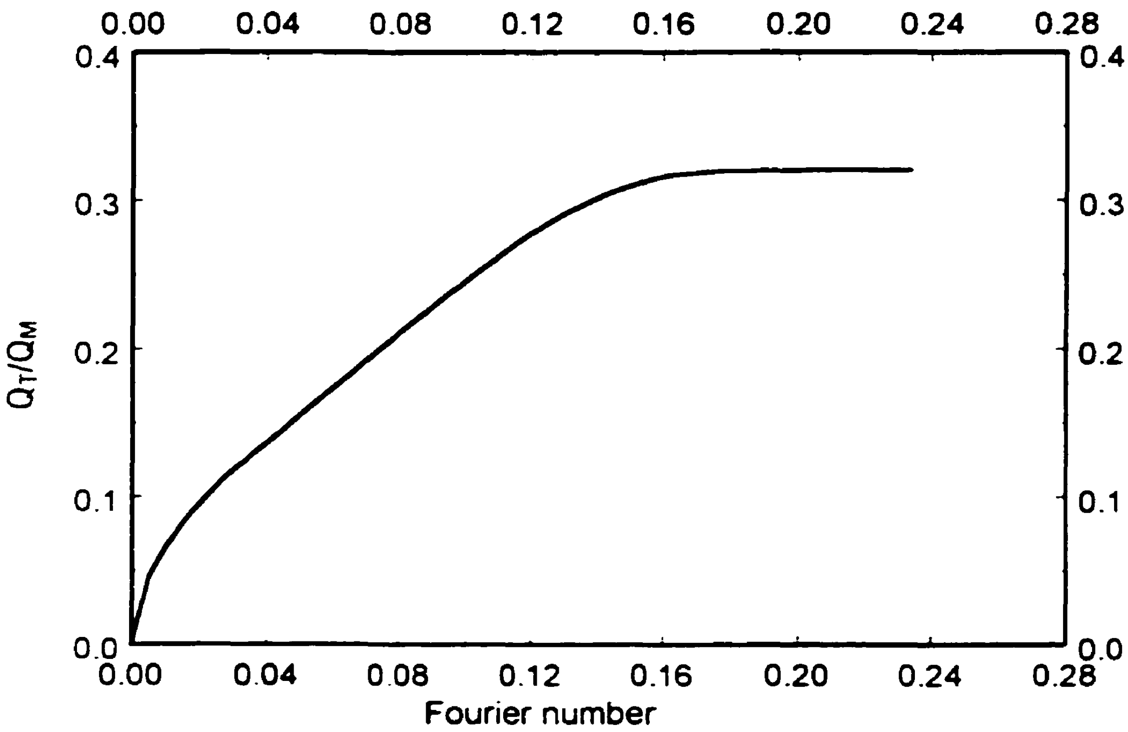

Fig 4 48 Dimensionless energy charge curve (Ra=2.844× 10^6)

Thus, from the aforementioned results it can be deduced that the effect of heating both walls on the streamlines and isotherms is similar to heating inside wall and the outside wall separately in type B horizontal annulus at lower dimensionless times when no interaction between the two melt takes place. This is clearly visible for Fo=0.0432 in Figures 4.35,4.40 and 4 43 for heating the inside wall, outside wall and both walls respectively. No thermal stratification is observed for heating outside and both walls of type B horizontal annulus although it is predominant for higher Rayleigh numbers when heated from inside wall.

4.2.2 Effect of Flipping on the Enhancement of Heat Transfer Rate

To enhance the heat transfer rate during the latter stages of the melting process, Flipping or inverting of the PCM container in the type B horizontal annulus at the appropriate elapsed time after melting begins is proposed as a innovative passive method. A schematic representing the idea is shown in Fig.4.49. Numerical experiments were carried out to determine to what extent the heat transfer rate can be enhanced using this simple procedure. Moreover it is reasonable to assume that the liquid (melt) phase is well-mixed and the melt is stationary after the PCM container is flipped or inverted and melting proceeds without interruption. Numerical simulations indicated that as the initial condition after the PCM container is inverted whether the liquid phase is well mixed and stationary with original temperature distribution or not has little effect on the heat transfer rate. Therefore, in subsequent simulations the temperature and velocity fields were not modified after the container is inverted

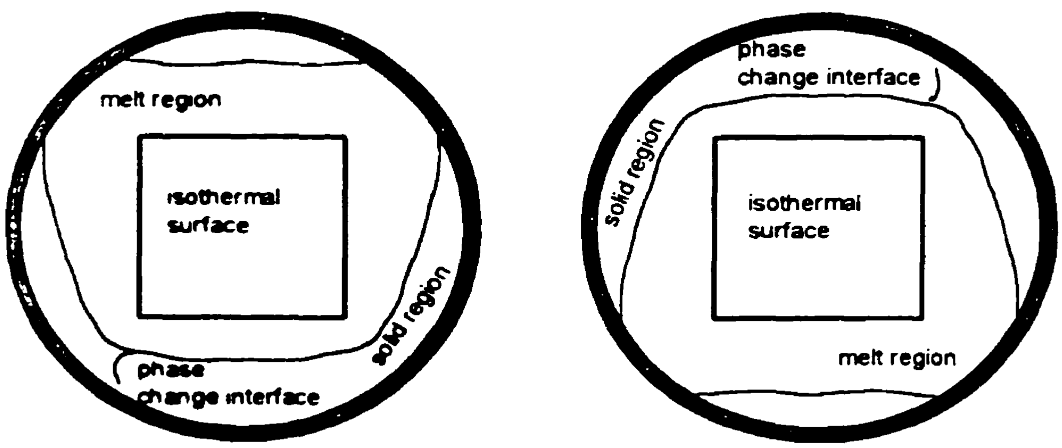

Fig 4 49 Schematic of the physical system for annulus type B

Consider the case of heating only the inside wall of type B horizontal annulus. The PCM container is flipped at Fo = 0.13 and held in that position for subsequent heating. The effect of flipping on the melting and the heat transfer rate is studied numerically

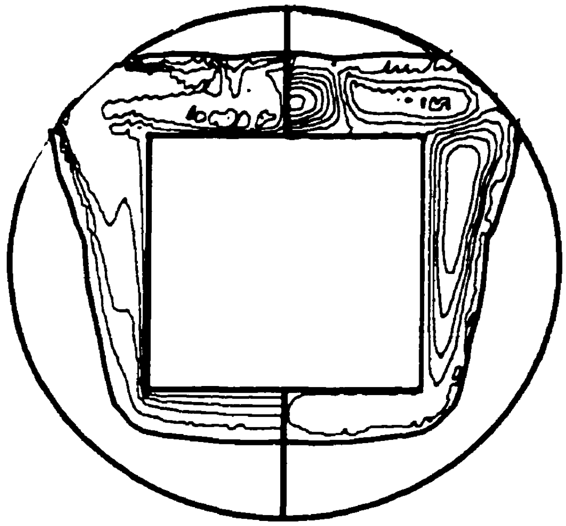

(a) Fo=0.1296

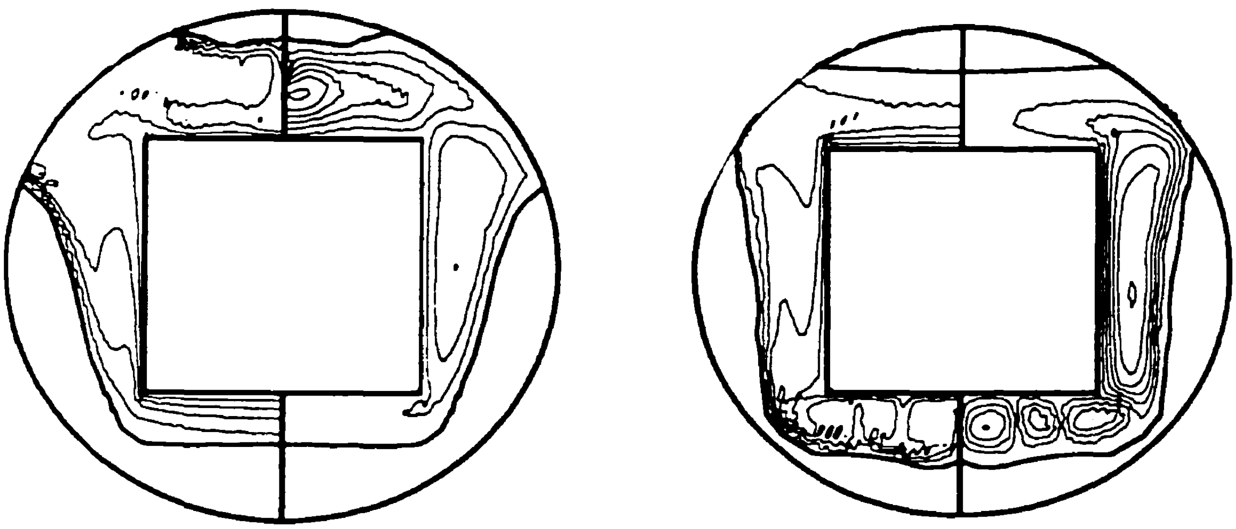

(a2) Fo=0.1728 (b2) Fo=0.1728

Fig. 4.50x Streamlines(right) and isotherms(left) in the melt zone with Ra=2.844×10^6 for heating from inside in case of unflipped and flipped annuli of type B

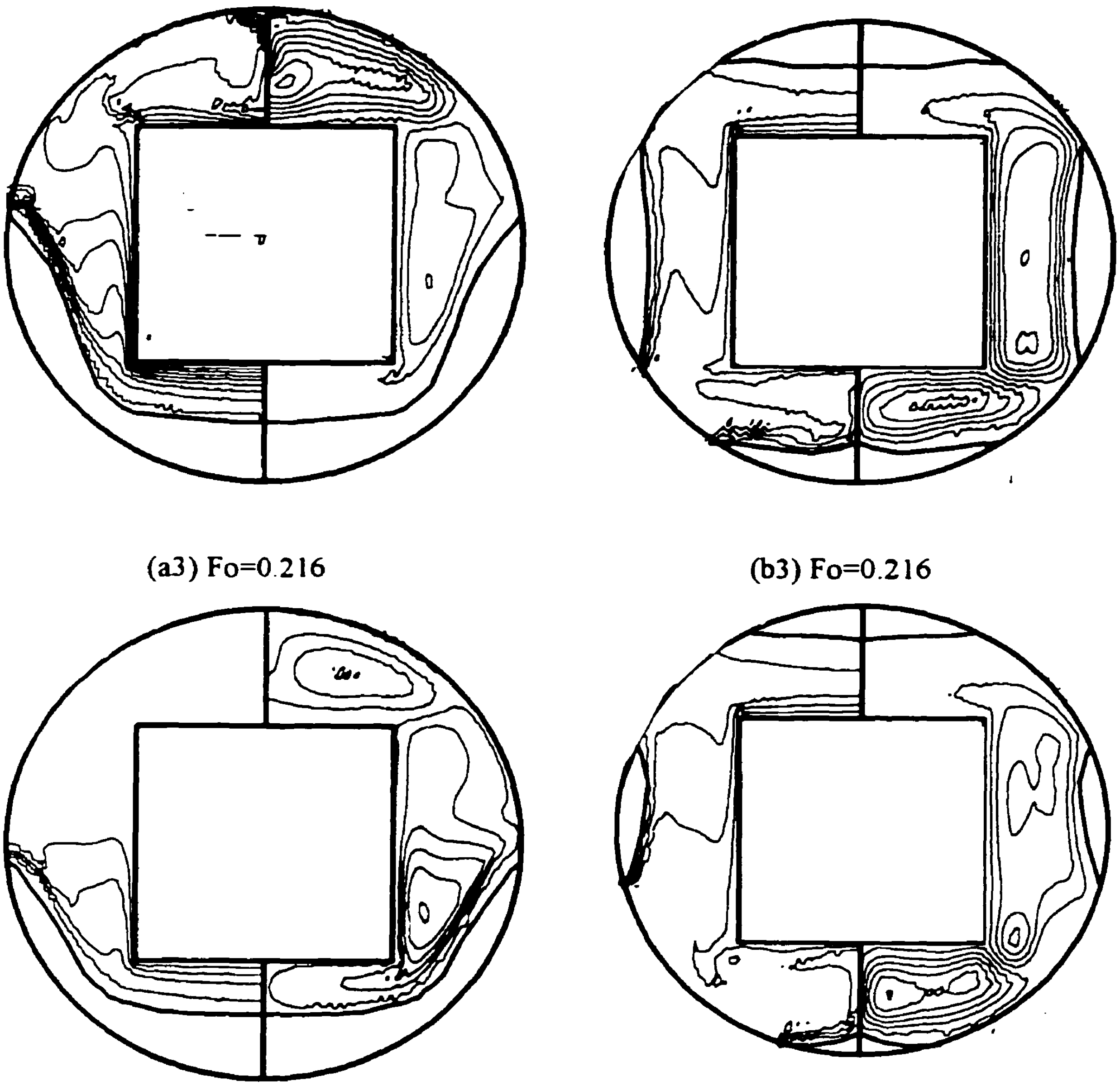

(a3) Fo=0.216 (b3) Fo=0.216

(a4) Fo=0.259 (b4) Fo=0.259

Fig. 4.50y Streamlines(right) and isotherms(left) in the melt zone with Ra=2.844×10^6 for heating from inside in case of unflipped and flipped annuli of type B

As can be seen from the isotherms plotted in Fig. 4.35(a4) thermal stratification occurs during the last stage of the melting process at Fo=0.259. Hence for heating from inside in a type B horizontal annulus the PCM container is inverted at Fo=0.1296. Fig. 4.50x and Fig.4.50y present the predicted streamlines and isotherm contours at different dimensionless times (Fourier numbers) for the unflipped annulus (type B) and for the second period in the case of the flipped horizontal annulus (type B) for a Rayleigh number of 2.84×10^6. In Fig. 4.50x (a) since the container is inverted at Fo > 0.1296, the streamline and isotherm distribution are similar to those for the unflipped annulus case. No thermal stratification occurs in the flipped container at Fo=0.259 when compared to that of unflipped annulus (Fig.4.50y (a4)) and free convection continues to play a significant role as can be seen in Fig.4.50y (b4). In fact the inversion of the container gives rise to a higher melting rate. This explains why the energy charge rate is enhanced by flipping the horizontal annulus of type B.

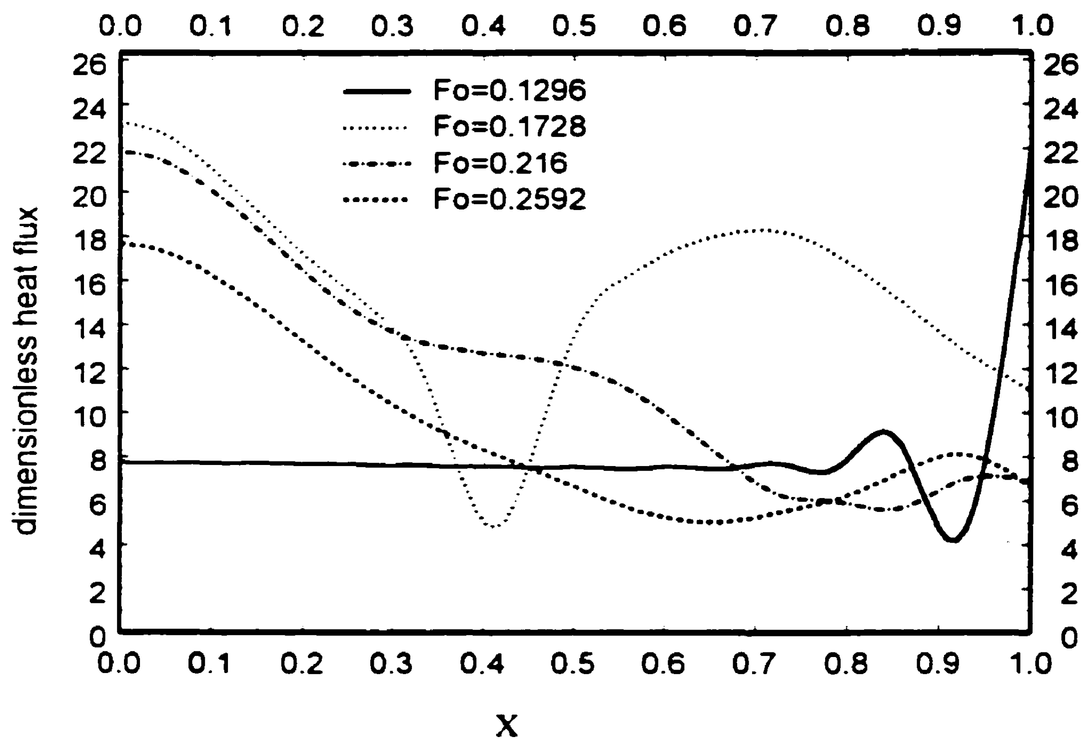

Fig. 4.51 Dimensionless heat flux $\partial\Theta/\partial Y$ along the heated bottom wall at different dimensionless times

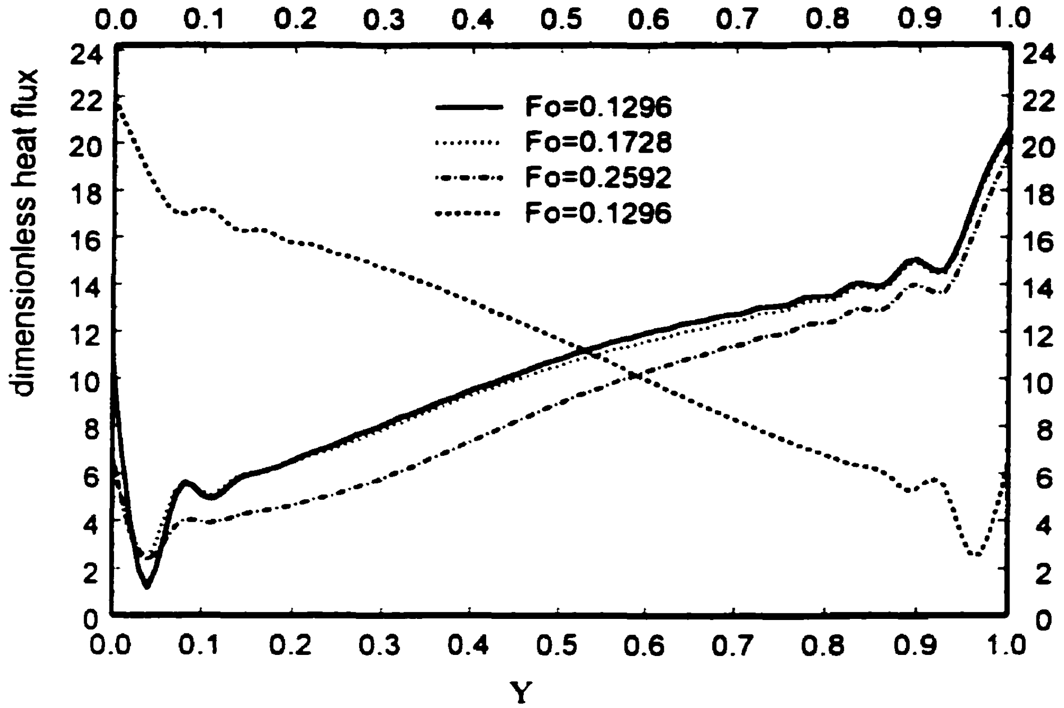

Fig. 4.52 Dimensionless heat Flux $\partial\theta/\partial X$, along the heated vertical wall at different dimensionless times

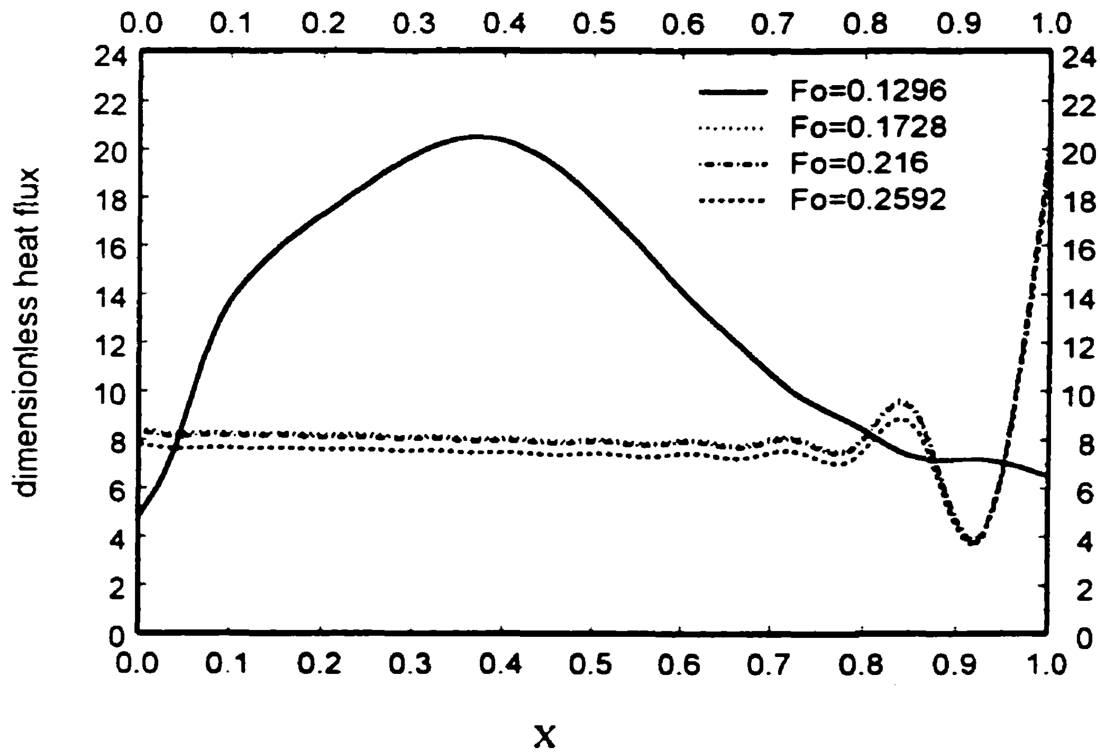

Fig. 4.53 Dimensionless heat flux $\partial\theta/\partial Y$ along the heated top wall at different dimensionless times

Figures 4.51, 4.52 and 4.53 display the dimensionless heat flux distributions $\partial\theta/\partial Y$, $\partial\theta/\partial X$, $\partial\theta/\partial Y$ along the heated bottom wall, vertical wall and top wall for the flipped annulus type B respectively, corresponding to the flow patterns shown in Figures 4.50x and 4.50y. Along the heated bottom wall of the inner tube the heat flux obtained for Fo=0.13 is the same as obtained for unflipped annulus of type B. However, after inversion of the container the heat flux, moving from left to right of the bottom heated wall, at various Fourier numbers is found to decrease steadily. In fact, at Fo=0.173 a trough and a crest is observed which basically corresponds to the junctions of the convection cells in Fig.4.50x(b2). For the inverted container the dimensionless heat flux along the heated vertical wall increases from the bottom to the top. Also the heat flux distribution along the heated top wall of the inner tube from left to right appears to be the same after inversion as can be seen from Fig.4.53.

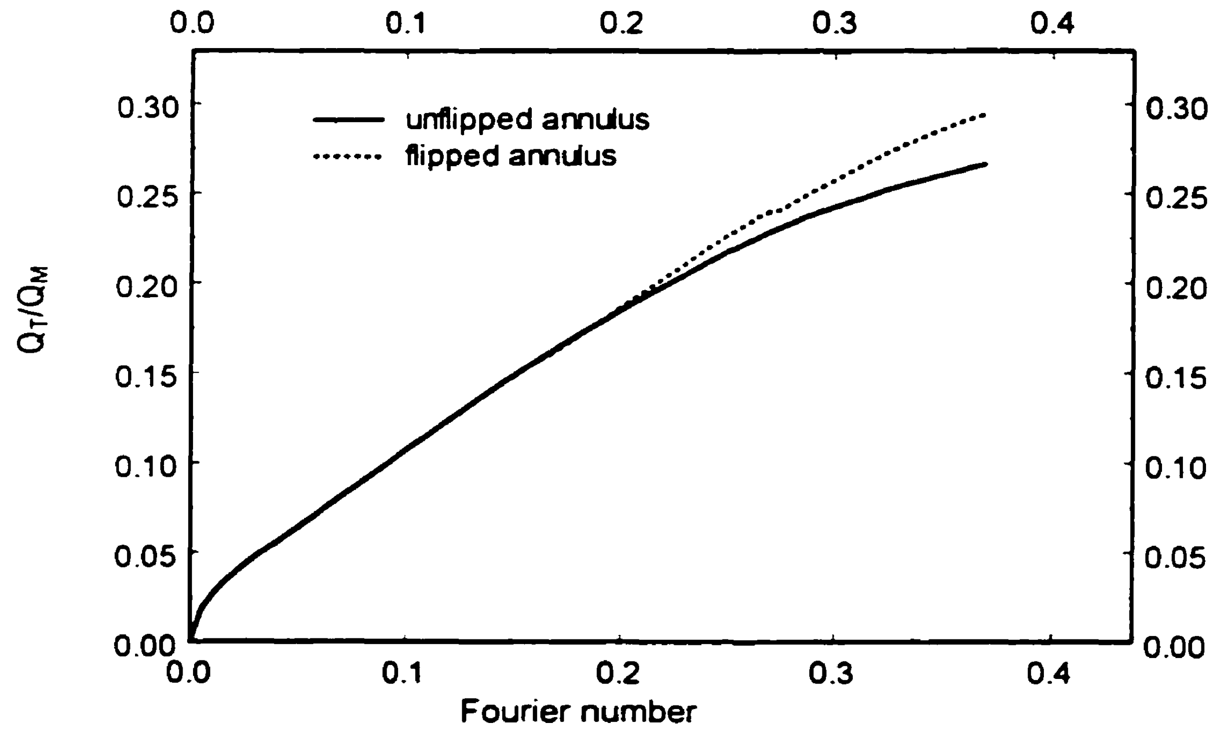

Fig. 4.54 Comparison of Dimensionless Cumulative Energy Charge as a function of the Fourier number(Ra=2.844×10^6)

Fig. 4.30 shows a comparison between the dimensionless cumulative energy charged in the system for both unflipped as well as flipped annuli. In Fig. 4.54 the energy charge curves with and without inverting the container are identical prior to Fo= 0.1296. This is because the flipping action takes place after Fo=0.1296. Fig. 4.31 reveals that the cumulative energy charged for the flipped case is higher than that for the unflipped case. Thus there is no obvious slow-down in the energy charge curve for the case of inverting the PCM container during the final stage of the melting process.

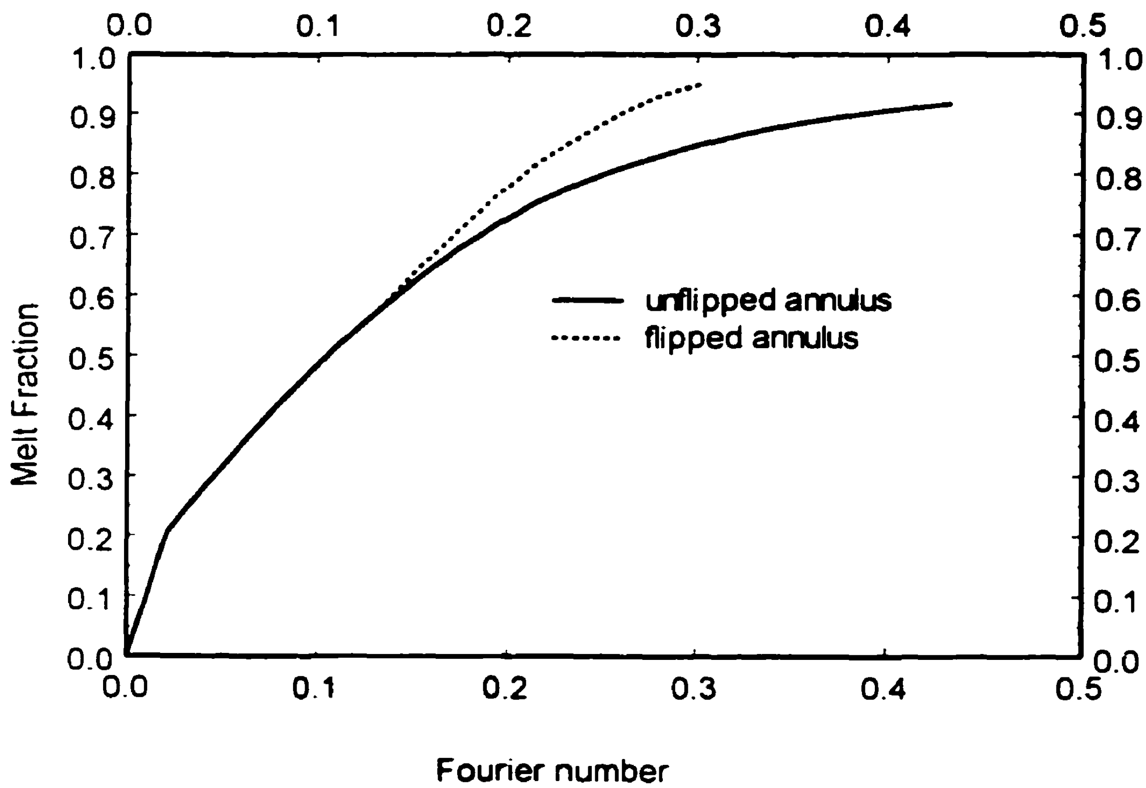

Fig. 4.55 Melt Fraction as a function of Fourier Number (Ra=2.844×10^6)

A comparison of the fraction melted for both the flipped and unflipped horizontal annulus of type B when only the inside wall is heated is presented in Fig.4.32. This figure reveals that there is a enhancement in the melting rate with the flipped container relative to the conventional unflipped case at long elapsed times. It can be deduced that the beneficial effects of flipping towards increase in the heat transfer rate is helpful only during the late stages of the melting process. Of course the magnitude of such enhancement will depend on the PCM used, the container geometry, boundary conditions as well as the time when the flipping occurs.

4.3 CONCLUDING REMARKS

Melting of a pure phase change material in tube geometries of two different configuration i.e type A horizontal annulus and type B horizontal annulus were studied numerically. Numerical experiments were carried out for each of the configurations for heating the inside wall, the outside wall and both walls simultaneously to determine which one is more effective for more rapid thermal storage.

Fig.4.56 displays a comparison of the dimensionless thermal energy charged for both horizontal annuli of type A and B for heating from inside as a function of the Fourier number. Although for type B annulus the energy charged is greater than that for the type A annulus during the first stage of the melting process, later on the rate of energy charged is more rapid for the type A annulus. Moreover there is an almost linear increase in the cumulative energy charged As can be seen in Fig. 4.57 the melt fraction for the type A annulus is lower than that of the type B annulus.

Fig 4.58 presents a comparison between the cumulative energy charged for heating from outside in both horizontal annuli of type A and B. Type A annulus has a higher cumulative energy charge rate rather than that of annulus type B. However a comparison of the corresponding melt fraction versus Fourier number curves shown in Fig. 4.59 shows that the melting rate is higher for type B annulus than type A annulus. This apparent anomaly is due to the fact that the melt fraction considers only the latent heat storage while the cumulative energy stored includes both sensible and latent heat components.

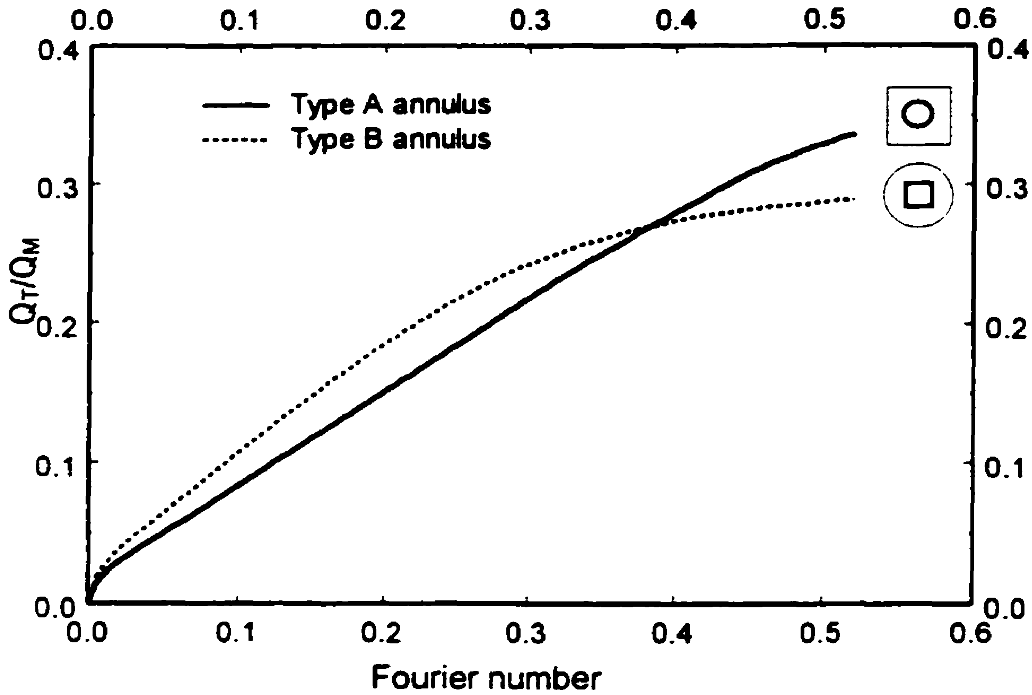

Fig. 4.56 Comparison of dimensionless cumulative energy charge curve for heating the inside wall (Ra=2.844×10^6)

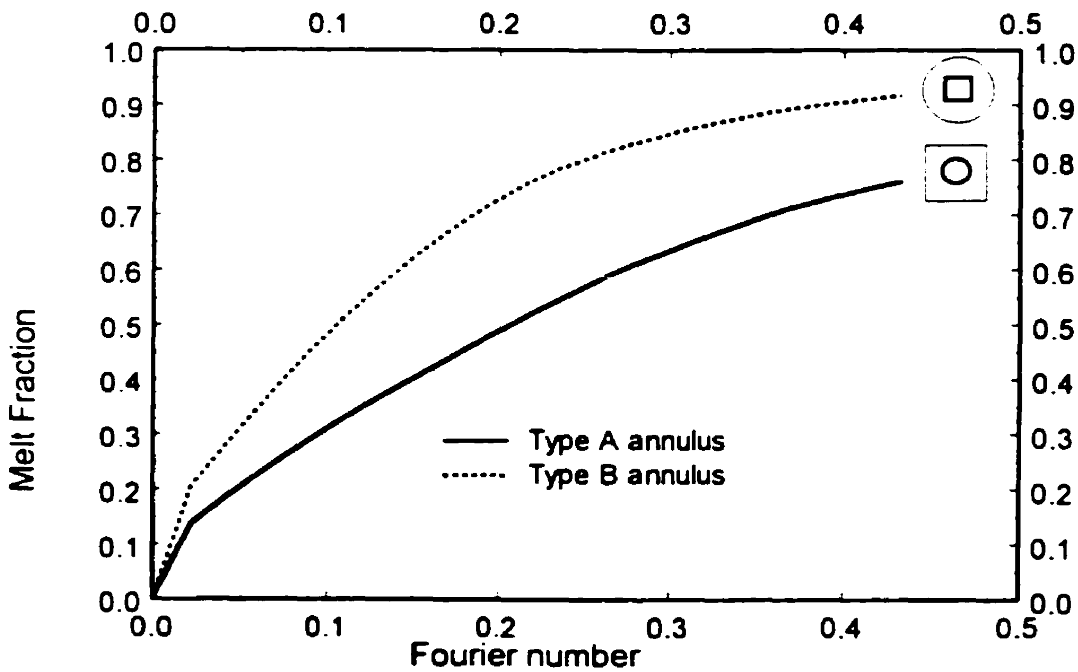

Fig. 4.57 Comparison of melt fraction as a function of Fourier number for heating the inside wall(Ra=2.844×10^6)

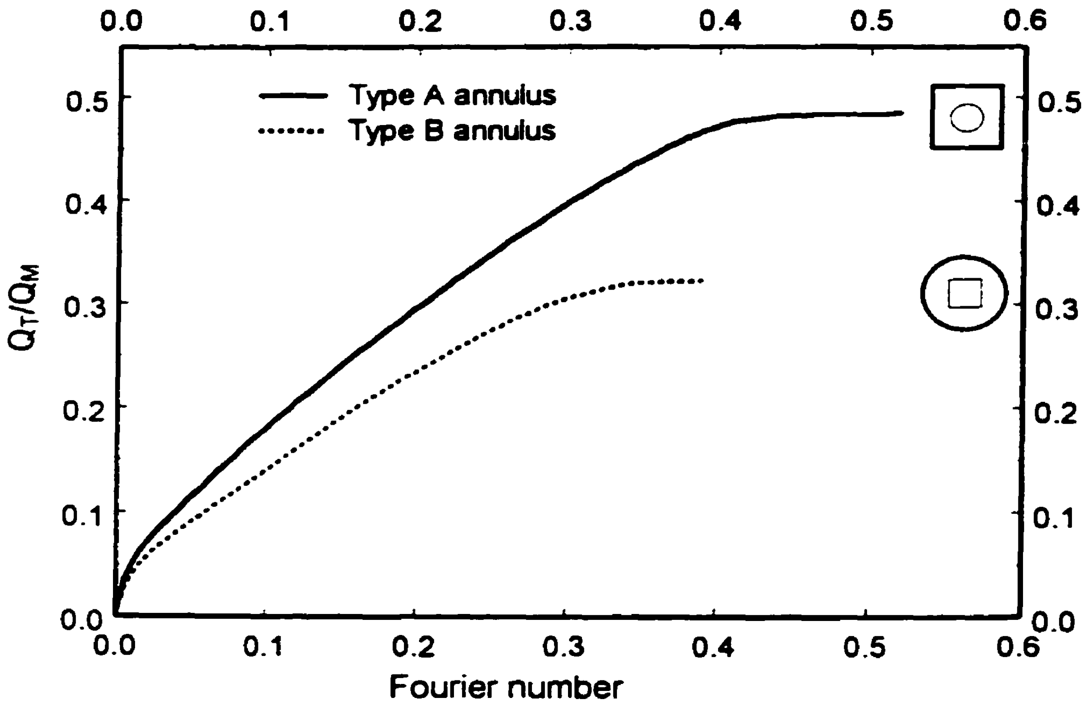

Fig. 4.58 Comparison of dimensionless cumulative energy charge curve for heating the outside wall (Ra=2.844×10^6)

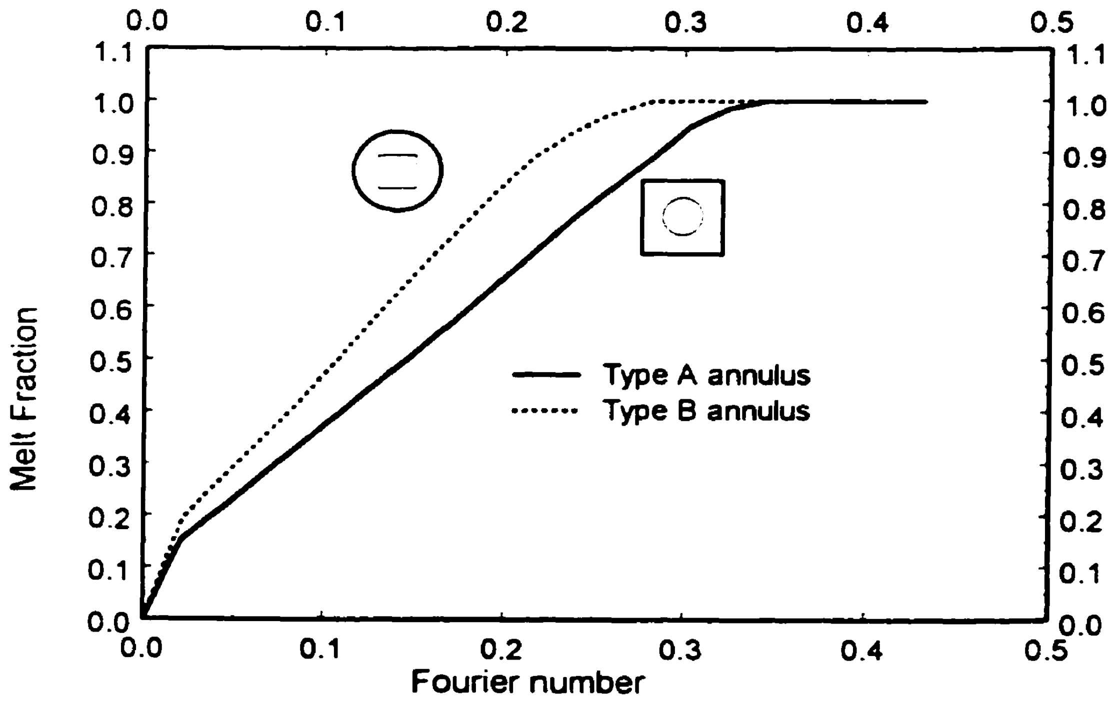

Fig. 4.59 Comparison of melt fraction as a function of Fourier number for heating outside wall (Ra=2.844×10^6)

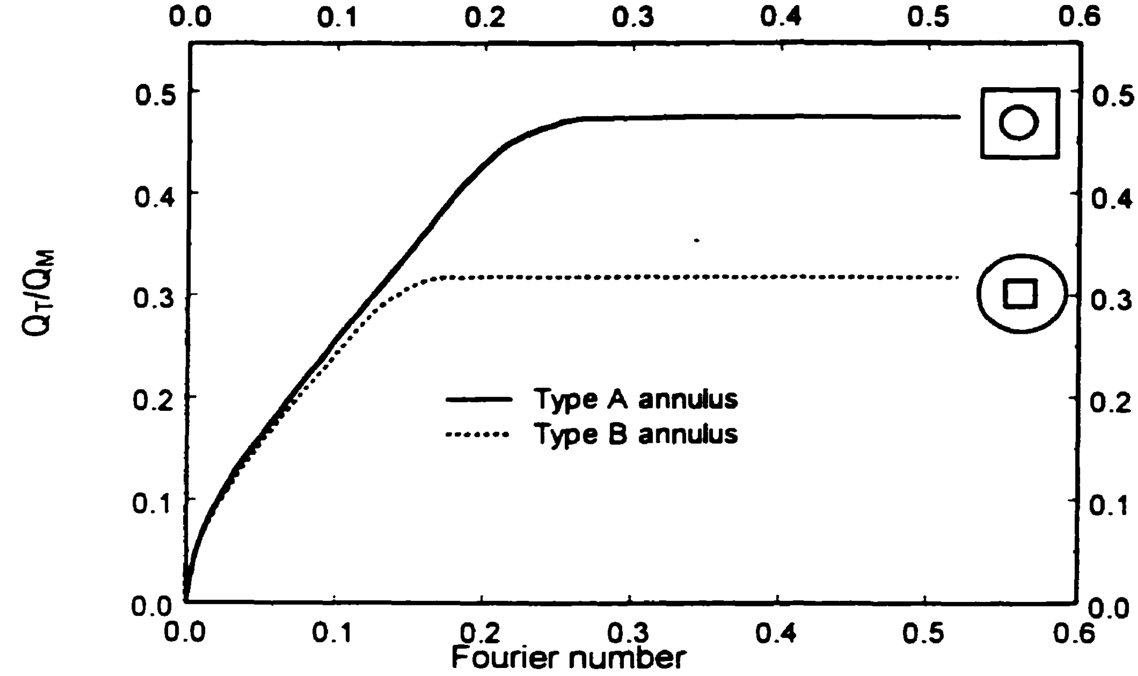

Fig. 4.60 Comparison of dimensionless cumulative energy charge curve for heating both inside and outside wall (Ra=2.844×10^6)

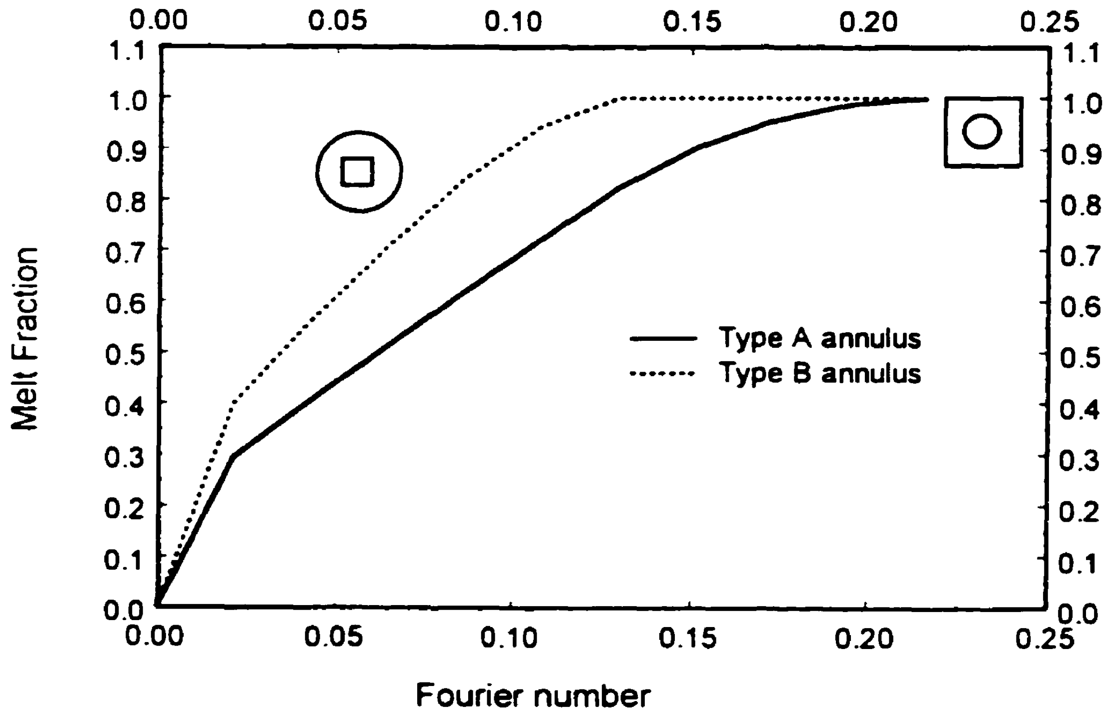

Fig. 4.61 Comparison of melt fraction as a function of Fourier number for heating both inside and outside wall (Ra=2.844×10^6)

Fig. 4.60 displays a comparison between the cumulative energy charged in horizontal annulus of type A and B when heated from both inside and outside wall, respectively. The energy charged in case of annulus type A is higher than that of annulus type B. Fig. 4.61 shows a comparison of the melt fraction as a function of Fourier number where annulus of type B melts at a faster rate thereby melting the entire solid PCM.

For both horizontal annuli of type A and B it is observed that the effect of heating both walls is the same as heating inside wall and outside wall separately until there is interaction between the two melt zones. However, during the late stages melting appears to occur at a faster rate due to good mixing between the melt zones formed by heating both the inside and the outside walls. This suppresses thermal stratification, which occurs in both horizontal annulus of type A and B for heating the inside wall. The thermal stratification is attained in the upper part of the cavity while the PCM at the bottom portion remains solid. This is due to the fact that the energy charged to the system is mainly carried upward by the free convective flow in the melt. Thus energy is used to raise the temperature of melt instead of melting the PCM. In other words energy storage in the system is in the form of sensible heat and not latent heat.

To counteract the problem of stratification for heating of the inside wall in type A annulus, introduction of eccentricity is proposed as a viable solution. This is supported by the numerical results obtained in this study. This is mainly attributed to the vertically oriented buoyancy force in the melt phase at high Rayleigh numbers, which facilitates melting. The extent of eccentricity determines the increase in melting as compared to the concentric case. The melting rate below the heated inner wall is controlled by conduction and hence is lower than that on the sides and top wall.

Another interesting yet simple approach to take care of stratification in both horizontal annulus of type A and B for heating the inside wall is flipping or inverting the container at pre-selected times after initiation of melting. The present numerical study reveals a good improvement in the melting rate, which indirectly reduces the melting time as compared to the conventional (unflipped) PCM container.

The numerical evaluation of heating the outside wall of both type A and B horizontal annuli of reveals that there is merit to heating the outer external bottom wall. It also eliminates the interference of thermal stratification as observed when heating only the inside wall.

REFERENCES

1. Hale, N.W. and Viskanta, R., 1980, "Solid-Liquid Phase Change Heat Transfer and Interface Motion in Materials Cooled or Heated from Above or Below," *Int. J. Heat Mass Transfer*, Vol. 23, pp. 283-292.
2. Benard, H., 1900, "Tourbillions Cellulaires dan une Nappe Liquid," *Revue Generale des Sciences Pures et Appliqees*, Vol. 11, pp. 1309-1328.
3. Devahastin, S., Siow, S. L., and Mujumdar, A. S., 1998, "Effect of Inclination on free Convective Heat transfer during Melting of a Phase Change Material in a Rectangular Enclosure," *Applied mechanics and Engineering*, Vol. 3, No.3, pp 491-515.
4. Gong, Z.X. and Mujumdar, A S , 1998, "Flow and Heat Transfer in Convection-Dominated Melting in a Rectangular Cavity Heated from below," *Int. J. Heat Mass Transfer*, Vol. 14, No 17, pp 2573-2580

NOMENCLATURE

d Diameter of the inner cylinder

f_H enthalpy-temperature function

g_i gravitational force vector

h enthalpy

k heat conductivity

Q instantaneous energy charged

Q_T total energy charged

Q_M maximum energy charged

r_s radius of inner cylinder

r_b radius of outer cylinder

r radial co-ordinate (see Fig. 1)

t time

T temperature

T_0 reference temperature

T_m melting point of PCM

T_w isothermal wall temperature

u_i velocity component

u_x velocity in x direction

u_y velocity in y direction

x, y coordinate

Greek symbols :

α diffusivity

β expansion coefficient

Δh latent heat

ϕ polar angle (see Fig. 1)

μ viscosity

ρ density

Subscripts :

l liquid

s solid

x component of x direction

y component of y direction

Dimensionless groups :

Fo Fourier number $Fo = \dfrac{t\alpha_l}{d^2}$

Pr Prandtl number $\Pr = \dfrac{c_l \mu}{k_l}$

R Normalized radial co-ordinate $\mathrm{R} = \dfrac{r - r_s}{r_b - r}$

Ra Rayleigh number $Ra = \dfrac{\rho^2 c_l g \beta d^3 (T_w - T_m)}{\mu k_l}$

Ste Stefan number $Ste = \dfrac{c_l (T_w - T_m)}{\Delta h}$

θ dimensionless temperature $\theta = \dfrac{T - T_m}{T_w - T_m}$

Φ normalized polar angle $\Phi = \phi/\pi$

Chapter 5

Conclusions

Using a mathematical model the free convection-dominated melting heat transfer characteristics of a phase change material (PCM) (n-octadecane (99% pure)) are determined for horizontal annuli of the following configurations:

(a) Square external tube with a circular tube inside - Annulus Type A

(b) Circular external tube with a square tube inside - Annulus Type B

Numerical experiments were carried out for each of the configurations for the following three cases: heating the inside wall, heating the outside wall and heating both walls simultaneously to a temperature above the melting point of the PCM. Additionally, various innovative passive methods such are introducing eccentricity to the annulus and inverting (or flipping) the assembly are proposed and examined as possible means of enhancing the melting heat transfer rates. The following conclusions are made based on this investigation subject to assumptions made in the model:

- Type A annulus appears to be more effective than type B annulus because the cumulative energy charged is more effective for all of the cases examined i.e heating the inside wall, the outside wall and both walls simultaneously. Although the melting rate appears to be better for annulus type B, it should be noted that melt fraction considers only the latent heat storage while the cumulative energy charged includes both sensible and latent heat components.
- Heating the inside wall in both configurations display that thermal stratification occurs in the upper part of the cavity while the PCM in the bottom portion remains

solid at longer dimensionless times (Fourier number), i.e in the late stages of melting. This happens due to the fact that the energy charged to system is mainly carried upward by the free convective flow in the melt. An increase in the Rayleigh number results in an earlier onset of convection thereby increasing the melting rate.

- For the case of heating the outside wall in both configurations it was observed that thermal stratification does not occur. This increases the melting rate to a considerable extent. Moreover, it can be inferred that the effect of heating both walls in horizontal annuli of type A and B is the same as the sum of heating inside wall and outside wall separately until there is interaction between the two melt zones.
- In horizontal annulus of type A, as a measure to suppress the thermal stratification on heating the inside wall, eccentricity is introduced. The numerical results indicate that the eccentric geometry with the inner cylinder moved lower is superior to the concentric one (all other parameters being held constant) due to the vertically upward orientation of the buoyancy force in the melt phase in free convection-dominated flows.
- Flipping or inverting the partially melted container at pre-selected times after initiation of melting was studied in horizontal annuli of type A and B. It is deduced that there is enhancement in the melting rate with the flipped container relative to the conventional unflipped one at long elapsed times.